The Dissertation Committee for Yonghwan Kwon Certifies that this is the approved version of the following dissertation:

Development and evaluation of an advanced microwave radiance data assimilation system for estimating snow water storage at the continental scale

Committee:

Zong-Liang Yang, Supervisor

Robert E. Dickinson

Rong Fu

Matthew Rodell

Robert D. Moser

Development and evaluation of an advanced microwave radiance data assimilation system for estimating snow water storage at the continental scale

by

Yonghwan Kwon, B.S.; M. City Planning

Dissertation

Presented to the Faculty of the Graduate School of

The University of Texas at Austin

in Partial Fulfillment

of the Requirements

for the Degree of

Doctor of Philosophy

The University of Texas at Austin

May 2016

Dedication

To my wife Jaeun Jung and my daughter Jamie Dahee Kwon

Acknowledgements

First and foremost, I am sincerely grateful to my supervisor, Dr. Zong-Liang Yang for his support, advice, inspiration, and encouragement. He is a great mentor to me. Without him, I would not be able to start my research journey with this challenging topic. His thoughtful understanding of my personal situation and his encouragement enabled me to complete my PhD research. All things I have learned from him will be priceless assets for my research and life.

I would like to express my gratitude to my committee members, Dr. Robert Dickinson, Dr. Rong Fu, Dr. Matthew Rodell, and Dr. Robert Moser for their constructive comments on my research. I also want to thank Dr. Matthew Rodell for allowing me to visit NASA and for providing continuous expert advice on my research. I am highly appreciative and grateful to Mr. Tim Hoar, Dr. Ally Toure, and Dr. Long Zhao for their time, efforts, and comments, which accelerated and enriched my research. Remote discussions with Dr. Michael Durand, Dr. Ghislain Picard, Dr. Mark Flanner, Dr. Alexandre Langlois, and Dr. Alexandre Roy were a great help to my research progress.

I want to thank my previous and current group members, Dr. Cédric David, Dr. Hua Su, Dr. Jiangfeng Wei, Dr. Mingjie Shi, Dr. Ahmad Tavakoly, Dr. Yongfei Zhang, Dr. Qinjian Jin, Dr. Xitian Cai, Lisa Helper, Peirong Lin, Sagar Parajuli, Alex Resovsk, Maryia Halubok, and Seungwon Chung for their help and beneficial discussions. In addition, I would like to express appreciation to Ms. Patricia Bobeck and Mr. Adam Papendieck for their help to improve my writing skill.

Most importantly, I am grateful to my parents and wife for their unfailing love and support.

My research was financially supported by the National Aeronautics and Space Administration under Grant NNX11AJ43G, the Jackson School of Geosciences, and the National Natural Science Foundation of China under Grant 91337217.

Development and evaluation of an advanced microwave radiance data assimilation system for estimating snow water storage at the continental scale

Yonghwan Kwon, Ph.D.

The University of Texas at Austin, 2016

Supervisor: Zong-Liang Yang

Snow cover modulates the Earth's surface energy and water fluxes, and snowmelt runoff is the principal source of water for humans and ecosystems in many of the middle to high latitudes in the Northern Hemisphere. Understanding spatial and temporal variation in snowpack is crucial for climate studies and water resource management and thus the climate and hydrological research communities have invested in improving large-scale snow estimates. This dissertation aims to develop an advanced snow radiance assimilation (RA) system to improve continental-scale snow water storage estimates. The RA system is comprised of the Community Land Model version 4 (CLM4) (for snow energy and mass balance modeling), radiative transfer models (RTMs) (for brightness temperature estimates), and the Data Assimilation Research Testbed (DART) (for ensemble-based data assimilation). Two snowpack RTMs, the Microwave Emission Model for Layered Snowpacks (MEMLS) and the Dense Media Radiative Transfer–Multi Layers model (DMRT-ML), are used to simulate T_B of a multi-layered snowpack.

Through an error characterization study, this dissertation presents that the correlations between snow water equivalent (SWE) error and brightness temperature (T_B)

error and subsequent RA performance in estimating snow are significantly affected by all physical properties of soil and snow involved in estimating T_B. Based on the error characterization results, it is hypothesized that the continental-scale RA performance in estimating snow water storage can be improved by simultaneously updating all model physical states and parameters determining T_B based on a rule, in which prior estimates are updated depending on their correlations with a prior T_B. The results of a series of RA experiments show that the improved continental-scale snow estimates are obtained by applying the hypothesis. This dissertation also shows that further improvement of the performance of the RA system can be achieved, especially for vegetated areas, by assimilating the best-performing frequency channels (i.e., 18.7 and 23.8 GHz) and by considering the vegetation single scattering albedo to represent the vegetation effect on T_B at the top of the atmosphere.

Table of Contents

List of Tables xi

List of Figures xii

CHAPTER 1: Introduction 1

CHAPTER 2: Error characterization of coupled land surface–radiative transfer models for snow microwave radiance assimilation 6

2.1 Abstract 6

2.2 Introduction 7

2.3 Methods 9

2.3.1 CLPX data 9

2.3.2 Land surface model 13

2.3.3 Radiative transfer model 14

2.3.4 Model parameter optimization 17

2.3.5 Synthetic experiments 19

2.4 Results and discussion 20

2.4.1 Point-scale error characterization: CLPX LSOS (non-vegetated case) 20

2.4.2 Mesoscale error characterization: CLPX MSA (vegetated case) 27

2.4.3 Synthetic experiments 35

2.5 Conclusions 44

2.5 Acknowledgment 49

CHAPTER 3: Estimating snow water storage in North America using CLM4, DART, and snow radiance data assimilation 51

3.1 Abstract 51

3.2 Introduction 52

3.3 Coupled radiance assimilation system, data sets, and experimental design 53

3.3.1 Coupled radiance assimilation system 53

3.3.2 Data sets 58
3.3.3 Experimental design 61
3.4 Results and discussion 65
3.4.1 Simultaneous update of states and parameters 65
3.4.2 Rule-based RA 71
3.4.3 Localization and adaptive inflation 77
3.5 Conclusions 82
3.6 Acknowledgement 84
CHAPTER 4: Improving the radiance assimilation performance in estimating snow water storage across snow and land cover types in North America 85
4.1 Abstract 85
4.2 Introduction 86
4.3 Coupled radiance assimilation system 87
4.4 Experimental design 90
4.4.1 Microwave frequency channels 92
4.4.2 Snowpack radiative transfer models 93
4.4.3 Vegetation single scattering albedo 94
4.5 Results and discussion 97
4.5.1 Performance of the RA system using AMSR-E frequencies and snowpack RTMs 97
4.5.2 The impact of the vegetation single scattering albedo (ω) on the RA performance 101
4.5.3 Snow water volume and snow cover area in North America 110
4.6 Conclusions 111
4.7 Acknowledgement 113
CHAPTER 5: Conclusions and future perspective 115
References 125
Vita 134

List of Tables

Table 2.1. DMRT-ML stickiness parameter optimization results using *in situ* snowpit and ground-based T_B data collected within the LSOS (RMSE: Root Mean Square Error, MBE: Mean Bias Error). The optimal stickiness parameter value was determined to be 0.17.....20

Table 2.2. Errors of T_B simulations by the coupled CLM4/DMRT-ML and CLM4/MEMLS for the LSOS. 24

Table 2.3. Optimization results of vegetation RTM parameters using *in situ* snowpit and AMSR-E T_B data collected over the Fraser and Rabbi Ears MSAs. 27

Table 2.4. Errors of T_B simulations by the coupled CLM4/DMRT-ML and CLM4/MEMLS for the Fraser and Rabbit Ears MSAs. 29

Table 3.1. List of experiments and updated states and parameters in each experiment. 62

Table 3.2. The snow depth RMSE of each case for snow classes as defined in *Sturm et al.* [1995]. The localization distance of 0.01 radians was used for all RA cases. Adaptive inflation was applied in the RASRTSP/INF and RASRTSP-R/INF cases. The percentage values in parentheses represent the relative improvement (negative values) or degradation (positive values) in the performance of the RA cases compared to the open-loop run. 81

Table 3.3. Same as Table 3.2 but for land covers. 81

Table 4.1. Radiance assimilation (RA) experimental cases with respect to snowpack RTMs, frequency channels, and single scattering albedo.....91

List of Figures

Figure 2.1. Maps of the NASA CLPX Small Regional Study Area (SRSA), the Rabbit Ears and Fraser Meso-cell study areas (MSAs), and the Local Scale Observation Site (LSOS). Figures from the National Snow and Ice Data Center (NSIDC) website (http://nsidc.org/data/clpx/clpx_pits.html and http://nsidc.org/data/docs/daac/nsidc0169_clpx_lsos_snow/). Red and blue stars indicate the locations of the CLPX region and Rocky Mountains, respectively, where the synthetic experiments were conducted. 10

Figure 2.2. CLM4 simulation results for the LSOS: (a) SWE and (b) normalized errors (=(simulation – observation)/observation) of snow depth, density, grain radius, and temperature.....23

Figure 2.3. Results of T_B simulation by the coupled CLM4/DMRT-ML and CLM4/MEMLS for the LSOS. 25

Figure 2.4. Relationships between errors (= simulation – observation) of SWE (ε_SWE) and T_B (ε_T_B) for the LSOS. 26

Figure 2.5. Relationships between errors (=simulation – observation) of snow depth (ε_d_{snow}) and density (ε_ρ_{snow}) and errors of (a) SWE (ε_SWE) and (b) snow grain radius (ε_r_e), respectively, for the LSOS. 26

Figure 2.6. Observed AMSR-E T_B versus simulated T_B by DMRT-ML and MEMLS, which are coupled with the vegetation and atmospheric RTMs, using the optimized parameters (in Table 2.3) and in situ snowpit measurements collected from ISAs within the Fraser and Rabbit Ears MSAs. 27

Figure 2.7. Results of SWE simulation by CLM4 for each ISA within the Fraser and Rabbit Ears MSAs. RMSE and MBE were calculated for MSAs. ...29

Figure 2.8. Normalized errors (= (simulation – observation) / observation) of snow depth, density, grain radius, and temperature for each ISA within the Fraser and Rabbit Ears MSAs. Since both observations and simulations showed dry snowpack conditions, normalized error of wetness is not shown. 30

Figure 2.9. Observed versus simulated T_B by the coupled CLM4/DMRT-ML and CLM4/MEMLS for the Fraser and Rabbit Ears MSAs. 31

Figure 2.10. Relationships between errors (= simulation – observation) of SWE (ε_SWE) and T_B (ε_T_B) for the Fraser MSA: (a) all ISAs are included and (b) the St. Louis Creek ISA is excluded.....32

Figure 2.11. Relationships between errors (= simulation – observation) of SWE (ε_SWE) and T_B (ε_T_B) for the Rabbit Ears MSA: (a) all ISAs are included and (b) the Buffalo Pass ISA is excluded.....33

Figure 2.12. Relationships between SWE error (= simulation – observation) (ε_SWE) and errors of snow depth (ε_d_{snow}) and density (ε_ρ_{snow}), respectively, for the Fraser MSA ((a) all ISAs are included and (b) the St. Louis Creek ISA is excluded) and the Rabbit Ears MSA ((c) all ISAs are included and (d) the Buffalo Pass ISA is excluded). 34

Figure 2.13. Relationships between snow grain radius error (= simulation – observation) (ε_r_e) and errors of snow depth (ε_d_{snow}) and density (ε_ρ_{snow}), respectively, for the Fraser MSA ((a) all ISAs are included and (b) the St. Louis Creek ISA is excluded) and the Rabbit Ears MSA ((c) all ISAs are included and (d) the Buffalo Pass ISA is excluded). 35

Figure 2.14. Synthetic truth and ensemble mean of SWE and RMSE of ensemble SWE simulations over the (a) CLPX region (shallow snowpack conditions) and (b) Rocky Mountains (deep snowpack conditions) during 2003. 36

Figure 2.15. Relationships between SWE error (= ensemble simulations – synthetic truth) (ε_SWE) and errors of snow depth (ε_d_{snow}) and density (ε_ρ_{snow}), respectively, over the (a) CLPX region (shallow snowpack conditions) and (b) Rocky Mountains (deep snowpack conditions) during 2003.37

Figure 2.16. Scatter plots of correlation coefficients between ε_SWE and ε_T_B versus SWE RMSE difference (= $RMSE_{RA} - RMSE_{Open\text{-}loop}$) for each model and each frequency channel over the CLPX region during 2003: (a) original result, (b) no soil (water content and temperature) effect on ε_T_B, (c) no soil (water content and temperature) and snow wetness effects on ε_T_B, and (d) no soil (water content and temperature), snow wetness, and snow temperature effects on ε_T_B. Each point is corresponding to each day. 38

Figure 2.17. Same as Figure 2.16 but for the Rocky Mountains. 39

Figure 2.18. The classification of 13 cases based on the correlation coefficients between ε_r_e and ε_d_{snow} (x-axis) and ε_ρ_{snow} (y-axis), respectively: (a) CLPX region (shallow snowpack conditions) and (b) Rocky Mountains (deep snowpack conditions).....41

Figure 2.19. Scatter plots of correlation coefficients between ε_SWE and ε_T_B versus the normalized ε_r_e for each model and each frequency channel over the CLPX region during 2003. Each point is corresponding to each day. The 13 cases are based on Figure 2.18a. 42

Figure 2.20. Same as Figure 2.19 but for the Rocky Mountains. The 13 cases are based on Figure 2.18b. 43

Figure 2.21. Scatter plots of the normalized ε_r_e versus SWE RMSE difference (= $RMSE_{RA} - RMSE_{Open\text{-}loop}$) over the CLPX region during 2003 (R: correlation coefficient between ε_SWE and ε_r_e). Each point is corresponding to each day. 45

Figure 2.22. Same as Figure 2.21 but for the Rocky Mountains. 46

Figure 3.1. Schematic diagram of the coupled radiance assimilation system.....54

Figure 3.2. Simulation results of the open-loop case for (a) snow depth and (b) SCF. The root mean square error (RMSE) and mean bias error (MBE) were calculated by comparing the results with the CMC snow depth and MODIS SCF for December 2002 to February 2003. 66

Figure 3.3. RMSE differences for (a to i) snow depth and (j to r) SCF: (a and j) RA_{SWE} − Open-loop, (b and k) RA_{SR} − Open-loop, (c and l) RA_{SRT} − Open-loop, (d and m) RA_{SRTS} − Open-loop, (e and n) RA_{SRTSP} − Open-loop, (f and o) RA_{SR} − RA_{SWE}, (g and p) RA_{SRT} − RA_{SR}, (h and q) RA_{SRTS} − RA_{SRT}, and (i and r) RA_{SRTSP} − RA_{SRTS}. In the RA cases, the default update method was used. 67

Figure 3.4. Spatial distributions of the ensemble mean of the RTM parameters (i.e., snow stickiness in DMRT-ML and x and b' in the vegetation RTM) on 15 December 2002, 1 and 15 January 2003, and 28 February 2003.69

Figure 3.5. Sensitivity of brightness temperature to snow and soil physical properties (i.e., SWE, snow grain radius, snow temperature, soil temperature, and soil water content) and RTM parameters (i.e., snow stickiness in DMRT-ML and two empirical parameters (x and b') in the vegetation RTM). Dimensionless sensitivity indices were calculated based on the method suggested by *Lenhart et al.* [2002]. 72

Figure 3.6. RMSE differences for (a to i) snow depth and (j to r) SCF: (a and j) $RA_{SWE\text{-}R}$ − Open-loop, (b and k) $RA_{SR\text{-}R}$ − Open-loop, (c and l) $RA_{SRT\text{-}R}$ − Open-loop, (d and m) $RA_{SRTS\text{-}R}$ − Open-loop, (e and n) $RA_{SRTSP\text{-}R}$ − Open-loop, (f and o) $RA_{SR\text{-}R}$ − $RA_{SWE\text{-}R}$, (g and p) $RA_{SRT\text{-}R}$ − $RA_{SR\text{-}R}$, (h and q) $RA_{SRTS\text{-}R}$ − $RA_{SRT\text{-}R}$, and (i and r) $RA_{SRTSP\text{-}R}$ − $RA_{SRTS\text{-}R}$. In the RA cases, the rule-based update method was used.....73

Figure 3.7. The snow depth (a to e) and SCF (f to j) RMSE differences between the RA cases with a rule-based update and with default update.....74

Figure 3.8. Degradation of the RA performance due to: (a) incorrect relationships between the prior SWE (or snow depth) and T_B and (b) overestimation of both SWE (or snow depth) and T_B with a negative correlation between them. 76

Figure 3.9. The prior T_B RMSE of the RA cases with localization distances of 0.01, 0.03, 0.05, 0.07, 0.1, 0.15, 0.2, and 0.3 radians. The RMSE values were averaged over North America. The solid and hollow symbols represent the default and rule-based RA cases, respectively. The red triangle symbols denote the results of RA using the adaptive inflation and the localization distance of 0.01 radians, which are plotted slightly displaced laterally from their original position for clearness.....78

Figure 3.10. Maps of (a) snow classes and (b) land cover types over North America. Snow cover was classified into six classes (1: tundra, 2: taiga, 3: maritime, 4: ephemeral, 5: prairie, and 6: alpine) according to *Sturm et al.* [1995]. Land cover was classified into five groups (1: bare soil, 2: forest, 3: shrub, 4: grass, and 5: crop) using CLM4 plant functional types (PFTs). 79

Figure 3.11. Time series of snow depth (in meters) for land covers: (a) bare soil, (b) forest, (c) shrub, (d) grass, and (e) crop. The localization distance of 0.01 radians was used for the radiance assimilation (RA) cases. 82

Figure 4.1. Spatial distribution of the correlations between the SWE error and T_B error in February 2003 (where error = simulation – observation). The SWE error is calculated using the SWE estimates obtained by *Reichle et al.* [2011] from the CMC snow depth and climatological snow densities suggested by *Sturm et al.* [2010]. The T_B error is estimated using the AMSR-E T_B observations at 18.7 and 36.5 GHz vertical (V) and horizontal (H) polarization channels.....95

Figure 4.2. The snow depth RMSE (m) in the radiance assimilation (RA) experimental cases, using different snowpack RTMs (DMRT-ML and MEMLS) and assimilating different AMSR-E frequency channels, for North America. The horizontal dotted line represents the RMSE of the open-loop run (without assimilation).....98

Figure 4.3. Brightness temperature (T_B) at 10.65, 18.7, 23.8, 36.5, and 89 GHz vertical polarization channels estimated by (a) DMRT-ML and (b) MEMLS with varying snow depth (0.1 to 3 m). Other snow and soil physical properties were set as follows: snow grain radius=350 μm, snow temperature=270 K, snow density=300 kg m^{-3}, snow wetness=0 m^3 m^{-3}, soil temperature=270 K, and soil water content=0.1 m^3 m^{-3}. The snow stickiness in DMRT-ML was set to 0.2 and the exponential correlation length (p_{ex}) for MEMLS was calculated using equation (1). 99

Figure 4.4. Same as Figure 4.2 but for snow classes as defined in Sturm et al. (1995): (a) tundra, (b) taiga, (c) maritime, (d) ephemeral, (e) prairie, and (f) alpine.....102

Figure 4.5. Same as Figure 4.2 but for land cover types: (a) bare soil, (b) forest, (c) shrub, (d) grass, and (e) crop. 103

Figure 4.6. The snow depth RMSE (m) in the radiance assimilation (RA) experimental cases using different snowpack RTMs (DMRT-ML and MEMLS) and assimilating two frequency channels simultaneously (i.e., 18.7 and 23.8 GHz or 18.7 and 36.5 GHz) for North America. The vegetation single scattering albedo (ω) was neglected (in the D1823, D1836, M1823 and M1836 cases), was set to 0.064 (in the D1823(ω), D1836(ω), M1823(ω), and M1836(ω) cases), or was updated during the assimilation (in the D1823(ω_up), D1836(ω_up), M1823(ω_up), and M1836(ω_up) cases). The horizontal dotted line represents the RMSE of the open-loop run (without assimilation).....106

Figure 4.7. Same as Figure 4.6 but for snow classes as defined in Sturm et al. (1995): (a) tundra, (b) taiga, (c) maritime, (d) ephemeral, (e) prairie, and (f) alpine. 107

Figure 4.8. Same as Figure 4.6 but for land cover types: (a) bare soil, (b) forest, (c) shrub, (d) grass, and (e) crop. 108

Figure 4.9. The estimated (ensemble mean) vegetation transmissivity in the (a) D1823 and (b) M1823 cases. The values were averaged over two frequency channels (18.7 and 23.8 GHz vertical polarizations) during the assimilation period. 109

Figure 4.10. The ratio of the estimated (ensemble mean) $T_{B,v}$ (T_B emitted by the vegetation canopy) to the estimated (ensemble mean) $T_{B,TOA}$ (T_B at the top of the atmosphere) in the cases neglecting ω ((a) D1823 and (b) M1823) and in the cases considering ω ((c) D1823(ω) and (d) M1823(ω)). The values were averaged over two frequency channels (18.7 and 23.8 GHz vertical polarizations) during the assimilation period. 109

Figure 4.11. The estimated (ensemble mean) (a) snow water volume (10^3 km^3) and (b) snow cover area (10^6 km^2) in North America. 111

Figure 5.1. The improvement of the RA performance in estimating snow depth for (a) North America, (b) bare soil land cover, and (c) forest land cover by simultaneously updating all model physical states and parameters determining T_B based on a rule (RA_{rule}), by assimilating the best-performing frequency channels, i.e., 18.7 and 23.8 GHz (RA_{1823}), and by considering the vegetation single scattering albedo ($RA_{1823(\omega)}$). 117

Figure 5.2. T_B estimated by DMRT-ML for four- and five-layered snowpack with and without ice layer. 120

CHAPTER 1: Introduction

Snow cover modulates the Earth's surface energy and water fluxes, especially at northern mid and high latitudes, because of its optical (high albedo), thermal (low thermal conductivity), and hydrologic (water holding capacity) characteristics. Snow cover affects not only regional atmospheric conditions [*Chapin et al.*, 2005] but also large-scale circulation patterns, leading to long-range teleconnections [*Cohen and Entekhabi,* 1999]. One reason suggested for the recent acceleration of the Arctic sea ice loss is wind-driven sea ice circulation intensified by the Arctic Oscillation (AO) or the Northern Annular Mode/Northern Hemisphere Annular Mode (NAM) [*Nghiem et al.*, 2007; *Stroeve et al.*, 2007], which may be affected by the Siberian snow cover anomalies [*Gong et al.*, 2003]. Furthermore, because natural snowpacks form one of the world's most important freshwater reservoirs [*Lemke et al.*, 2007], an understanding of its spatial and temporal variations is crucial for climate studies and water management.

Methods for quantifying snowpack characteristics include ground based *in situ* measurement, remote sensing observations, and model simulations. Ground based *in situ* measurements provide the most accurate snow cover information but are limited in their ability to describe spatial and temporal variability of snowpack properties over large areas. Although remote sensing observations are expected to yield large-scale snowpack variations, they involve errors resulting from sensor and retrieval algorithms. Furthermore, they do not provide fine temporal resolution. Current state-of-the-art land surface models (LSMs) are capable of producing spatially and temporally continuous snow fields, but their results can have large uncertainties due to imperfect parameterizations (including unknown parameters) and inaccurate meteorological forcing (especially precipitation).

Data assimilation (DA) has emerged as a means to overcome the above-mentioned limitations because it merges observations with model estimates for the complementary use of both approaches. Snow DA using satellite products such as snow cover fraction (SCF) [e.g., *Rodell and Houser*, 2004; *Andreadis and Lettenmaier*, 2006; *Clark et al.*, 2006; *Su et al.*, 2008, 2010; *Zaitchik and Rodell*, 2009; *De Lannoy et al.*, 2012] and snow water equivalent (SWE) [e.g., *Sun et al.*, 2005; *Andreadis and Lettenmaier, 2006*; *Dong et al.*, 2007; *De Lannoy et al.*, 2012] has been studied extensively but several limitations render them suboptimal for continental-scale snow state estimation. When the ground is fully covered with snow (i.e., SCF is equal to 100% or is saturated), satellite SCF data cannot detect additional snow mass variations, which makes SCF assimilation appropriate only for ephemeral snowpack [*Rodell and Houser*, 2004; *Clark et al.*, 2006; *Su et al.*, 2010; *De Lannoy et al.*, 2012]. *Andreadis and Lettenmaier* [2006] have shown that SCF assimilation has almost no effect during snow accumulation when SCF is usually 100%, whereas the improvement is evident for snowmelt periods when snow coverage is partial. Furthermore, the proper assimilation increment (quantity of SWE to be added during a SCF update) cannot be known from the SCF observation alone, a deficiency that *Zaitchik and Rodell* [2009] attempted to address using the model's forcing data.

It has been demonstrated that the Advanced Microwave Scanning Radiometer–Earth Observing System (AMSR-E) SWE product is degraded by microwave signal saturation over moderately deep snowpack (i.e., SWE exceeding the 100-mm threshold) [*Dong et al.*, 2007]. In general, SWE is retrieved using empirical equations based on the difference in scattering properties of brightness temperatures (T_B) at 18 and 37 GHz horizontal polarization channels [e.g., *Chang et al.*, 1987; *Foster et al.*, 2005]. The emitted radiation is more readily scattered by the snow at higher frequencies (i.e., 36–37

GHz) than at lower frequencies (i.e., 18–19 GHz) [*Chang et al.*, 1987]. Due to the fact that the microwave signal at 36–37 GHz saturates at depths greater than approximately 1 m [*Foster et al.*, 2005], several studies [e.g., *Andreadis and Lettenmaier*, 2006; *De Lannoy et al.*, 2012; *Dong et al.*, 2007] have shown that assimilating SWE retrievals can provide improvements only for shallow snowpacks. For the same reason, the assimilation of passive microwave retrieved SWE cannot reproduce the interannual variability of SWE for deep snowpack regions [*De Lannoy et al.*, 2012].

Several previous studies have suggested that radiance assimilation (RA), which incorporates microwave brightness temperature (T_B) observations directly into LSMs, shows promise for improving SWE estimates compared to the assimilation of T_B-based SWE retrievals at the point scale [e.g., *Durand et al.*, 2009; *Toure et al.*, 2011], mesoscale [e.g., *Durand and Margulis*, 2007], and basin scale [e.g., *Dechant and Moradkhani*, 2011]. *Durand and Margulis* [2006] conducted a point-scale synthetic test, in which they demonstrated that RA can recover the true SWE and addressed the relative contributions of microwave frequency channels to correcting the SWE estimates in the RA scheme. In their follow-on study [i.e., *Durand and Margulis*, 2007], they also performed the mesoscale synthetic RA experiments and showed that RA can be an alternative to existing retrieval algorithms [e.g., *Foster et al.*, 2005], which have limitations with respect to the characterization of SWE exceeding the 100-mm threshold [*Dong et al.*, 2007]. *Durand et al.*, [2009], a point-scale snow RA study, assimilated (ground-based) real microwave radiance observations and demonstrated that SWE estimated by the RA scheme is more accurate than that estimated by an empirical retrieval algorithm. Using the same data set, *Toure et al.* [2011] showed that the additional use of horizontally polarized T_B with a more elaborated representation of snowpack stratigraphy further enhances the snow RA performance. *Dechant and*

Moradkhani [2011] successfully applied the RA method to the basin-scale SWE estimates and subsequent operational streamflow forecasts. However, continental-scale applications of RA require a substantial amount of further research because of various snow and vegetation cover conditions in the continental domain.

The primary objective of this dissertation is to develop an advanced RA system to improve snow water storage estimates at the continental scale. This dissertation addresses the following research questions:

(a) Is the RA method applicable to continental-scale snow water storage estimations?

(b) Which error characteristics of estimated snow physical properties and brightness temperature (T_B) impede continental-scale applications of the RA method?

(c) Can the effect of these error sources be mitigated in the RA system?

(d) How to improve the performance of the RA system in characterizing snow under the vegetation canopy?

In Chapter 2, an analysis of error characteristics of coupled land surface–radiative transfer models is conducted for a successful RA study. The chapter focuses on the Community Land Model version 4 (CLM4) [*Oleson et al.*, 2010; *Lawrence et al.*, 2011] as the land surface model, and the Microwave Emission Model for Layered Snowpacks (MEMLS) [*Wiesmann and Mätzler*, 1999] and the Dense Media Radiative Transfer–Multi Layers model (DMRT-ML) [*Picard et al.*, 2013] as radiative transfer models (RTMs). The analysis is conducted at point scale (without considering the vegetation effect) and mesoscale (considering the vegetation effect) using *in situ* measurements. The synthetic experiments are additionally carried out for shallow and deep snowpack conditions.

Chapter 3 addresses continental-scale applications of the RA method to estimate snow water storage. Two hypotheses are established based the results in Chapter 2: 1) the simultaneous update of model states and parameters can improve snow estimation by minimizing the effects of their errors on the T_B error; and 2) updating states and parameters based on a rule, the degradation of RA performance, which is attributed to incorrect relationships between the prior SWE (or snow depth) and T_B, can be managed. A series of experiments are conducted to demonstrate the feasibility of RA to improve snow estimates at the continental scale.

Chapter 4 presents an improvement of the RA system in estimating snow across snow classes and land cover types in North America by addressing three research questions related to microwave frequency channels, snowpack RTMs, and vegetation single scattering albedo. The enhanced continental-scale snow estimates are achieved for vegetated areas, especially for densely forested areas, by assimilating the best-performing frequency channels and by better representing the contribution of the vegetation canopy to brightness temperature at the top of the atmosphere.

Chapter 5 summarizes the key findings obtained in this dissertation and suggests further works that need to be addressed in future studies.

CHAPTER 2: Error characterization of coupled land surface–radiative transfer models for snow microwave radiance assimilation[1]

2.1 ABSTRACT

Snow microwave radiance assimilation (RA) or brightness temperature data assimilation has shown promise for improving snow water equivalent (SWE) estimation. A successful RA study requires, however, an analysis of error characteristics of coupled land surface–radiative transfer models. This study focuses on the Community Land Model version 4 (CLM4) as the land surface model, and the Microwave Emission Model for Layered Snowpacks (MEMLS) and the Dense Media Radiative Transfer–Multi Layers model (DMRT-ML) as radiative transfer models (RTMs). Using the NASA Cold Land Processes Field Experiment (CLPX) datasets and through synthetic experiments, the errors of the coupled CLM4/DMRT-ML and CLM4/MEMLS are characterized by: a) evaluating the CLM4 snowpack state simulations, b) assessing the RTMs performance in simulating brightness temperature (T_B), and c) analyzing the correlations between SWE error (ε_SWE) and T_B error (ε_T_B) from the RA perspective. The results using the CLPX datasets show that given a large error of snow grain radius (ε_r_e) under dry snowpack conditions (along with a small error of snow temperature (ε_T_{snow})), the correlations between ε_SWE and ε_T_B are mainly determined by the relationship between ε_r_e and snow depth error (ε_d_{snow}) or snow density error (ε_ρ_{snow}). The synthetic experiments were carried out for the CLPX region (shallow snowpack conditions) and Rocky Mountains (deep snowpack conditions) using the atmospheric ensemble reanalysis

[1]This chapter was previously published in Kwon, Y., A. M. Toure, Z.-L. Yang, M. Rodell, and G. Picard (2015), Error characterization of coupled land surface–radiative transfer models for snow microwave radiance assimilation, *IEEE Trans. Geosci. Remote Sens.*, 53, 5247–5268, doi:10.1109/TGRS.2015.2419977. Y. Kwon designed and performed research, and wrote the paper; A. M. Toure prepared part of the data and contributed to analyzing the data; Z.-L. Yang contributed to research design, discussions, and revisions; and M. Rodell and G. Picard contributed to discussions and revisions.

produced by the coupled Data Assimilation Research Testbed (DART)/Community Atmospheric Model (CAM4). The synthetic experiments support the results from the CLPX datasets and additionally show that errors of soil (water content and temperature), snow wetness, and snow temperature mostly result in positive correlations between ε_SWE and ε_T_B. CLM4/DMRT-ML and CLM4/MEMLS tend to produce different RA performances, with more positive and negative correlations between ε_SWE and ε_T_B, respectively. These results suggest the necessity of using multiple snowpack RTMs in RA to improve the SWE estimation at the continental scale. The results in this study also show that the magnitude of ε_r_e and its relationship to ε_SWE are important for RA performance. Most of the SWE estimations in RA are improved when ε_SWE and ε_r_e show a high positive correlation (greater than 0.5).

2.2 INTRODUCTION

For RA, the RTM should be incorporated into a DA system as an observational operator predicting T_B. Therefore, the quality of the assimilation results will be impacted by the uncertainty of the RTM [*Tedesco and Kim*, 2006; *Durand et al.*, 2008] as well as the LSM. Several published RTMs for snowpack have been developed by different groups and used in RA schemes. However, due to their differing sensitivities to snow properties that determine T_B of snowpack, the models show a large variability in simulated T_B for various snow conditions, as demonstrated in [*Tedesco and Kim*, 2006].

Using only one snowpack RTM, previous RA studies were able to achieve promising improvements in estimating SWE or snow depth at the point or local scales; however, the use of only a single RTM may have limitations for continental-scale RA. Snowpack physical properties, such as snow texture, stratigraphy, and crystal morphology, are closely related to local climate conditions [*Sturm et al.*, 1995]; therefore,

various snow conditions can be found in the continental domain. However, no particular existing snowpack RTM can accurately reproduce the observed T_B for all snow conditions [*Tedesco and Kim*, 2006]. Consequently, the use of multiple snowpack RTMs (i.e., multi-RTM ensemble RA) that are based on different theories may reduce errors related to RTM uncertainties for continental-scale SWE estimations.

An understanding of errors in the coupled LSM/RTMs is essential for a successful RA study. Therefore, as a preliminary study for multi-RTM ensemble RA, our goal is to analyze the error characteristics of two coupled LSM/RTMs. Here we used the Community Land Model version 4 (CLM4) [*Oleson et al.*, 2010] and two snowpack RTMs, the Microwave Emission Model for Layered Snowpacks (MEMLS) [*Wiesmann and Mätzler*, 1999] and the Dense Media Radiative Transfer–Multi Layers model (DMRT-ML) [*Picard et al.*, 2013] that simulate T_B of a multi-layered snowpack.

Our error characterizations involved: a) evaluating the CLM4 snowpack state simulations, b) assessing the RTMs performance in simulating T_B, and c) analyzing the relationships between SWE error (ε_SWE) and T_B error (ε_T_B). The importance of the performance of LSMs (or snow models) in RA has been emphasized in previous studies [e.g., *Durand et al.*, 2008]. In this study, we focused more on addressing the differences between the snowpack RTMs given the errors of the simulated snowpack states in the LSM. Using in situ snowpit, T_B, and meteorological data collected during the NASA Cold Land Processes Field Experiment (CLPX), we characterized the errors over a small clearing within the Local Scale Observation Site (LSOS) (point-scale analysis without considering the vegetation effect) and the Meso-cell Study Areas (MSAs) (mesoscale analysis considering the vegetation effect). Continental-scale (or larger) error characterizations were not conducted in this study because snowpit observations (e.g., snow depth, density, temperature, wetness (liquid water content within the snowpack),

and grain size) required for the analyses were unavailable. To support the results from the CLPX datasets, we additionally carried out synthetic experiments in which the correlations between ε_SWE and ε_T_B were analyzed for shallow and deep snowpack conditions from the RA perspective.

For the same study areas, *Andreadis et al.* [2008] analyzed the error characteristics of their coupled model, the Variable Infiltration Capacity (VIC) [*Liang et al.*, 1994] model and DMRT, based on a single snow layer representation. *Brucker et al.* [2011] simulated hourly snowpack T_B in southern Quebec, Canada using the snow evolution model Crocus [*Brun et al.*, 1992] and MEMLS and interpreted their results at the local scale. Unlike these previous studies that focused on one snowpack RTM, we used two coupled models, CLM4/DMRT-ML and CLM4/MEMLS, and performed different analyses as the first step toward multi-RTM ensemble RA for improved continental-scale SWE estimation.

In the following section, we describe the datasets (snowpit, T_B, and meteorological data) and models (LSM and RTMs) used in this research. In section 2.4, we analyze the performance of the coupled models in simulating snowpack states and T_B and we discuss the relationships between ε_SWE and ε_T_B. Conclusions are provided in section 2.5.

2.3 METHODS

2.3.1 CLPX data

For point-scale and mesoscale experiments, we used in situ snowpit, T_B, and meteorological data collected during CLPX (see http://nsidc.org/data/clpx). The Small Regional Study Area (SRSA) of CLPX had three MSAs: the North Park, Rabbit Ears, and

Fraser MSA (Figure 2.1). The Fraser MSA included the LSOS and each MSA involved three Intensive Study Areas (ISAs): 1) the St. Louis Creek, Fool Creek, and Alpine ISAs within the Fraser MSA; 2) the Spring Creek, Buffalo Pass, and Walton Creek ISAs within the Rabbit Ears MSA; and 3) the Illinois River, Potter Creek, and Michigan River ISAs within the North Park MSA. Measurements were made in mid-winter (February) and early spring (March) to coincide with dry and wet periods, respectively. Four Intensive Observation Periods (IOPs) were conducted in 2002 (IOP1 and IOP2) and 2003 (IOP3 and IOP4).

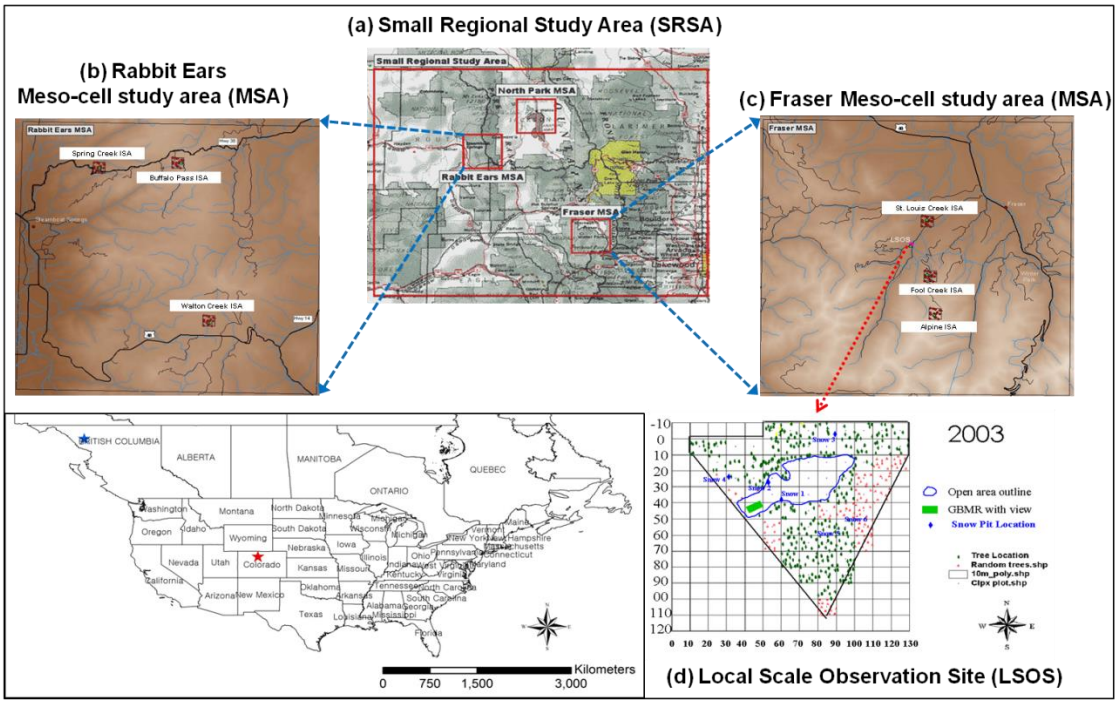

Figure 2.1. Maps of the NASA CLPX Small Regional Study Area (SRSA), the Rabbit Ears and Fraser Meso-cell study areas (MSAs), and the Local Scale Observation Site (LSOS). Figures from the National Snow and Ice Data Center (NSIDC) website (http://nsidc.org/data/clpx/clpx_pits.html and http://nsidc.org/data/docs/daac/nsidc0169_clpx_lsos_snow/). Red and blue stars indicate the locations of the CLPX region and Rocky Mountains, respectively, where the synthetic experiments were conducted.

In situ snowpit data include snowpack stratigraphy, density, temperature, grain size, and wetness. These data were collected from 16 snowpits in each ISA [*Cline et al.*, 2002] and six snowpits in the LSOS [*Cline et al.*, 2003]. The snow grain size measured in CLPX snowpits was the maximum extent of the intermediate grain size, which can be converted to the exponential correlation length (defined by *Mätzler* [2002]) on the basis of an empirical relationship suggested by *Durand et al.* [2008], as follows:

$$p_{ex} = \begin{cases} a_0 + a_1 \ln D_{\max}, & f_v > 0.2 \, and \\ & D_{\max} > 0.125 mm \\ p_0, & otherwise \end{cases} \quad (2.1)$$

where $D_{\max}$ is the maximum extent of the intermediate grain size (mm), p_{ex} is the exponential correlation length (mm), a_0, a_1 and p_0 are 0.18, 0.09 and 0.05 mm [*Durand et al.*, 2008], respectively, and f_v is the volume fraction (snow density divided by ice density).

Microwave measurements at 18.7, 23.8, 36.5, and 89 GHz vertical (V) and horizontal (H) polarization channels were made using the University of Tokyo's Ground-Based Microwave Radiometer (GBMR-7) installed in a small clearing within the LSOS [*Graf et al.*, 2003]. Airborne multi-band polarimetric T_B observations were carried out over MSAs during IOP1, IOP3, and IOP4 using a Polarimetric Scanning Radiometer (PSR/A) [*Stankov and Gasiewski*, 2004]. Meteorological data including air temperature, relative humidity, wind speed, precipitation, and downward short-wave radiation were observed at 11 sites throughout the SRSA. Among them, nine meteorological towers were located near the center of each ISA [*Elder and Goodbody*, 2004] and the other two were located close to the LSOS [*Elder and Goodbody*, 2004] and in the GBMR-7 location [*Graf et al.*, 2003], respectively.

For the point-scale analysis without considering the vegetation effect, LSOS in situ snowpit and GBMR-7 T_B data collected during IOP3 (19–25 February 2003), the same datasets used in *Durand et al.* [2008, 2009] and *Toure et al.* [2011], were used. To exclude the effect of vegetation, snow data from only two snowpits (snowpit #1 and #2) located in a small clearing within the LSOS were used. Meteorological data collected near the GBMR-7 location were used to force CLM4.

For the mesoscale analysis considering the vegetation effect, ISA in situ snowpit and the Advanced Microwave Scanning Radiometer–Earth Observing System (AMSR-E) T_B observations were used. For these datasets to be usable, snowpit and T_B data should be available for the same dates. However, only one day (21 February 2002) of both ISA snowpit and PSR/A data was available over the North Park MSA, while datasets for four days (23 February 2002, 24–25 February and 30 March 2003) were available for the Rabbit Ears MSA. Meanwhile, no ISA snowpit and PSR/A T_B data were collected during the same period for the Fraser MSA. Therefore, we used AMSR-E T_B data, which covered the period from 1 February to 31 May 2003 [*Elder and Goodbody*, 2004], instead of PSR/A data to have more data points for the analysis, although AMSR-E data have a coarser spatial resolution. The original AMSR-E T_B data (25 km × 25 km resolution) were resampled to the spatial resolution (1 km × 1 km resolution) of ISAs. Snow data from 16 snowpits within each ISA were averaged. The North Park MSA was excluded from the analysis because the quality of snow data is not good. ISA meteorological tower data were used to force CLM4 for each ISA, except for precipitation; due to the lack of precipitation data for ISAs, GBMR-7 precipitation data were used.

2.3.2 Land surface model

In this study, we used CLM4 [*Oleson et al.*, 2010] to simulate snow dynamics. CLM4 is forced by air temperature, humidity, atmospheric pressure, wind speed, precipitation, and downward short-wave radiation. In CLM4, the snow/soil column is composed of 15 soil layers, up to five snow layers (depending on snowpack depth), and one vegetation layer. CLM4 calculates soil temperature for all soil layers but only the top 10 layers are subject to hydrologic calculations.

CLM4 is advantageous for snow RA because it represents a snowpack with multiple layers and is capable of simulating snow thermodynamics such as melt-refreeze cycles and densification processes. All these stratigraphic details about snow are needed as input for the RTMs.

In CLM4, the effective snow grain radius is defined as follows:

$$r_e = \frac{3}{\rho_{ice} SSA} \tag{2.2}$$

where r_e is the effective grain radius (m), ρ_{ice} is the ice density (=917 kg m^{-3}), and *SSA* is the specific surface area (m^2 kg^{-1}). Evolution of r_e is represented as follows [*Oleson et al.*, 2010]:

$$r_e(t) = \left[r_e(t-1) + dr_{e,dry} + dr_{e,wet}\right] f_{old} + r_{e,0} f_{new} + r_{e,rf} f_{rf} \tag{2.3}$$

where $dr_{e,dry}$ and $dr_{e,wet}$ are r_e changes by dry snow and liquid water-induced metamorphism, which are calculated based on *Flanner and Zender* [2006] and *Brun* [1989], respectively; $r_{e,0}$ and $r_{e,rfz}$ are the effective radius of freshly-fallen snow (=54.5 μm) and refrozen liquid water (=1000 μm), respectively; f_{old}, f_{new}, and f_{rfz} are the fractions

of snow from the previous time step t–1, freshly-fallen snow, and refrozen liquid water, respectively. When snow layers are combined or subdivided depending on the layer thickness, r_e is recalculated by the mass-weighted average of the two layers.

2.3.3 Radiative transfer model

Microwave T_B measured by satellite at the top of the atmosphere (TOA) is a mixture of microwave signals from snowpack, soil, vegetation, atmosphere, and space. T_B at the TOA can be estimated as follows [*Durand and Margulis*, 2007]:

$$T_{B,TOA} = \left[\{1 + (t_c - 1)V_c\}T_{B,sn} + V_c(1 - t_c)T_c\right]t_a + T_{B,a} \tag{2.4}$$

where $T_{B,TOA}$ is the brightness temperature at the TOA (K); t_c and t_a are the transmissivities of the vegetation canopy and atmosphere, respectively; V_c is the vegetation fraction covering the grid cells; $T_{B,sn}$ is the snowpack brightness temperature (K) (it includes T_B emitted from the underlying soil), which is simulated by DMRT-ML or MEMLS; T_c is the physical temperature of the vegetation (K); and $T_{B,a}$ is the atmospheric brightness temperature (K).

To predict the upwelling brightness temperature from the snowpack ($T_{B,sn}$), DMRT-ML and MEMLS require the boundary condition brightness temperature ($T_{B,BC}$), which is the combination of downwelling radiative fluxes emitted from space, atmosphere, and vegetation. $T_{B,BC}$ is calculated according to the method suggested by Durand and Margulis [*Durand and Margulis*, 2007]:

$$T_{B,BC} = \{1 + (t_c - 1)V_c\}(T_{B,sp}t_a + T_{B,a}) + V_c(1 - t_c)T_c \tag{2.5}$$

where $T_{B,sp}$ is the space brightness temperature (=2.7 K). In equations (2.4) and (2.5), multiple reflections between vegetation canopy and snowpack are neglected.

DMRT-ML [*Picard et al.*, 2013] estimates T_B of a layered snowpack based on the Dense Media Radiative Transfer (DMRT) theory [*Tsang and Kong*, 2001]. In this model, snow grains are assumed to be ice spheres and each snow layer is represented by layer thickness, density, temperature, snow grain radius, and wetness. The microwave scattering and absorption coefficients of snowpack are modeled based on the DMRT theory. This model considers multiple scattering between the layers and employs the discrete ordinate radiative transfer (DISORT) method [*Jin*, 1994] to calculate the microwave emission and propagation for 32 streams (directions). DMRT-ML can be applied to a frequency range of 1 to 200 GHz. To consider the contribution of the underlying soil to the microwave emission, we used the rough bare soil reflectivity model suggested by *Wegmüller and Mätzler* [1999] in DMRT-ML.

MEMLS [*Wiesmann and Mätzler*, 1999] also simulates T_B of a multi-layered snowpack; however, it is based on radiative transfer theory. Like DMRT-ML, each snow layer in MEMLS is characterized by layer thickness, density, temperature, snow grain size, and wetness; however, the grain size is represented by an exponential correlation length that depends on grain size and snow density. Multiple volume scattering, absorption, and the consequent propagation through the snowpack are modeled based on the six-flux theory. As suggested in *Mätzler and Wiesmann* [1999], we used the improved Born approximation [*Mätzler*, 1998] to calculate the extinction coefficient (sum of the scattering and absorption coefficients). MEMLS can be applied to a frequency range of 5 to 100 GHz and a correlation length range of 0.05 to 0.6 mm. For the reflectivity of the underlying soil, the same soil model [*Wegmüller and Mätzler*, 1999] and the same permittivity values in DMRT-ML were used for MEMLS.

DMRT-ML has a tunable stickiness parameter [*Ding et al.*, 2001] that affects the extinction coefficient because it determines the degree of particle clustering and thus is related to the size of the scatterers. However, a realistic stickiness value is not easily obtained from snow microstructure images, field measurements, or model simulations [*Picard et al.*, 2013]. The sensitivity analysis by *Picard et al.* [2013] shows that the scattering coefficient increases as the stickiness value decreases. Lower stickiness parameter values lead to stronger attractions between snow grains (i.e., greater clustering effect); in addition, snow density at which the maximum scattering coefficient appears is influenced by stickiness values. *Tsang et al.* [2008] suggest using 0.1 for the stickiness parameter while *Mätzler* [1998] suggests using 0.2; *Andreadis and Lettenmaier* [2012] use a stickiness value of 0.1 for the CLPX LSOS but a stickiness value of 0.2 for the Arctic regions. In this study, we optimized the stickiness parameter using *in situ* snowpit and GBMR-7 T_B data collected in the LSOS.

MEMLS does not have tunable parameters except that it uses an exponential correlation length to represent the grain size, whereas DMRT-ML and CLM4 use an effective grain radius. According to *Debye et al.* [1957] and *Mätzler* [2002], the exponential correlation length is given by

$$p_{ex} = \frac{3}{4} p_c = \frac{3(1 - f_v)}{\rho_{ice} SSA} \tag{2.6}$$

where p_{ex} is the exponential correlation length (m) and p_c is the correlation length (m). From equations (2.2) and (2.6), the relationship between p_{ex} and r_e is obtained as follows:

$$p_{ex} = r_e(1 - f_v) = r_e\left(1 - \frac{\rho}{\rho_{ice}}\right) \tag{2.7}$$

where ρ is the snow density (kg m^{-3}).

In this study, the atmosphere is assumed to be clear-sky and is modeled using the atmospheric RTM suggested by *Ulaby et al.* [1981] as used in *Durand and Margulis* [2007]. Vegetation transmissivity is estimated from the vegetation optical depth (τ_c) [*Schmugge and Jackson*, 1992], which is calculated using an empirical equation by *Jackson and Schmugge* [1992]:

$$t_c = \exp(-\tau_c) \tag{2.8}$$

$$\tau_c = b' \lambda^x w_c / \cos\theta \tag{2.9}$$

where λ is the wavelength (cm), w_c is the vegetation water content (kg m^{-2}), θ is the incident angle, and b' and x are empirical parameters depending on the vegetation canopy structure. Vegetation water content can be estimated from the leaf area index (LAI) [*Paloscia and Pampaloni*, 1988]:

$$w_c = \exp(LAI / 3.3) - 1. \tag{2.10}$$

2.3.4 Model parameter optimization

Each analysis was preceded by model parameter optimization (snow stickiness in DMRT-ML and empirical parameters in vegetation RTM) using observed datasets. To optimize the stickiness parameter, DMRT-ML was forced by the LSOS *in situ* snowpit measurements and the simulated T_B was compared to the GBMR-7 T_B observations. For DMRT-ML grain size information, the measured D_{max} values were converted to the effective grain radius (r_e) using equations (2.1) and (2.7). Stickiness optimization was

conducted for four frequency channels (i.e., 18.7 and 36.5 GHz V and H polarizations) by minimizing the root mean square error (RMSE).

To estimate the contribution of the underlying soil, DMRT-ML needs soil information such as sand and clay fractions, soil temperature, volumetric soil water content, and roughness length. We used 0.39 and 0.22 for sand and clay fractions, respectively, which were obtained from the surface input dataset provided in CLM4. As in *Durand et al.* [2008], soil temperature was assumed to be the same as snow bottom layer temperature. Since volumetric soil water content simulated by CLM4 for this area was about 0.1 throughout the simulation period, we set it to a constant value of 0.1, whereas *Durand et al.* [2008] used 0.12. For the surface roughness length, we used 0.01 m.

Vegetation RTM used in this study has two empirical parameters (b' and x in equation (2.9)), which depend on the vegetation canopy structure. It has been reported that the Rabbit Ears MSA consists of dense coniferous forest, moderate-density deciduous forest, and meadow while the Fraser MSA is composed of moderate-density coniferous forest and alpine tundra (see http://www.nohrsc.nws.gov/~cline/clp/Field_exp/clpx_plan/tables/CLPX_plan_table9.html). However, because we do not have exact information about vegetation canopy properties for these MSAs, vegetation variables required for estimating the vegetation effect on T_B were provided by CLM4 simulation (LAI and physical temperature of the vegetation) and surface input dataset (vegetated area fraction in grid cells). Therefore, we optimized b' and x to minimize the error caused by inaccurate vegetation information. For optimization, we used *in situ* snowpit and AMSR-E T_B datasets collected over ISAs within the Fraser and Rabbit Ears MSAs. The optimization was conducted on a MSA basis for 18.7 and 36.5 GHz channels by

minimizing the RMSE; the same parameter values were used for all ISAs within the same MSA.

2.3.5 Synthetic experiments

An 80-member ensemble atmospheric reanalysis [*Raeder et al.,* 2012], which has a physical consistency between forcing fields, has been produced by the coupled Data Assimilation Research Testbed (DART) [*Anderson et al.,* 2009]/Community Atmospheric Model (CAM4) [*Gent, et al.*, 2011]. As used in [*Zhang et al.*, 2014], among 80 forcing members, 40 randomly chosen ensemble members were used for the synthetic experiments to consider a compromise between the performance and computational efficiency of the DA scheme.

The experiments were conducted for the CLPX region and Rocky Mountains (marked with red and blue stars, respectively, in Figure 2.1) during 2003. CLM4 simulations using the DART/CAM4 atmospheric ensemble reanalysis showed that the snowpack is shallow over the CLPX region and relatively deep over the Rocky Mountains (the maximum ensemble mean snow depth was 0.098 m and 0.581 m, respectively). For the synthetic experiments, the first member of the 40 ensemble members was assumed to be a synthetic truth and the remaining 39 ensemble members were used for ensemble model simulations. Four microwave frequency channels (18.7 and 36.5 GHz V and H polarizations) were used in the analysis. To analyze the relationship between the correlations (between ε_SWE and ε_T_B) and RA performance, we did a simple RA test in which the ensemble Kalman filter (EnKF) method [*Evensen*, 1994] was used and the synthetic truth of T_B was assumed to be perfect (i.e., no observation error).

2.4 RESULTS AND DISCUSSION

In this section, we present the error characterization results of two coupled models: CLM4/DMRT-ML and CLM4/MEMLS. As previously mentioned, the analyses were carried out at point scale and mesoscale; the vegetation effect was considered for the mesoscale error characterization but not at the point scale. The results of the synthetic experiments were analyzed with respect to the effects of errors of snow grain radius (ε_r_e), snow wetness (ε_W_{snow}), snow temperature (ε_T_{snow}), and soil (water content and temperature) (ε_WT_{soil}) on the relationships between ε_SWE and ε_T_B, and subsequent RA performance.

2.4.1 Point-scale error characterization: CLPX LSOS (non-vegetated case)

1) Optimization of the DMRT-ML Stickiness Parameter: From optimization, the stickiness parameter was determined to be 0.17. RMSE and the mean bias error (MBE) for each of the frequency channels are summarized in Table 2.1. The simulated T_B using the stickiness parameter of 0.17 agrees well with the observations; RMSE ranges from 2.3 to 10.6 K and MBE ranges from −0.1 to 6.5 (Table 2.1). Although each snowpack layer can have a different stickiness value, we assumed in this study that all layers have the same stickiness parameter values due to the difficulty of optimization for all snowpack layers.

Table 2.1. DMRT-ML stickiness parameter optimization results using *in situ* snowpit and ground-based T_B data collected within the LSOS (RMSE: Root Mean Square Error, MBE: Mean Bias Error). The optimal stickiness parameter value was determined to be 0.17.

	18.7 GHz		36.5 GHz	
	T_BV	T_BH	T_BV	T_BH
RMSE (K)	2.3	7.3	9.5	10.6
MBE (K)	-0.1	6.5	2.8	5.7

Brucker et al. [2011] and *Roy et al.* [2013] demonstrated that the snow grain radius in equation (2.2) is not the effective grain radius in DMRT-ML and thus introduced a tunable scaling factor (ϕ) to minimize the difference between the simulated and observed T_B:

$$r_e = \frac{3}{\rho_{ice} SSA} \phi \tag{2.11}$$

From calibrations, they obtained scaling factor values much greater than unity (2.85 in *Brucker et al.* [2011] and 3.3 in *Roy et al.* [2013]) without considering the stickiness. *Brucker et al.* [2011] suggest that their large scaling factor could be attributed to three possible reasons: stickiness (cohesion between snow grains), snow grain size distribution (heterogeneity of snow grain size), and grain shape. *Roy et al.* [2013] provides detailed discussions of the effect of the stickiness and grain size distribution on the scaling factor. However, a physically robust basis for the scaling factor and its reasonable range have not yet been established, although *Roy et al.* [2013] have made a qualitative analysis of the scaling factor. Therefore, in this study, we optimized the stickiness parameter without the use of the scaling factor. *Roy et al.* [2013] showed that when both the scaling factor and stickiness parameter were optimized, they achieved the minimum RMSE using a scaling factor of 2.6 and a stickiness of 0.44. This stickiness value is somewhat greater than the 0.17 obtained here. This implies that other significant factors, including grain shape and the size distribution of sticky spheres as *Brucker et al.* [2011] and *Roy et al.* [2013] emphasized, must be explicitly addressed in DMRT-ML for more accurate T_B predictions. However, since this topic is outside the scope of this paper and the stickiness value of 0.17 is within the range of values (from 0.1 to 0.2) suggested by previous studies

[e.g., *Mätzler*, 1998; *Tsang et al.*, 2008; *Andreadis and Lettenmaier*, 2012], we concluded that the stickiness of 0.17 could be reasonably used in this study.

2) SWE and T_B Simulations by the Coupled Models: SWE and T_B for a small clearing within the LSOS were simulated by the coupled CLM4/DMRT-ML and CLM4/MEMLS for seven days (19–25 February 2003) when snowpit and GBMR-7 T_B data were available. CLM4 was forced by GBMR-7 meteorological data and the simulated SWE was compared to the LSOS *in situ* snowpit measurements (Figure 2.2a). The simulated SWE showed fairly good agreement with the observations (RMSE = 16 mm; MBE = –2.5 mm).

However, CLM4 simulations for snowpack characteristics such as snow depth, density, grain radius, and temperature, all of which determine T_B of snowpack, showed some errors as indicated by normalized errors (=(simulation – observation)/observation) in Figure 2.2b. To calculate the normalized errors, snow layer thickness was summed and snow density, grain radius, and temperature were averaged (weighted by snow layer thickness) over all snow layers. Because both simulations and observations showed dry snowpack conditions during the simulation period, the results of snow wetness were not indicated in the figure. Figure 2.2b shows that grain radius was greatly overestimated while snow depth and density were slightly underestimated and overestimated, respectively; snow temperature bias was very small. Since in CLM4 snow density is estimated by dividing SWE (kg m^{-2}) by snow depth (m), we see that the overestimation of snow density was caused primarily by the underestimation of snow depth.

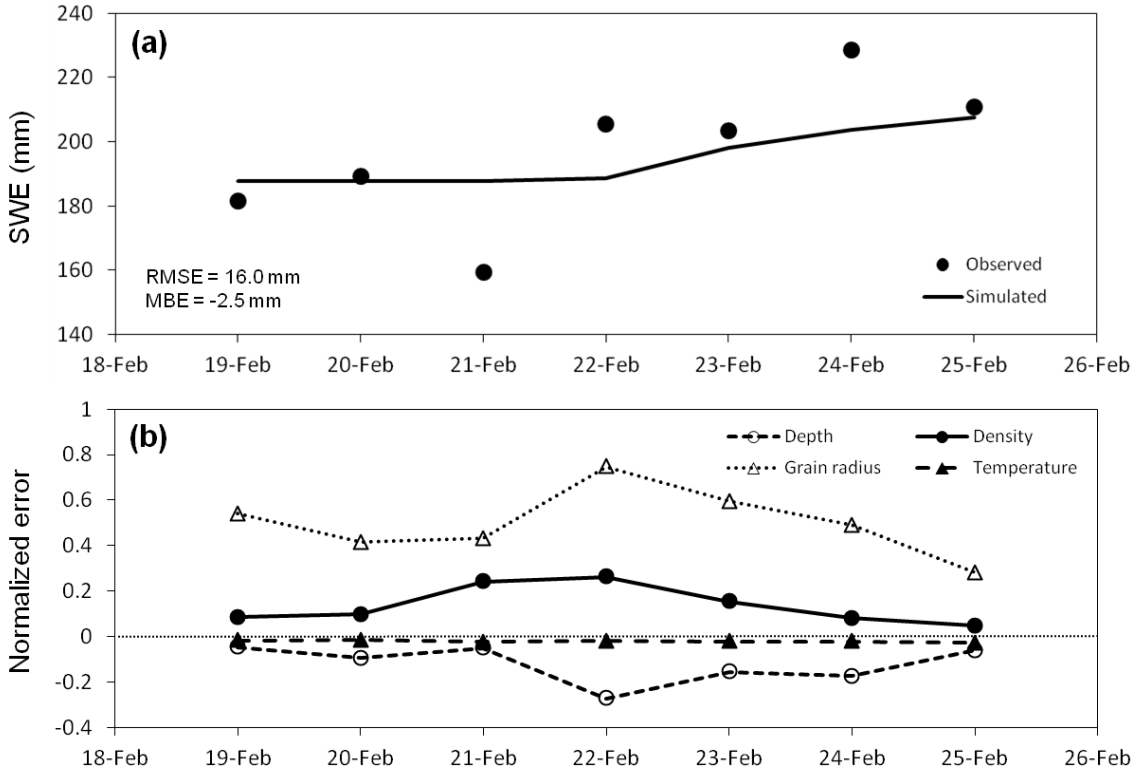

Figure 2.2. CLM4 simulation results for the LSOS: (a) SWE and (b) normalized errors (=(simulation – observation)/observation) of snow depth, density, grain radius, and temperature.

Brightness temperatures at 18.7 and 36.5 GHz V and H polarization channels were predicted by DMRT-ML and MEMLS using simulated snowpack physical properties and were compared with the GBMR-7 T_B observations (Figure 2.3 and Table 2.2). Two snowpack RTMs showed similar performance; DMRT-ML showed slightly better performance, except for 18.7 GHz H polarization channel (18.7-H). Simulation errors of both models were the smallest for 18.7 GHz V polarization channel (18.7-V), whereas they were relatively large for 36.5 GHz channels (Table 2.2), which may be attributed to the large error of snow grain radius because microwave emission at a higher frequency is more affected by snow grain size than at a lower frequency.

Table 2.2. Errors of T_B simulations by the coupled CLM4/DMRT-ML and CLM4/MEMLS for the LSOS.

	CLM4/DMRT-ML				CLM4/MEMLS			
	18.7 GHz		36.5 GHz		18.7 GHz		36.5 GHz	
	T_BV	T_BH	T_BV	T_BH	T_BV	T_BH	T_BV	T_BH
RMSE (K)	1.9	14.9	29.0	19.3	9.9	10.2	39.8	20.5
MBE (K)	-0.6	14.5	-28.9	-19.1	-9.8	9.7	-39.7	-20.4

3) The Relationship Between ε_SWE and ε_T_B: In RA using the EnKF, update of a prior (e.g., SWE simulated by a LSM) is based on the assumption that ε_SWE is correlated to ε_T_B. Therefore, to address the feasibility of the coupled models to properly update SWE in the RA scheme, it is necessary to analyze the relationship between ε_SWE and ε_T_B.

Figure 2.4 shows the relationship between ε_SWE and ε_T_B for the LSOS. For this study area, we did not observe any significant correlation between ε_SWE and ε_T_B; this may be attributed to the effect of ε_r_e. Snow depth error (ε_d_{snow}) and ε_SWE determined snow density error (ε_ρ_{snow}) while ε_T_B was mainly determined by snow density, depth, and grain size for this area; therefore, we analyzed the results by focusing on errors of these three snow physical properties (i.e., snow density, depth, and grain radius). Based on a sensitivity test (not shown here), T_B is positively sensitive to snow density and negatively sensitive to snow depth and grain radius. Because ε_SWE was more correlated to ε_d_{snow} (R = 0.76) (even though they were calculated separately in the model) than ε_ρ_{snow} (R = 0.28) (Figure 2.5a), we may expect from the LSOS results that ε_SWE would be negatively correlated with ε_T_B. However, T_B is affected by snow grain radius as well as density and depth. Snow grain radius was greatly overestimated (Figure 2.2b) and its error was negatively and positively correlated to ε_d_{snow} (R = –0.66) and ε_ρ_{snow} (R = 0.70), respectively (Figure 2.5b). Therefore, we can infer that the effect of ε_r_e on T_B was

opposite to those of ε_d_{snow} and ε_ρ_{snow} during the simulation period. As a result, for the LSOS, there was no significant correlation between ε_SWE and ε_T_B.

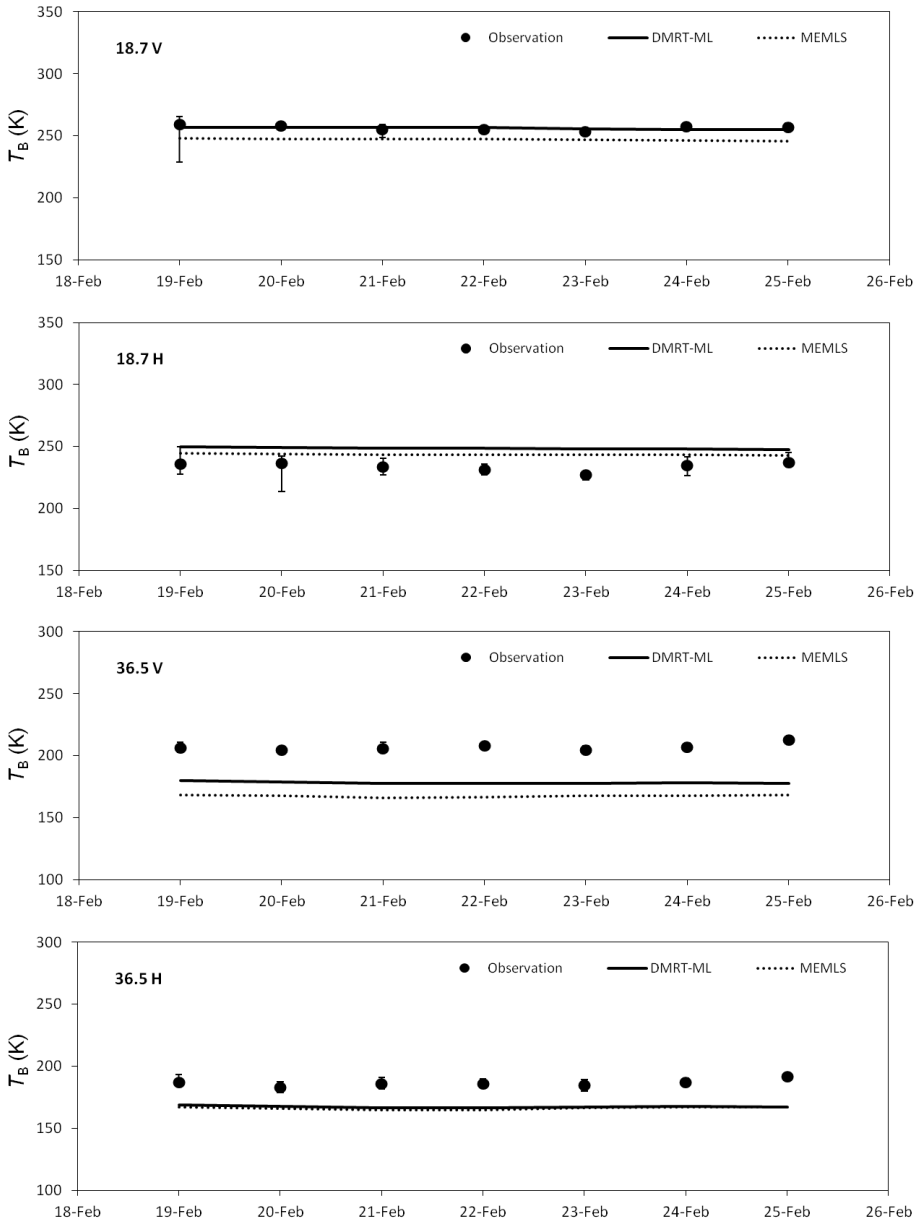

Figure 2.3. Results of T_B simulation by the coupled CLM4/DMRT-ML and CLM4/MEMLS for the LSOS.

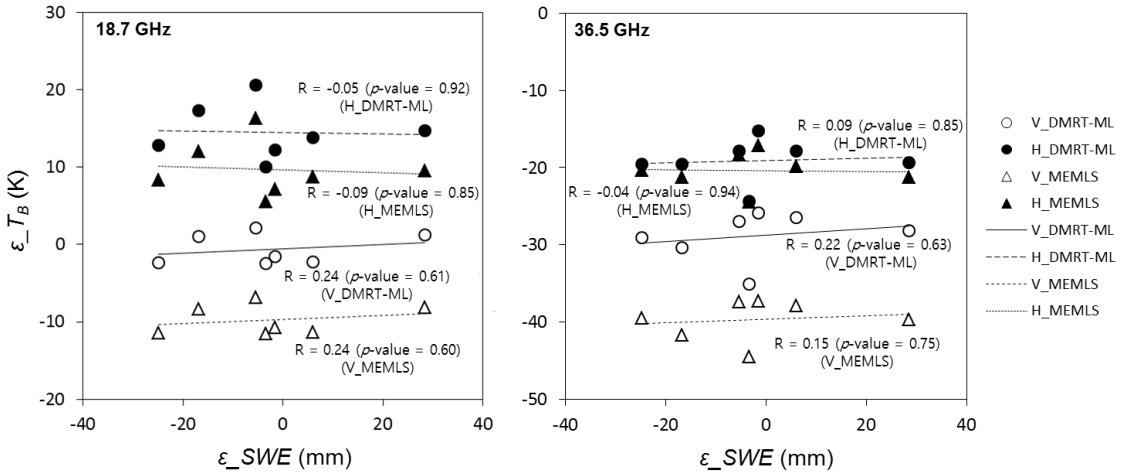

Figure 2.4. Relationships between errors (= simulation – observation) of SWE (ε_SWE) and T_B (ε_T_B) for the LSOS.

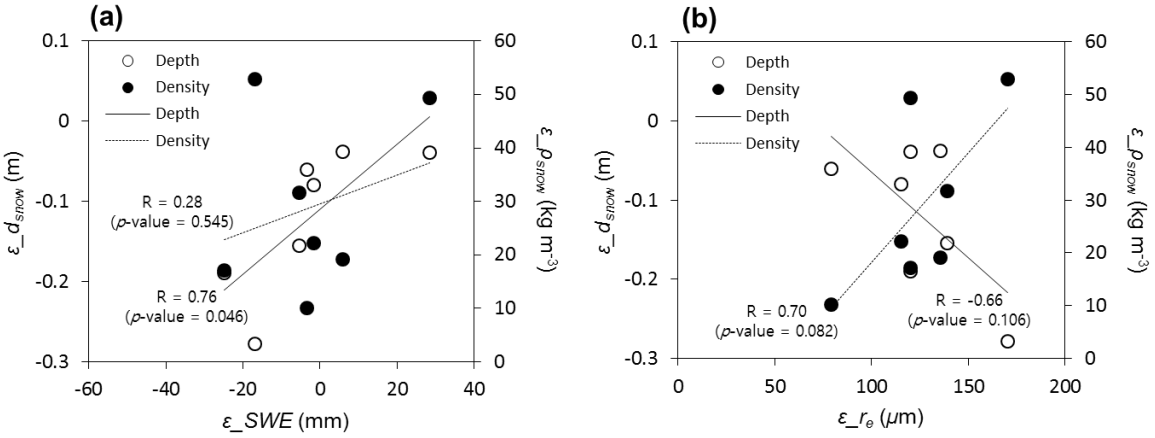

Figure 2.5. Relationships between errors (=simulation – observation) of snow depth (ε_d_{snow}) and density (ε_ρ_{snow}) and errors of (a) SWE (ε_SWE) and (b) snow grain radius (ε_r_e), respectively, for the LSOS.

2.4.2 Mesoscale error characterization: CLPX MSA (vegetated case)

1) Optimization of the Vegetation RTM Parameters: The optimized parameters for each MSA are indicated in Table 2.3; two parameters (b' and x) in vegetation RTM were determined to be 0.40 and –1.48, respectively, for the Fraser MSA and 0.10 and –1.38, respectively, for the Rabbit Ears MSA. The results of T_B predictions using these parameter values are shown in Figure 2.6.

Table 2.3. Optimization results of vegetation RTM parameters using *in situ* snowpit and AMSR-E T_B data collected over the Fraser and Rabbi Ears MSAs.

	Fraser MSA	Rabbit Ears MSA
b'	0.40	0.10
x	-1.48	-1.38

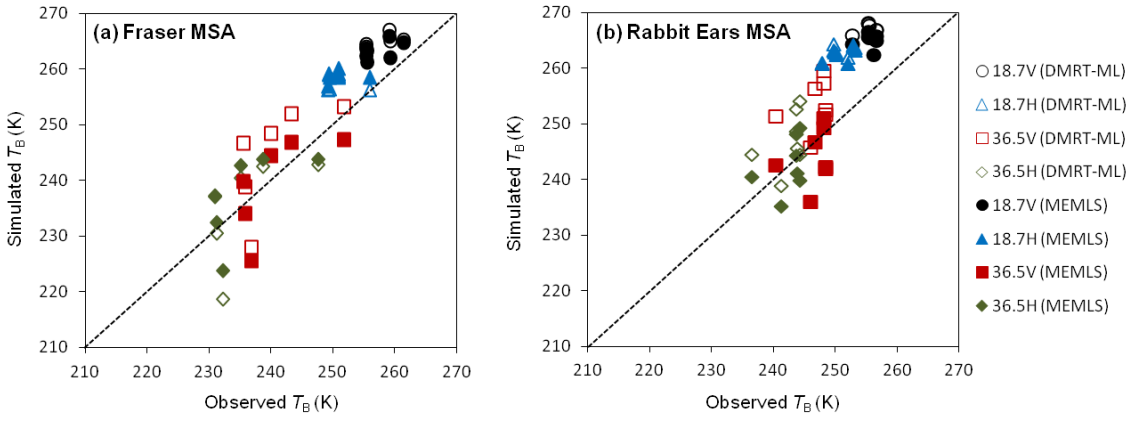

Figure 2.6. Observed AMSR-E T_B versus simulated T_B by DMRT-ML and MEMLS, which are coupled with the vegetation and atmospheric RTMs, using the optimized parameters (in Table 2.3) and in situ snowpit measurements collected from ISAs within the Fraser and Rabbit Ears MSAs.

2) SWE and T_B Simulations by the Coupled Models: Due to the lack of 2002 meteorological tower data, SWE and T_B for ISAs within the Fraser and Rabbit Ears MSAs were simulated by the coupled models only for 2003. Figure 2.7 shows the SWE

simulation results over both MSAs; overall, SWE was slightly overestimated for the Fraser MSA (MBE = 2.3 mm) and greatly underestimated for the Rabbit Ears MSA (MBE = –360.4 mm) (Figure 2.7). Because GBMR-7 precipitation data (collected over the LSOS within the Fraser MSA) were used for SWE simulations due to the lack of precipitation data for ISAs, CLM4 could not reproduce a deep snowpack in the Rabbit Ears MSA (RMSE = 385.8 mm) while it showed good performance for the Fraser MSA (RMSE = 54.2 mm).

Figure 2.8 shows the normalized errors of snow depth, density, grain radius, and temperature for both MSAs. Snow temperature simulations showed fairly good agreement with the observations, whereas for both MSAs, the largest error was that of snow grain size. Over the Fraser MSA, snow depth was overestimated for the St. Louis Creek and Alpine ISAs while it was underestimated for the Fool Creek ISA (Figure 2.8a). Snow depth was largely underestimated for all ISAs within the Rabbit Ears MSA (Figure 2.8b). ε_ρ_{snow} was relatively small compared to ε_d_{snow} and ε_r_e for both MSAs. Because observations showed dry snowpack conditions for all ISAs during the simulation period, the normalized error of wetness was not indicated.

Brightness temperatures at 18.7 and 36.5 GHz channels predicted by the coupled models were compared with the AMSR-E T_B observations (Figure 2.9 and Table 2.4). As shown in Table 2.4, two coupled models show comparable performance; they exhibit fairly good performance for 18.7 GHz channels, whereas their T_B simulation errors are relatively large for 36.5 GHz channels, which are primarily consequences of the large ε_r_e. For the Rabbit Ears MSA, the simulation errors of T_B at 18.7 GHz channels are small (Figure 2.9b), even though SWE was greatly underestimated (Figure 2.7) mainly due to snow depth underestimations (Figure 2.8b). This is attributed to that highly

overestimated snow grain radius offsets the effect of the underestimated snow depth on ε_T_B.

Table 2.4. Errors of T_B simulations by the coupled CLM4/DMRT-ML and CLM4/MEMLS for the Fraser and Rabbit Ears MSAs.

		CLM4/DMRT-ML				CLM4/MEMLS			
		18.7 GHz		36.5 GHz		18.7 GHz		36.5 GHz	
		T_BV	T_BH	T_BV	T_BH	T_BV	T_BH	T_BV	T_BH
Fraser MSA	RMSE (K)	3.1	3.4	15.5	17.7	4.4	2.8	22.6	19.4
	MBE (K)	2.0	2.2	-14.2	-16.6	-3.0	0.1	-21.9	-18.7
Rabbit Ears	RMSE (K)	4.2	3.9	29.4	34.4	2.3	3.6	39.9	37.2
MSA	MBE (K)	2.9	1.1	-28.7	-33.8	1.1	2.6	-39.4	-36.7

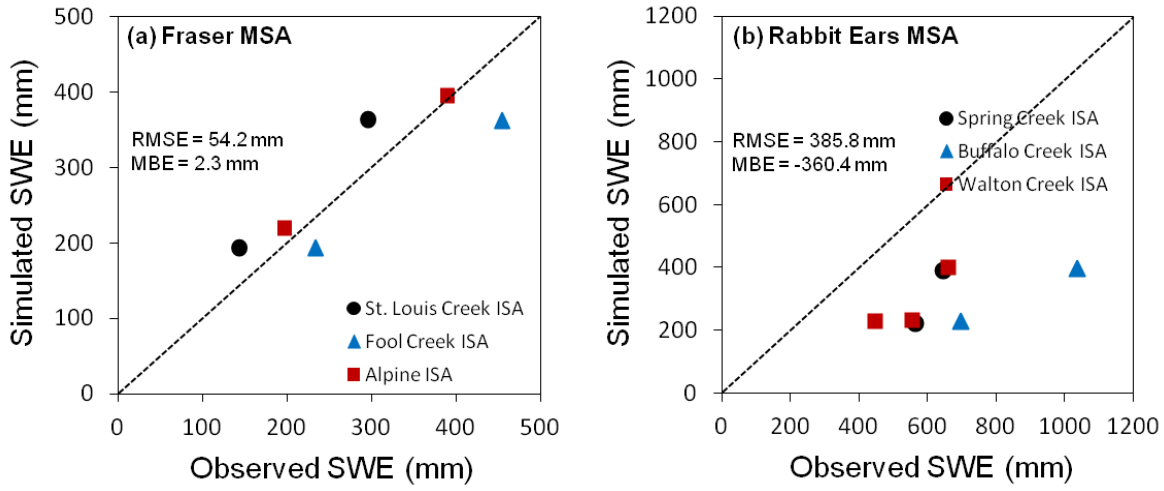

Figure 2.7. Results of SWE simulation by CLM4 for each ISA within the Fraser and Rabbit Ears MSAs. RMSE and MBE were calculated for MSAs.

Figure 2.8. Normalized errors (= (simulation – observation) / observation) of snow depth, density, grain radius, and temperature for each ISA within the Fraser and Rabbit Ears MSAs. Since both observations and simulations showed dry snowpack conditions, normalized error of wetness is not shown.

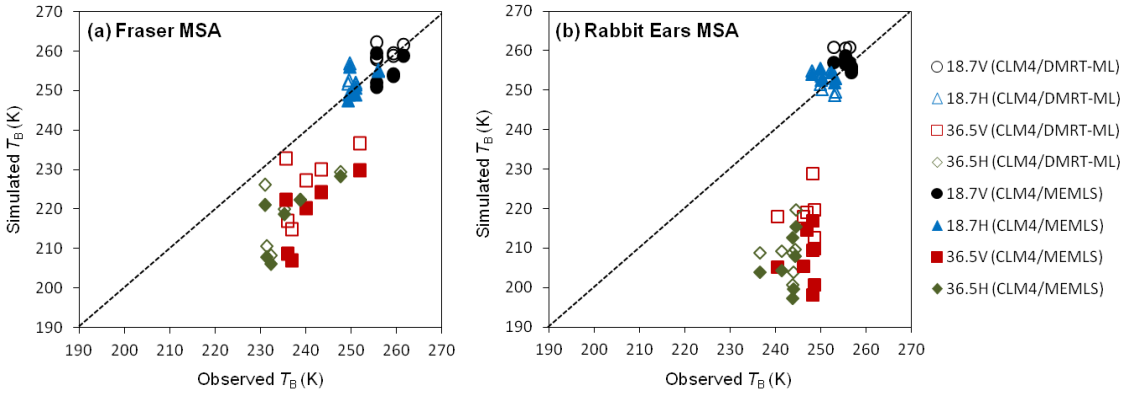

Figure 2.9. Observed versus simulated T_B by the coupled CLM4/DMRT-ML and CLM4/MEMLS for the Fraser and Rabbit Ears MSAs.

3) The Relationship Between ε_SWE and ε_T_B: Similar to the LSOS case, *ε_SWE* and *ε_*T_B did not show distinct correlations for both MSAs (Figure 2.10a and Figure 2.11a). For MSAs, *ε_*d_{snow} was much greater than *ε_*ρ_{snow} (Figure 2.8) and was more correlated to *ε_SWE* (Figure 2.12); therefore, *ε_SWE* was mainly caused by *ε_*d_{snow} for both MSAs. However, because snow grain radius was greatly overestimated (Figure 2.8), most *ε_*T_B was resulted from *ε_*r_e. In this case, as for the LSOS, the relationship between *ε_*r_e and *ε_*d_{snow} determines the correlation between *ε_SWE* and *ε_*T_B. During the simulation period, *ε_*d_{snow} was not significantly correlated to *ε_*r_e for both MSAs (R = –0.32 for the Fraser MSA and R = –0.37 for the Rabbit Ears MSA) (Figure 2.13a and Figure 2.13c). Consequently, we did not see any significant correlation between *ε_SWE* and *ε_*T_B for MSAs.

By excluding the St. Louis Creek ISA (from the Fraser MSA) and the Buffalo Pass ISA (from the Rabbit Ears ISA), we obtained higher positive correlations between *ε_SWE* and *ε_*T_B (Figure 2.10b and Figure 2.11b). These are mainly consequences of increased negative relationships between *ε_*d_{snow} and *ε_*r_e (Figure 2.13b and Figure 2.13d)

because in this case, even though snow depth decreases, increased snow grain radius results in decreased T_B. Meanwhile, like the LSOS, ε_ρ_{snow} was more (positively) correlated with ε_r_e than ε_d_{snow} (Figure 2.13b and Figure 2.13d). However, for both MSAs, ε_ρ_{snow} did not significantly affect the relationships between ε_SWE and ε_T_B, because ε_ρ_{snow} was relatively small for these areas (Figure 2.8).

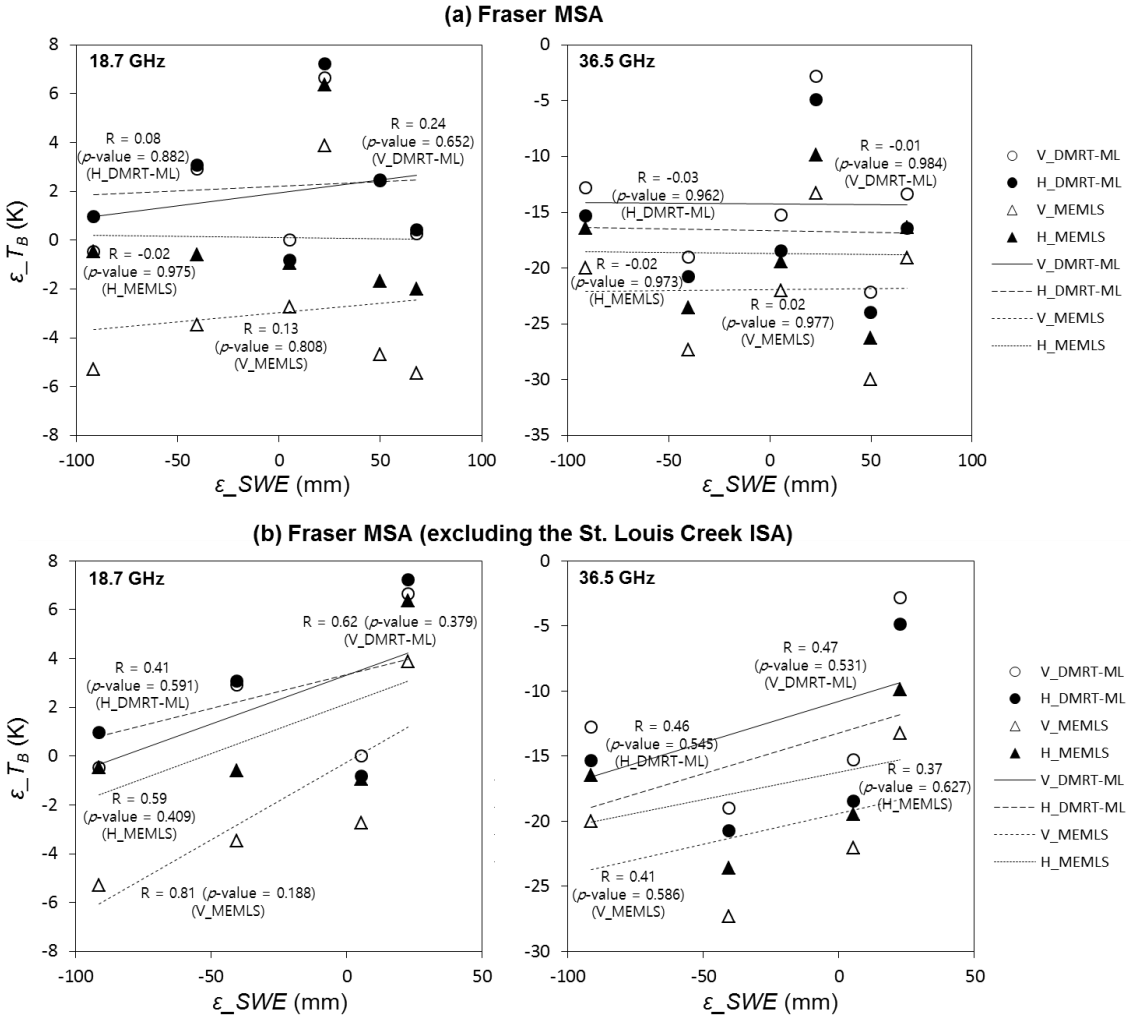

Figure 2.10. Relationships between errors (= simulation – observation) of SWE (ε_SWE) and T_B (ε_T_B) for the Fraser MSA: (a) all ISAs are included and (b) the St. Louis Creek ISA is excluded.

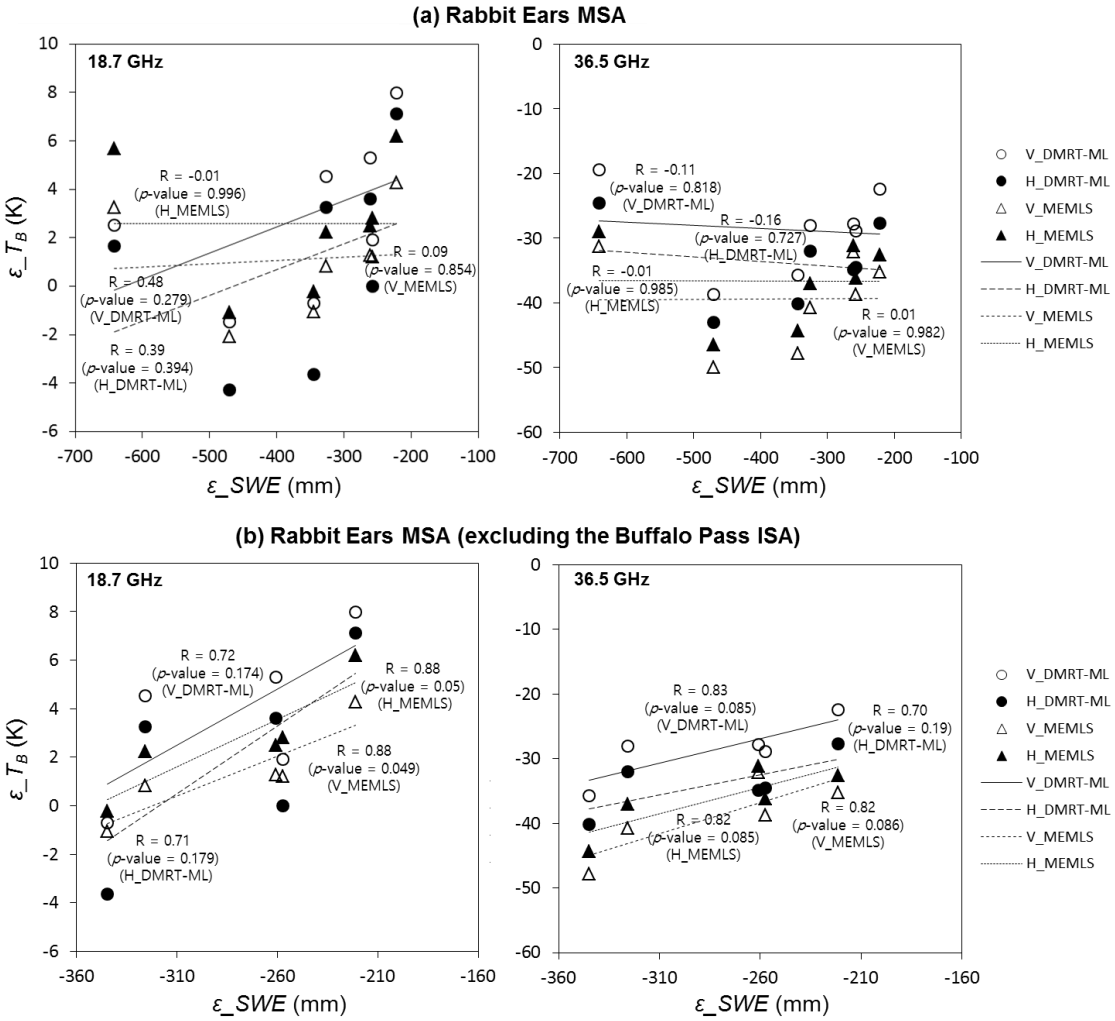

Figure 2.11. Relationships between errors (= simulation – observation) of SWE (ε_SWE) and T_B (ε_T_B) for the Rabbit Ears MSA: (a) all ISAs are included and (b) the Buffalo Pass ISA is excluded.

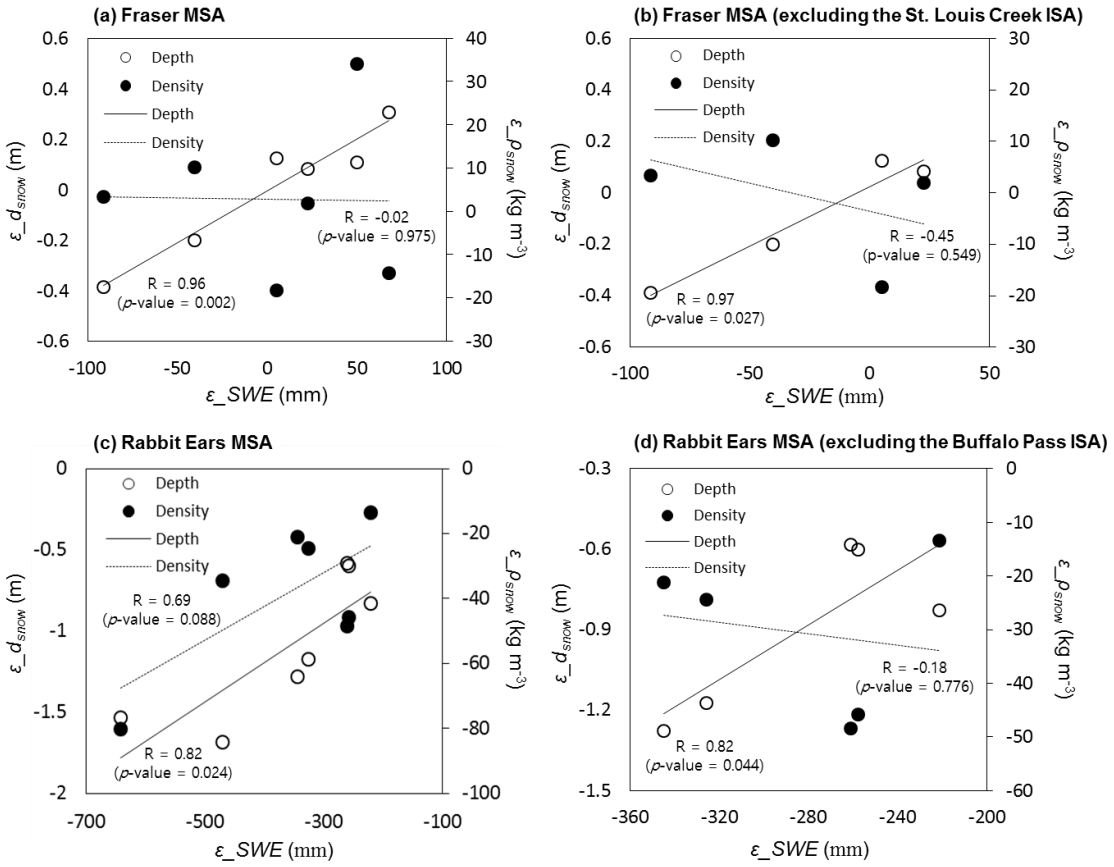

Figure 2.12. Relationships between SWE error (= simulation – observation) (ε_SWE) and errors of snow depth (ε_d_{snow}) and density (ε_ρ_{snow}), respectively, for the Fraser MSA ((a) all ISAs are included and (b) the St. Louis Creek ISA is excluded) and the Rabbit Ears MSA ((c) all ISAs are included and (d) the Buffalo Pass ISA is excluded).

The analyses using the CLPX datasets for the LSOS and MSAs show that given the large ε_r_e, the relationship between ε_r_e and ε_d_{snow} or ε_ρ_{snow}, and the relative magnitude of ε_d_{snow} and ε_ρ_{snow} mainly determine the direction of correlations between ε_SWE and ε_T_B. However, the CLPX datasets used in these analyses involve the spatial and temporal variability, while RA updates SWE at a given time and location. In addition, mainly due to the small number of observations, the correlation results are not significant (p-values are greater than 0.05 in Figure 2.10 to Figure 2.13, except for some

results). Therefore, in the following section, we carried out synthetic experiments to overcome the limitations of using the CLPX datasets and to support the above discussion.

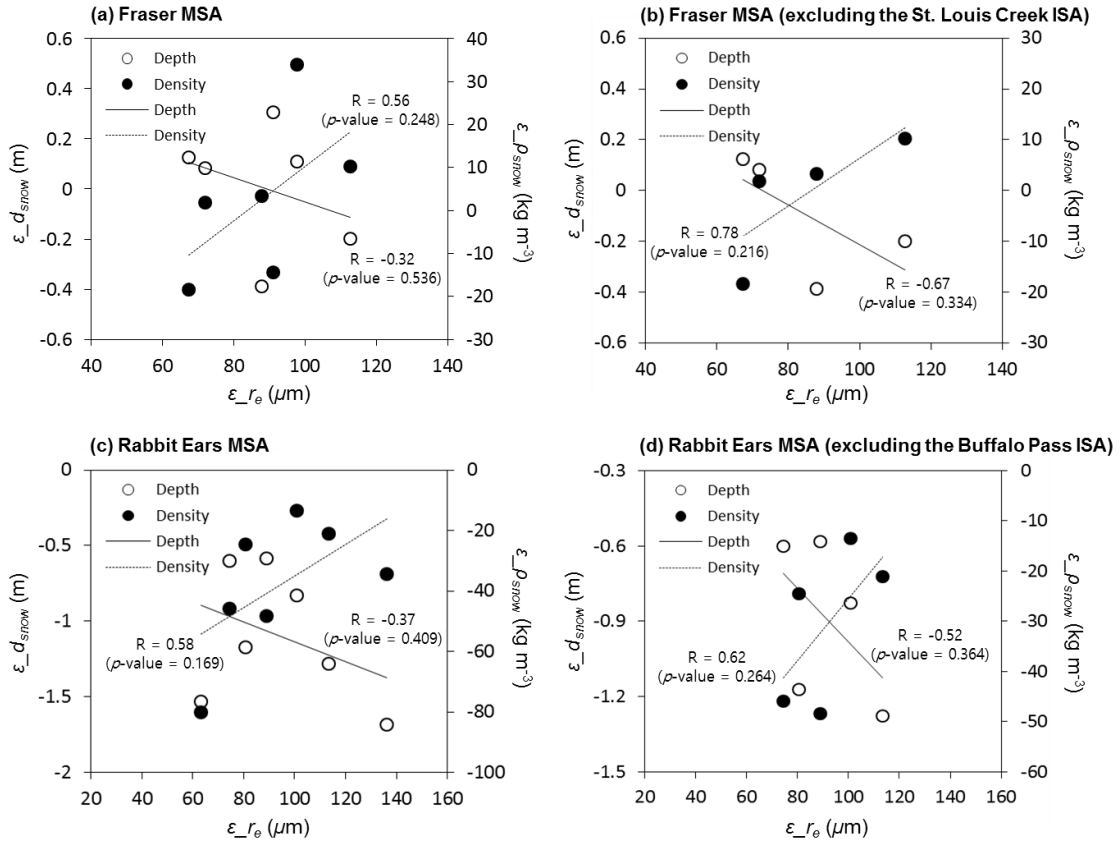

Figure 2.13. Relationships between snow grain radius error (= simulation – observation) (ε_r_e) and errors of snow depth (ε_d_{snow}) and density (ε_ρ_{snow}), respectively, for the Fraser MSA ((a) all ISAs are included and (b) the St. Louis Creek ISA is excluded) and the Rabbit Ears MSA ((c) all ISAs are included and (d) the Buffalo Pass ISA is excluded).

2.4.3 Synthetic experiments

In the synthetic experiments, we used the 40 randomly chosen ensemble members of the DART/CAM4 atmospheric ensemble reanalysis. Figure 2.14 shows the synthetic

truth and ensemble mean (from the open-loop run) of SWE for the CLPX region (shallow snowpack conditions) and Rocky Mountains (deep snowpack conditions) during 2003. The simulated SWE was about 10 times greater over the Rocky Mountains than over the CLPX region. During the simulation period, ε_SWE (ensemble simulations – synthetic truth) was mostly a result of ε_d_{snow} for both regions (Figure 2.15).

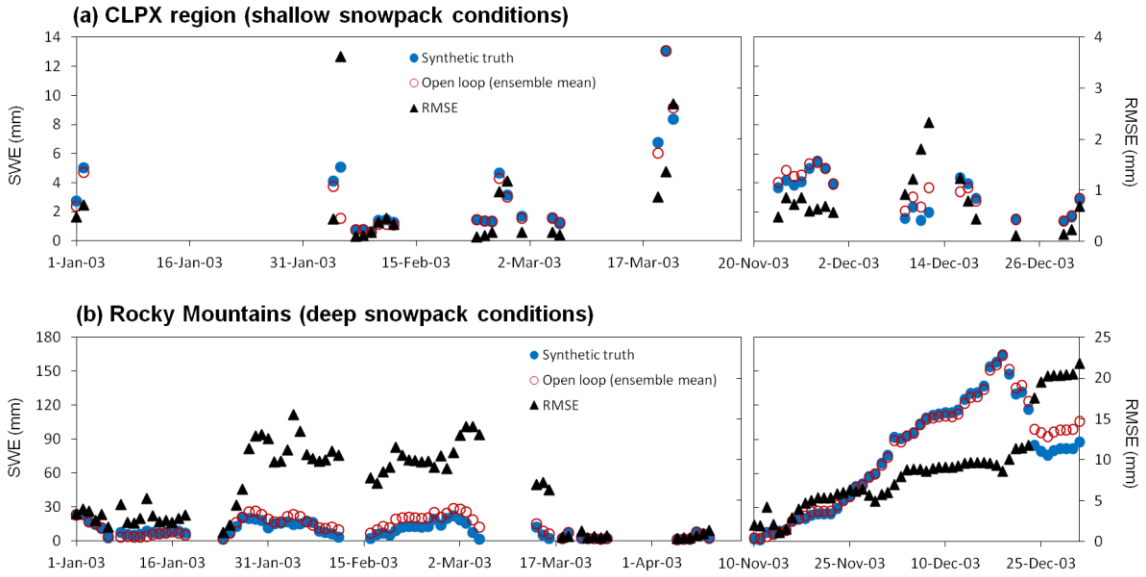

Figure 2.14. Synthetic truth and ensemble mean of SWE and RMSE of ensemble SWE simulations over the (a) CLPX region (shallow snowpack conditions) and (b) Rocky Mountains (deep snowpack conditions) during 2003.

Figure 2.16 and Figure 2.17 show the correlations between ε_SWE and ε_T_B and the SWE RMSE difference between the RA and open-loop cases (= $RMSE_{RA}$ – $RMSE_{Open\text{-}loop}$) for the CLPX region and Rocky Mountains, respectively. Negative (or positive) values of the RMSE difference indicate that RA improves (or degrades) the estimation of SWE in comparison with the open-loop case. As shown in the figures, RA

improved the SWE estimation for most of the simulation period; however, it also degraded the SWE estimation for some periods. Overall, greater (positive or negative) correlations between ε_SWE and ε_T_B led to more improvement of SWE in RA. The degradation of SWE estimates in RA was mainly caused by some ensemble members that did not obey the correlation between ε_SWE and ε_T_B. When the correlation was insignificant, the SWE update in RA was marginal and thus the degree of degradation of SWE was small. Meanwhile, when the correlation coefficient approaches 1 or –1, RA improved the SWE estimation for most cases. Therefore, most of the degradation of SWE estimates in RA was observed around the correlation coefficient of 0.5 or –0.5.

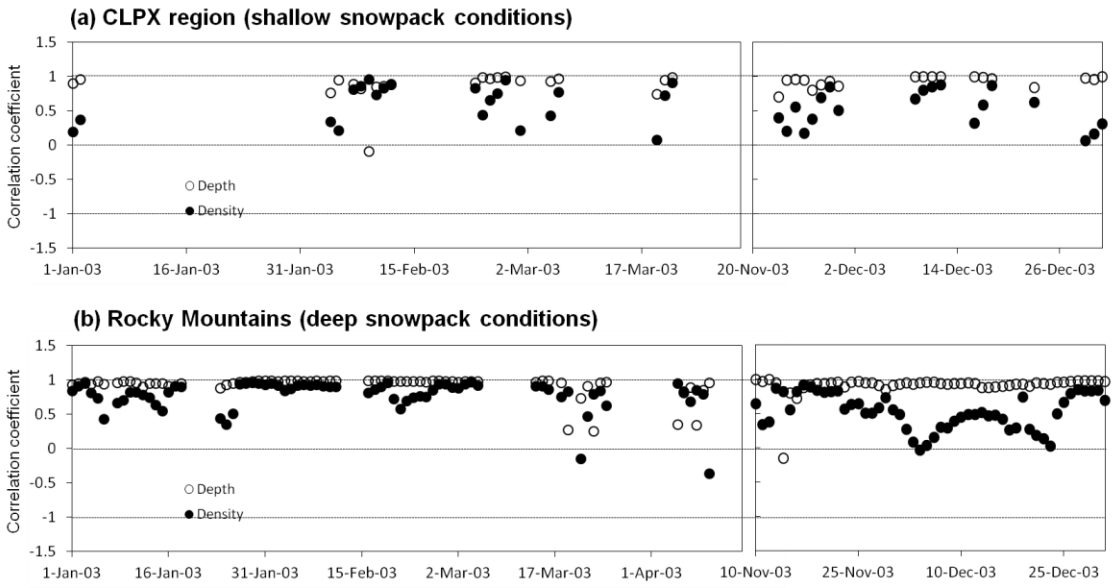

Figure 2.15. Relationships between SWE error (= ensemble simulations – synthetic truth) (ε_SWE) and errors of snow depth (ε_d_{snow}) and density (ε_ρ_{snow}), respectively, over the (a) CLPX region (shallow snowpack conditions) and (b) Rocky Mountains (deep snowpack conditions) during 2003.

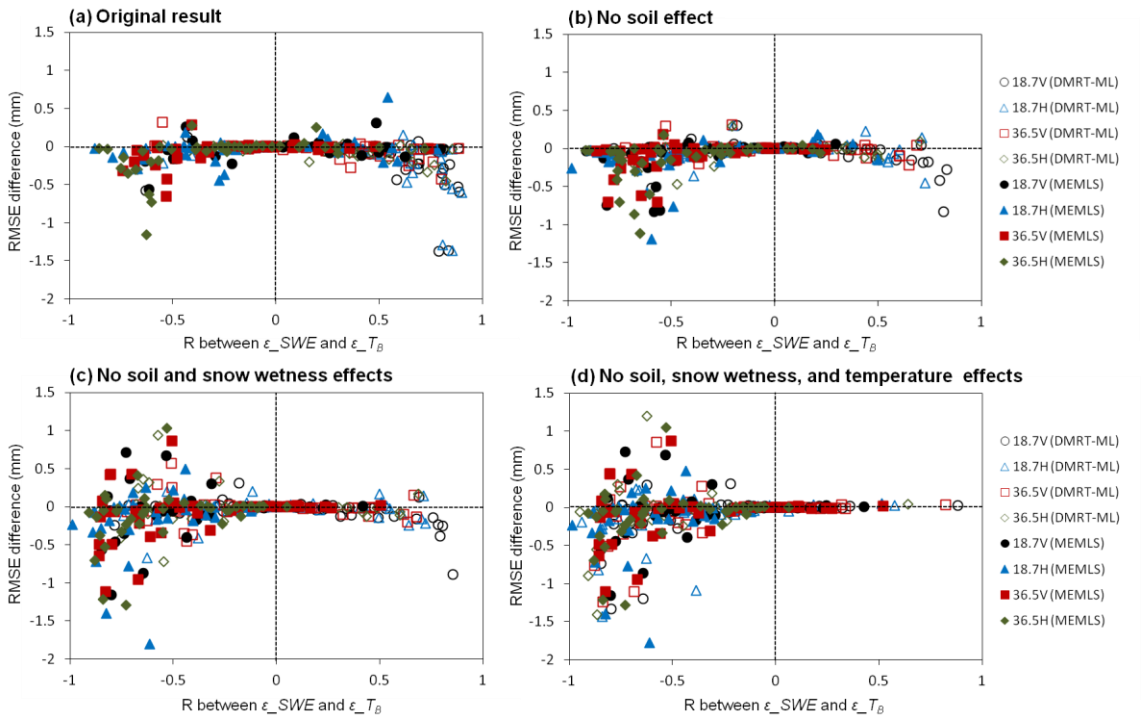

Figure 2.16. Scatter plots of correlation coefficients between ε_SWE and ε_T_B versus SWE RMSE difference (= $RMSE_{RA} - RMSE_{Open\text{-}loop}$) for each model and each frequency channel over the CLPX region during 2003: (a) original result, (b) no soil (water content and temperature) effect on ε_T_B, (c) no soil (water content and temperature) and snow wetness effects on ε_T_B, and (d) no soil (water content and temperature), snow wetness, and snow temperature effects on ε_T_B. Each point is corresponding to each day.

For shallow snowpack conditions over the CLPX region, more positive and negative correlations between ε_SWE and ε_T_B were produced by CLM4/DMRT-ML and CLM4/MEMLS, respectively (Figure 2.16a). In order to analyze the effects of ε_WT_{soil}, ε_W_{snow}, and ε_T_{snow}, some of these physical properties were assumed to be perfect so that no ε_T_B was introduced by errors of these properties: 1) soil water content and temperature (Figure 2.16b); 2) soil water content, soil temperature, and snow wetness (Figure 2.16c); and 3) soil water content, soil temperature, snow wetness, and snow

temperature (Figure 2.16d). Comparing Figure 2.16b with Figure 2.16a, we can see that for this shallow snowpack condition, the effect of soil on T_B resulted in positive correlations between ε_SWE and ε_T_B, especially in DMRT-ML. The additional exclusion of the snow wetness effect on ε_T_B from Figure 2.16b did not make much difference in the correlations but led to more degradation of SWE estimates in RA (Figure 2.16c). For the CLPX region, ε_T_{snow} was also one of the significant factors causing a positive correlation between ε_SWE and ε_T_B, particularly in DMRT-ML (compare Figure 2.16d to Figure 2.16c).

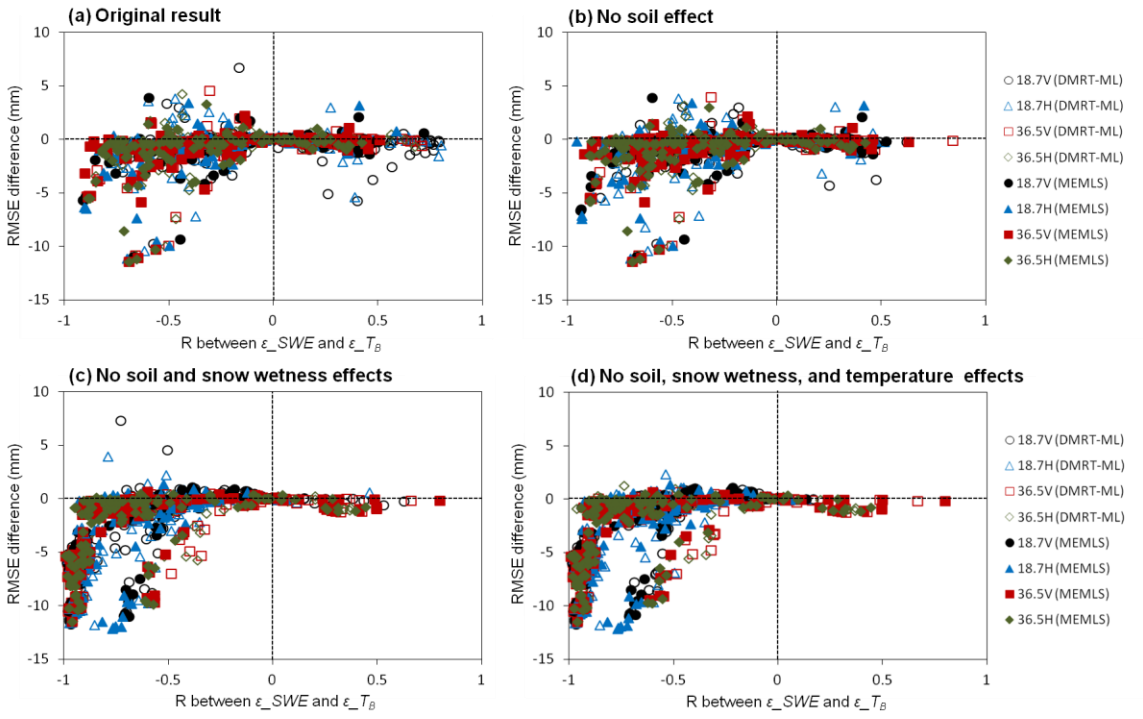

Figure 2.17. Same as Figure 2.16 but for the Rocky Mountains.

Unlike the CLPX region (Figure 2.16a), for deep snowpack conditions over the Rocky Mountains, more negative correlations between ε_SWE and ε_T_B were produced by the coupled models but CLM4/DMRT-ML tends to yield more (and higher) positive correlations than CLM4/MELMS (Figure 2.17a). The effect of ε_WT_{soil} on the positive correlation between ε_SWE and ε_T_B (compare Figure 2.17b with Figure 2.17a) is reduced compared to that for the CLPX region, mainly due to the increased snow depth. In contrast to the CLPX region (Figure 2.16c and Figure 2.16d), the SWE estimation in RA was improved by additionally excluding the effects of snow wetness and snow temperature on ε_T_B (Figure 2.17c and Figure 2.17d).

As previously mentioned, over the LSOS and MSAs, both simulations and observations showed dry snowpack conditions (no effect of snow wetness on ε_T_B) and ε_T_{snow} was very small (the effect of snow temperature on ε_T_B was negligible). Therefore, we further analyzed the results shown in Figure 2.16d and Figure 2.17d because they were considered appropriate to support the results from the CLPX datasets.

From the results in Figure 2.16d and Figure 2.17d, the classification of 13 cases was made based on the correlation coefficients between ε_r_e and ε_d_{snow} or ε_ρ_{snow} (Figure 2.18). Figure 2.19 and Figure 2.20 show the effects of the magnitude of ε_r_e and its relationship to ε_d_{snow} and ε_ρ_{snow} (see the 13 cases in Figure 2.18) on the correlations between ε_SWE and ε_T_B for the CLPX region and Rocky Mountains, respectively.

Most of the positive or insignificant correlations between ε_SWE and ε_T_B occurred when ε_r_e was small, especially for cases 1 to 8 where ε_r_e was positively correlated to ε_ρ_{snow} (Figure 2.19 and Figure 2.20). Based on a sensitivity test, the effects of snow density and grain radius on T_B are opposite in direction, whereas both snow depth and grain radius are negatively correlated with T_B. In contrast to the results from the CLPX datasets (Figure 2.12), ε_ρ_{snow} was also highly correlated with ε_SWE in the

synthetic experiments (Figure 2.15). Therefore, in cases 1 to 8, the effects of ε_d_{snow} and ε_r_e on the relationships between ε_SWE and ε_T_B were canceled out by ε_ρ_{snow}. However, in these cases, the correlation between ε_SWE and ε_T_B negatively increased as ε_r_e increased (Figure 2.19 and Figure 2.20).

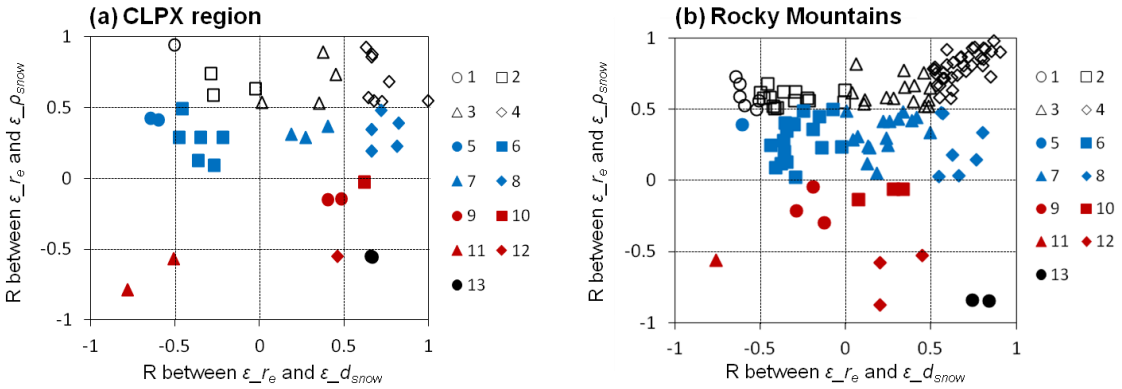

Figure 2.18. The classification of 13 cases based on the correlation coefficients between ε_r_e and ε_d_{snow} (x-axis) and ε_ρ_{snow} (y-axis), respectively: (a) CLPX region (shallow snowpack conditions) and (b) Rocky Mountains (deep snowpack conditions).

Cases 9 (only for the Rocky Mountains) and 11, where ε_r_e was negatively correlated to both ε_d_{snow} and ε_ρ_{snow}, exhibited relatively high negative correlations between ε_SWE and ε_T_B (Figure 2.19 and Figure 2.20). Because in these cases, ε_r_e was small and the magnitude of ε_d_{snow} and its relationship with ε_SWE were much greater than those of ε_ρ_{snow}, the negative correlations between ε_SWE and ε_T_B were mainly determined by ε_d_{snow}.

In cases 9 (only for the CLPX region), 10, 12, and 13, we may expect negative correlations between ε_SWE and ε_T_B when ε_r_e is large. However, some points in these cases showed insignificant or positive correlations (Figure 2.19 and Figure 2.20), which

was also mostly attributed to the much larger ε_ρ_{snow} and its higher correlation with ε_SWE than those of ε_d_{snow}.

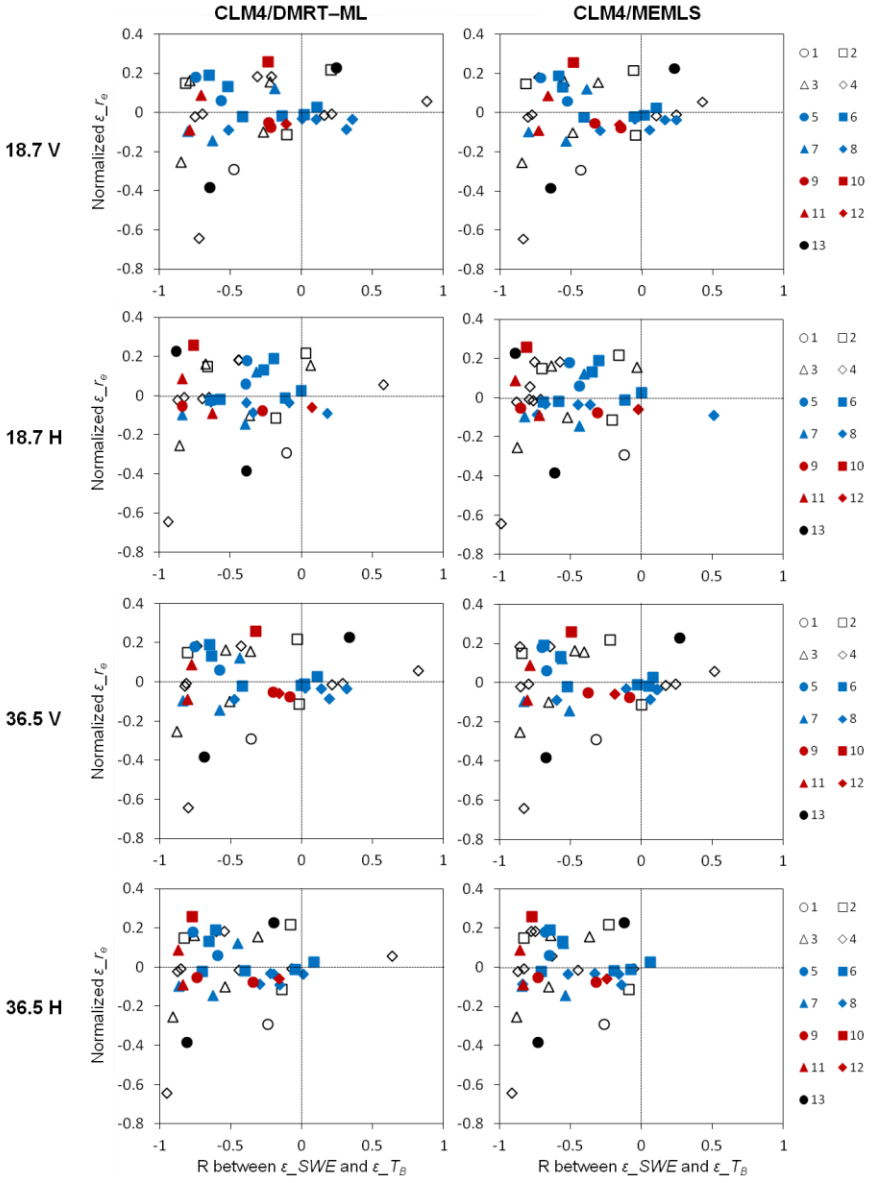

Figure 2.19. Scatter plots of correlation coefficients between ε_SWE and ε_T_B versus the normalized ε_r_e for each model and each frequency channel over the CLPX region during 2003. Each point is corresponding to each day. The 13 cases are based on Figure 2.18a.

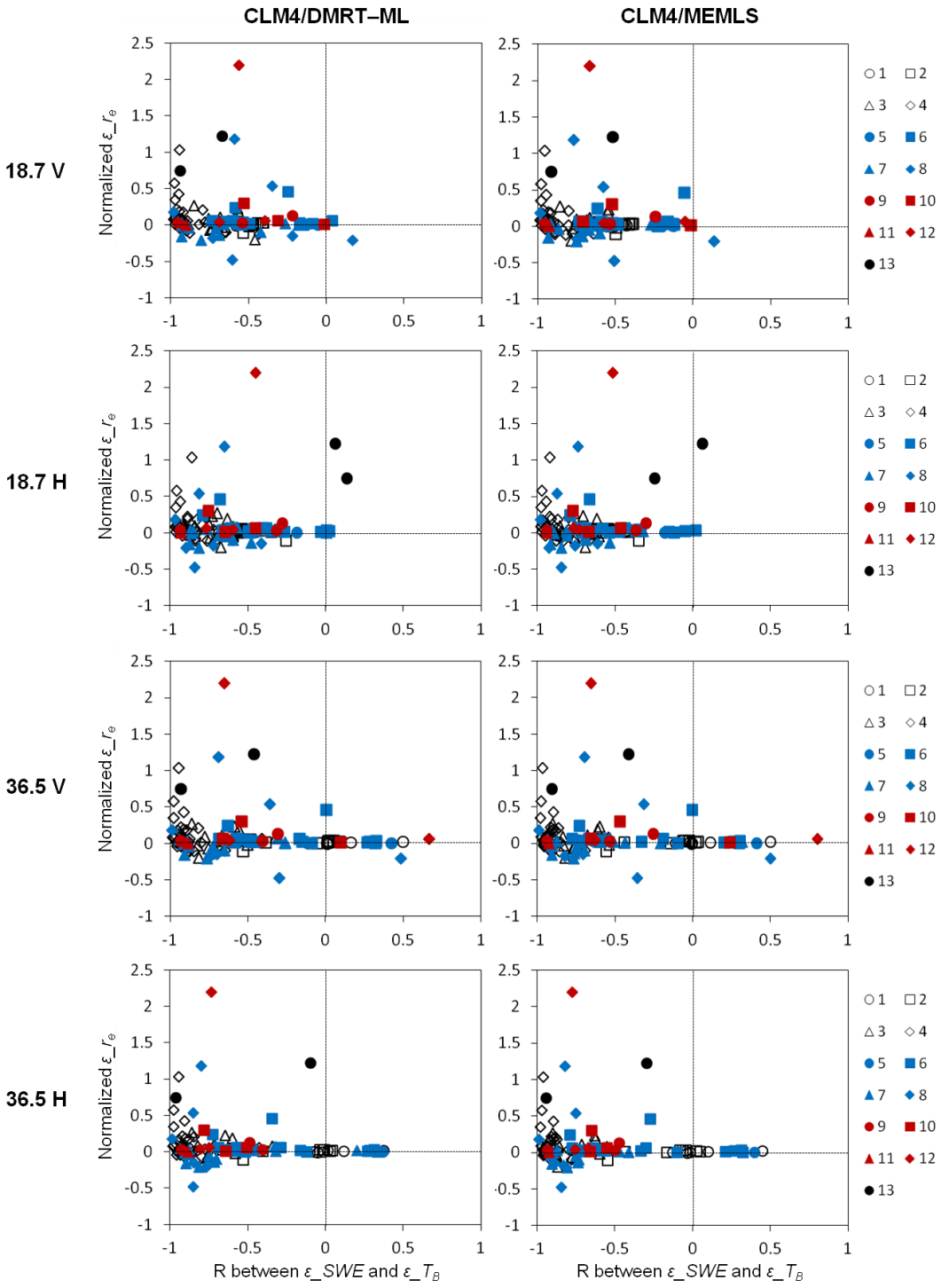

Figure 2.20. Same as Figure 2.19 but for the Rocky Mountains. The 13 cases are based on Figure 2.18b.

Figure 2.21 and Figure 2.22 show the relationships between the normalized ε_r_e and SWE RMSE difference (= $RMSE_{RA} - RMSE_{Open\text{-}loop}$) for the CLPX region and Rocky Mountains, respectively. Each symbol in the figures represents the range of correlation coefficients between ε_SWE and ε_r_e. When ε_r_e was small, most of the degradation of SWE estimates in RA was resulted from the relative magnitude of ε_d_{snow} and ε_ρ_{snow} and their relationships to ε_SWE. Although large ε_r_e led to high negative correlations between ε_SWE and ε_T_B (Figure 2.19 and Figure 2.20), it did not result in an improvement of SWE in RA (Figure 2.21 and Figure 2.22) because much of the signal of ε_T_B was due to ε_r_e. However, when the correlation coefficient between ε_SWE and ε_r_e was greater than 0.5, most of the SWE estimations in RA were improved, even though ε_r_e was large.

2.5 CONCLUSIONS

SWE and T_B at 18.7 and 36.5 GHz V and H polarization channels were simulated by the coupled CLM4/DMRT-ML and CLM4/MEMLS for non-vegetated (LSOS) and vegetated areas (Fraser and Rabbit Ears MSAs). To minimize errors caused by uncertainties of snow stickiness (in DMRT-ML only) and vegetation parameters (in vegetation RTM), optimizations were conducted using snowpit and T_B observations. Based on optimization, the stickiness parameter was set to 0.17, which is lower than that obtained in *Roy et al.* [2013]; the lower value results from the effects of grain shape and size distribution of sticky spheres, which were not considered in DMRT-ML. The lower value (0.17) is, however, within the range (from 0.1 to 0.2) suggested by previous studies. Two empirical vegetation parameters (b' and x) were determined to be 0.40 and −1.48, respectively, for the Fraser MSA and 0.10 and −1.38, respectively, for the Rabbit Ears MSA.

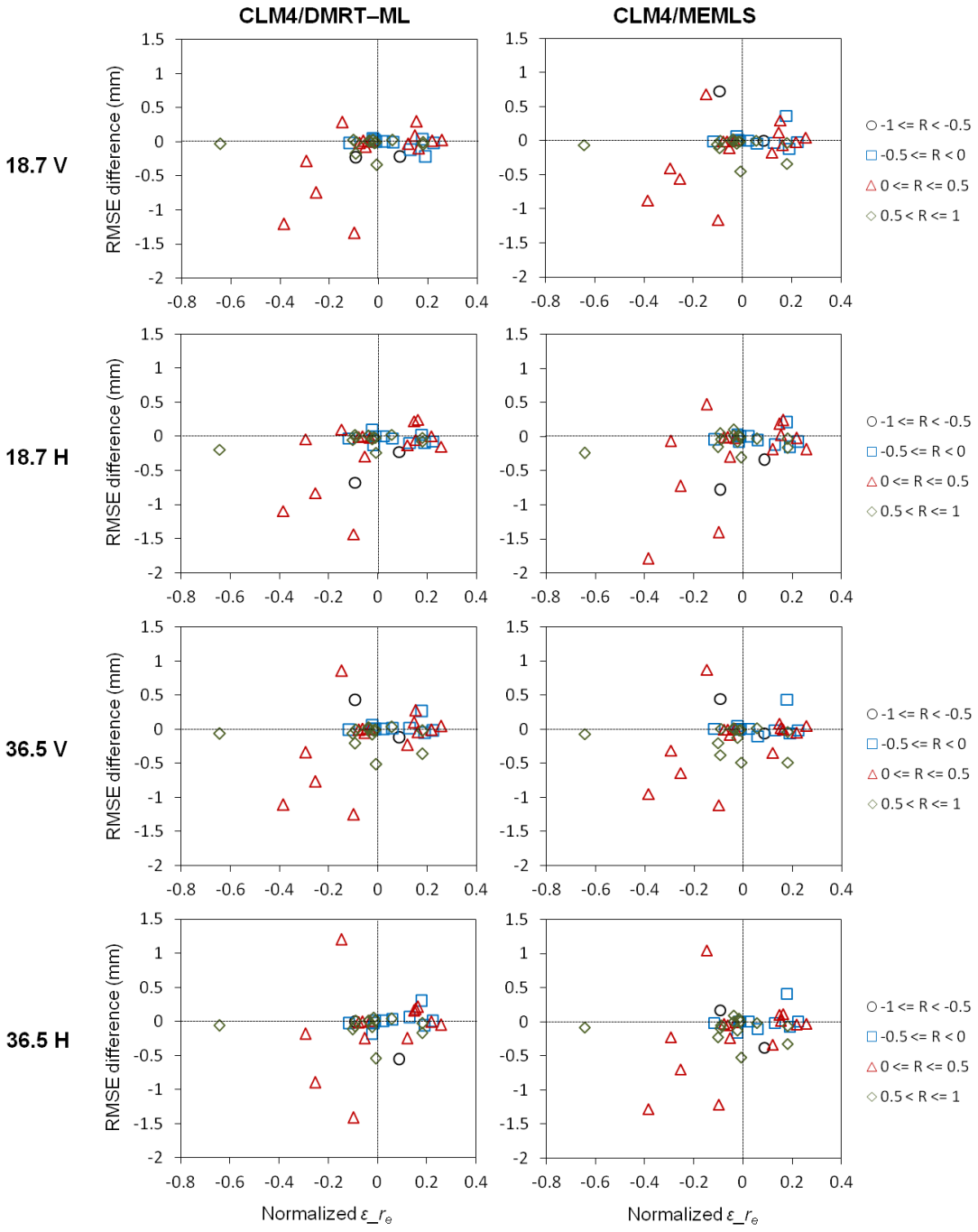

Figure 2.21. Scatter plots of the normalized ε_r_e versus SWE RMSE difference (= $RMSE_{RA} - RMSE_{Open\text{-}loop}$) over the CLPX region during 2003 (R: correlation coefficient between ε_SWE and ε_r_e). Each point is corresponding to each day.

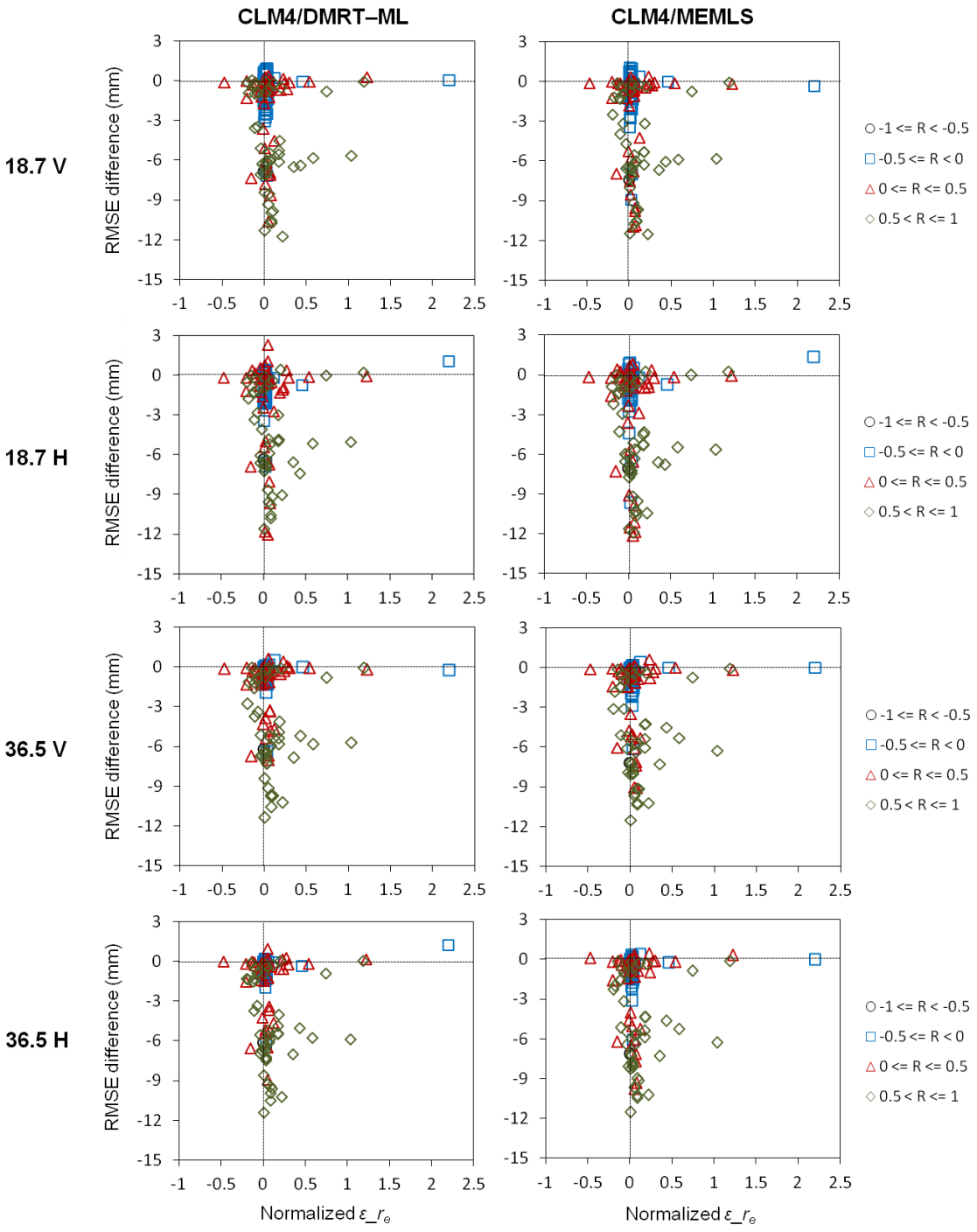

Figure 2.22. Same as Figure 2.21 but for the Rocky Mountains.

We characterized the errors of the coupled models by evaluating the CLM4 snowpack state simulations, by assessing the RTMs performance in simulating T_B, and by analyzing the correlations between ε_SWE and ε_T_B. SWE simulations by CLM4 showed fairly good agreement with the observations for the LSOS and Fraser MSA while SWE was underestimated for the Rabbit Ears MSA. Among the snowpack physical properties required to run the snowpack RTMs, the highest normalized error in all study areas was that of snow grain radius. Both coupled models showed comparable performance in predicting T_B; they show fairly good performance for 18.7 GHz channels but their simulation errors of T_B were relatively great for 36.5 GHz channels due to the large ε_r_e. The results using the CLPX datasets show that given the large ε_r_e for dry snowpack conditions, the correlations between ε_SWE and ε_T_B are determined by the relationship between ε_r_e and ε_d_{snow} or ε_ρ_{snow}, and the relative magnitude of ε_d_{snow} and ε_ρ_{snow}.

The synthetic experiments conducted for the CLPX region (shallow snowpack conditions) and Rocky Mountains (deep snowpack conditions) support the results from the CLPX datasets. When no ε_T_B was resulted from ε_WT_{soil}, ε_W_{snow}, and ε_T_{snow}, the relationships between ε_SWE and ε_T_B were mainly determined by the magnitude of ε_r_e and its relationship to ε_d_{snow} and ε_ρ_{snow}. Overall, large ε_r_e led to high negative correlations between ε_SWE and ε_T_B, and most of the positive or insignificant correlations were consequence of larger ε_ρ_{snow} and its higher correlation with ε_SWE than those of ε_d_{snow}. Errors of soil (water content and temperature), snow wetness, and snow temperature mostly resulted in positive correlations between ε_SWE and ε_T_B. The effect of soil on the correlations was obvious for shallow snowpack conditions, especially in CLM4/DMRT-ML.

The synthetic experiments show that greater (positive or negative) relationships between ε_SWE and ε_T_B led to more improvement of SWE in RA while most of the

degradation was observed around the correlation coefficient of 0.5 or –0.5. When simulations of soil water content, soil temperature, snow wetness, and snow temperature are assumed to be perfect, the magnitude of ε_r_e and its relationship to ε_SWE are important for RA performance. Most of the SWE estimations in RA were improved when ε_SWE and ε_r_e show a high positive correlation (greater than 0.5).

CLM4/DMRT-ML and CLM4/MEMLS tended to produce more positive and negative correlations between ε_SWE and ε_T_B, respectively, and thus they showed different performances in RA. This emphasizes the necessity of using multiple snowpack RTMs to improve the SWE estimation at the continental scale. The results in this study also show that errors of all physical properties of soil and snow required to estimate T_B have significant effects on the relationships between ε_SWE and ε_T_B and subsequent RA performance. Therefore, as well as SWE (snow depth and density), all of these physical properties have to be properly updated in the RA scheme to reduce errors related to them. To minimize ε_T_B resulted from ε_W_{snow}, we may be able to use only nighttime observations.

It should be noted that we used the conversion equations (e.g., equations (2.1), (2.6), and (2.7)) for three different snow grain size parameters, i.e., D_max (observed grain size), r_e (in CLM4 and DMRT-ML), and p_ex (in MEMLS). This can lead to uncertainty in simulated T_B by the coupled models and thus some results (e.g., parameter optimizations, and the magnitude of ε_T_B and ε_r_e) might be affected. However, the overall discussions on the relationships between errors are unaffected by this incompatibility among the snow grain size parameters.

Model error characterization in a DA system is the greatest challenge, especially for large-scale applications. Furthermore, because in snow RA, model error can be resulted from RTMs and parameterizations of various snow and soil variables in the

LSM, not just from SWE-related variables, model error characterization is much difficult. Although further studies are required, the results obtained in this study (e.g., relationships between errors of T_B and snow and soil states, and their effects on RA performance) can contribute to characterization of model error in future real RA studies. In addition, they can also be used for a rule-based approach in updating SWE in the RA scheme to minimize the degradation of SWE estimates.

The error characteristics of CLM4/DMRT-ML and CLM4/MEMLS were analyzed only at point and local scales. For continental-scale multi-RTM ensemble RA, optimizations of stickiness in DMRT-ML and empirical parameters in vegetation RTM would be a laborious task. For this, several approaches could be taken: 1) dual-pass approach (calibration + assimilation) [*Yang et al.*, 2009], 2) simultaneous updates of states and parameters in the data assimilation system [*Su et al.*, 2011], and 3) the use of published values by classifying snow cover and vegetation types. These issues will be addressed in future studies.

2.5 ACKNOWLEDGMENT

This work was supported in part by the National Aeronautics and Space Administration under Grant NNX11AJ43G and in part by the National Natural Science Foundation of China under Grant 91337217. The authors appreciate to the Jackson School of Geosciences (JSG) for providing travel funds to visit NASA Goddard Space Flight Center (GSFC). The authors would like to thank C. Mätzler and M. Durand for providing their computer codes and all of the CLPX participants for collecting the data used in this study. The authors also wish to thank M. Durand and M. Flanner for their discussions on CLM4 snow grain radius simulations and P. A. Bobeck for language assistance. The DART/CAM4 atmospheric ensemble reanalysis data are prepared by K.

Raeder (raeder@ucar.edu). Computational resources were provided by the UT Texas Advanced Computing Center (TACC).

CHAPTER 3: Estimating snow water storage in North America using CLM4, DART, and snow radiance data assimilation[2]

3.1 ABSTRACT

This paper addresses continental-scale snow estimates in North America using a recently developed snow radiance assimilation (RA) system. The RA system is comprised of the Community Land Model version 4 (CLM4), the Dense Media Radiative Transfer–Multi Layers model (DMRT-ML), and the Data Assimilation Research Testbed (DART). A series of RA experiments with the ensemble adjustment Kalman filter are conducted by assimilating the Advanced Microwave Scanning Radiometer–Earth Observing System (AMSR-E) brightness temperature (T_B) at 18.7 and 36.5 GHz vertical polarization channels. Results demonstrate that the coupled RA system has the potential to improve continental-scale snow estimates. The RA performance in estimating snow depth and snow cover fraction (SCF) is improved by simultaneously updating model states and parameters involved in predicting T_B and by updating prior estimates based on their correlations with a prior T_B (i.e., rule-based RA). Radiance data assimilation can complement SCF data assimilation for relatively deep snowpack regions where SCF approaches 100%. The rule-based RA is more effective in estimating snow depth than the default RA (without a rule). Significant improvement of the snow depth estimates in the rule-based RA is observed for tundra snow class and bare soil land cover type. However, even in the most improved RA case, snow estimates are degraded for some specific snow classes and land covers like taiga and forest. The current RA system needs to be further refined to enhance snow estimates for various snow types and forested regions.

[2] This chapter was previously submitted to *Journal of Hydrometeorology*.

3.2 INTRODUCTION

Estimates of snow depth and snow water equivalent (SWE) are critical for climate studies and water resource management. Data assimilation (DA) has been identified as a powerful method to generate improved estimates by merging observations and model forecasts based on their uncertainties. As a DA method, radiance assimilation (RA) incorporates microwave brightness temperature (T_B) observations into a land-surface model (LSM) coupled with a microwave radiative transfer model (RTM).

In this study, we address the feasibility of RA to improve snow estimates at the continental scale. This work builds on our previous research [*Kwon et al.*, 2015] in which the Community Land Model version 4 (CLM4) [*Oleson et al.*, 2010; *Lawrence et al.*, 2011] is coupled with the Dense Media Radiative Transfer–Multi Layers model (DMRT-ML) [*Picard et al.*, 2013] to predict T_B from the snowpack. The observed T_B from the Advanced Microwave Scanning Radiometer–Earth Observing System (AMSR-E) is then assimilated using the ensemble adjustment Kalman filter (EAKF) [*Anderson*, 2001], which is an option in the Data Assimilation Research Testbed (DART) [*Anderson et al.*, 2009] developed by the National Center for Atmospheric Research (NCAR).

We hypothesize that the continental-scale RA performance in estimating snow depth and SWE can be improved through: 1) simultaneous updates of all model physical states and parameters involved in predicting T_B and 2) a rule-based approach in which prior estimates are updated depending on their correlations with a prior T_B. *Kwon et al.* [2015] emphasized that all physical states and parameters in the model used to estimate T_B should be appropriately updated in RA to minimize errors related to them. *Kwon et al.* [2015] also showed that the T_B signal can be dominated by snow and soil properties (in particular, snow grain size) instead of SWE (or snow depth). Such dominance in RA can degrade SWE (or snow depth) estimates because of incorrect relationships between the

prior SWE (or snow depth) and T_B estimates. A rule-based RA could ameliorate this issue.

The remainder of this chapter is organized as follows. Section 3.3 describes the coupled RA system, the data sets, and the experimental design. Results are analyzed and discussed in section 3.4. Conclusions are enumerated in section 3.5.

3.3 COUPLED RADIANCE ASSIMILATION SYSTEM, DATA SETS, AND EXPERIMENTAL DESIGN

3.3.1 Coupled radiance assimilation system

The coupled CLM4, DART, and RTMs data assimilation system is hereafter referred to as the coupled RA system (see Figure 3.1 for a schematic diagram of the coupled RA system). CLM4 simulates snow and soil states (snow depth and layer thickness, snow temperature, soil temperature and moisture) and snow characteristics (density, grain radius, and wetness). Whenever AMSR-E T_B observations are available, CLM4 creates restart files for each ensemble member. The forecasted states and characteristics in the restart files are then read by DART and fed to an observational operator (i.e., RTMs), which converts the model states and snow characteristics to T_B. At the same time, DART reads AMSR-E T_B observations and updates model states and snow characteristics by the assimilation process. These updated values in the restart files are used for subsequent model forecast.

1) DART

DART [*Anderson et al.*, 2009] is a community facility for ensemble-based DA studies. Given its flexibility, DART has been coupled with various atmospheric and oceanic models [*Anderson et al.*, 2009] and land surface models including CLM4 [*Zhang*

et al., 2014]. In this study, we additionally incorporated RTMs as an observational operator to predict T_B.

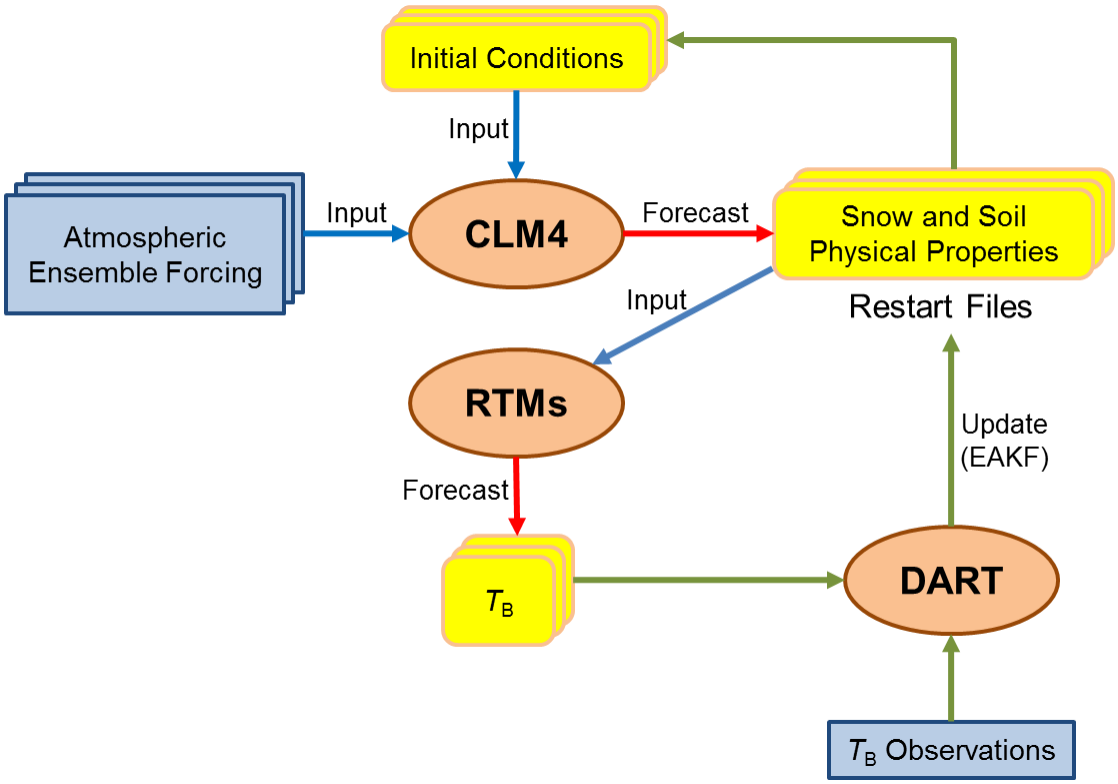

Figure 3.1. Schematic diagram of the coupled radiance assimilation system.

DART involves a variety of ensemble-based assimilation algorithms. One of them, the EAKF [*Anderson*, 2001], is applied in this study. The EAKF is a deterministic ensemble square root filter [*Tippett et al.*, 2003] whereas the traditional ensemble Kalman filter (EnKF) [*Evensen*, 1994; *Burgers et al.*, 1998] calculates model forecast error statistics based on a Monte Carlo method. In the EAKF, an updated (posterior) ensemble is generated by shifting the forecasted (prior) ensemble so that it has the same mean and

standard deviation as those of the continuous posterior [*Anderson et al.*, 2009]. *Anderson* [2001] suggests that, in particular for a small ensemble size, the EAKF significantly outperforms the traditional EnKF, which introduces a random perturbation to observation. More detailed descriptions of DART and the EAKF are available in *Anderson et al.* [2009] and *Anderson* [2001], respectively.

2) CLM4

CLM4 [*Oleson et al.*, 2010; *Lawrence et al*., 2011] is the land component of the Community Earth System Model (CESM) [*Gent et al.*, 2011]. CLM4 has 15 soil layers, up to five snow layers (depending on snow depth), and one canopy layer. In CLM4, soil temperature is calculated for all soil layers but hydrologic calculations are conducted only for the top 10 soil layers; frozen soil hydrology is represented based on the procedure described by *Niu and Yang* [2006].

CLM4 is advantageous for this study because a) it is a community developed model and b) it represents the snowpack as multiple layers and simulates snow thermodynamics. As a community model, CLM has been extensively evaluated in a wide range of applications and it evolves continuously from worldwide contributions. Recently, *Kwon et al.* [2015] linked CLM4 with two snow radiative transfer models, DMRT-ML [*Picard et al.*, 2013] and the Microwave Emission Model for Layered Snowpacks (MEMLS) [*Wiesmann and Mätzler*, 1999]. *Kwon et al.* [2015] also analyzed the error characteristics of these coupled models (CLM4/DMRT-ML and CLM4/MEMLS) from RA perspectives.

Durand et al. [2008] demonstrated that the use of a five-layer snow scheme of CLM4 provides more accurate T_B calculations than a three-layer snow scheme. Furthermore, CLM4 is capable of simulating snow melt-refreeze cycles (depending on

snow temperature and ice/liquid water content within each snow layer) and densification processes (e.g., destructive metamorphism, compaction resulting from snow load or overburden, and melting metamorphism), which are critical inputs for RTMs to predict T_B. Therefore, CLM4 coupled with RTMs could potentially provide improved estimates of snow physical properties through RA.

CLM4 computes snow depth, snow grain radius, and mass of liquid water and ice within the snowpack every time step. SWE is the sum of snow liquid water and snow ice. Snow density (kg m^{-3}) is equal to SWE (kg m^{-2}) divided by snow depth (m). Therefore, updating all these snow variables separately in RA would violate their physical relationships and cause excessive updating of snow mass. *Zhang et al.* [2014] updated SWE only through data assimilation. The updated SWE was redistributed to the mass of snow liquid water and ice, and snow depth was adjusted based on its physical relationship with SWE by using the prior snow density. This updating scheme was used in this study.

3) Radiative transfer models

In the RA system, the RTM is an observational operator predicting T_B. Here, we used DMRT-ML [*Picard et al.*, 2013] to estimate microwave T_B from the snowpack. DMRT-ML is a multilayer microwave emission model that calculates the microwave scattering and absorption coefficients of snowpack based on the Dense Media Radiative Transfer (DMRT) theory [*Tsang and Kong*, 2001]. To solve the radiative transfer equation, the model employs the discrete ordinate radiative transfer (DISORT) method [*Jin*, 1994], which considers multiple scattering within and between the layers. The model is applicable to a frequency range of 1 to 200 GHz. DMRT-ML provides several combinations of reflectivity models and dielectric constant models for the snow-bottom interface (see Table 1 in *Picard et al.* [2013]). To estimate the effect of the underlying

soil on microwave emission, we used the rough bare soil reflectivity model by *Wegmüller and Mätzler* [1999] and calculated the soil dielectric constant based on *Dobson et al.* [1985]. Snow and soil inputs required by DMRT-ML include snow layer thickness, density, wetness, snow grain radius, snow and soil temperature, and soil water content, all of which are simulated by CLM4.

DMRT-ML has a stickiness parameter [*Ding et al.*, 2001] that affects the size of the scatterers. Stickiness depends on snow type and is difficult to obtain [*Picard et al.*, 2013]. It can be optimized using measurements as presented in *Kwon et al.* [2015]. In this study, however, due to the difficulty of the continental-scale optimization, it is updated in the DA system.

T_B at the top of the atmosphere (TOA) is modeled based on *Durand and Margulis* [2007]. To consider the effects of atmosphere and vegetation, we used the atmospheric RTM by *Ulaby et al.* [1981] as implemented in *Durand and Margulis* [2007], and vegetation transmissivity was calculated from the optical depth of vegetation (τ_c) [*Jackson and Schmugge*, 1991]:

$$\tau_c = b' \lambda^x w_c / \cos\theta \tag{3.1}$$

where b' and x are empirical coefficients, λ is the wavelength (cm), w_c is the vegetation water content (kg m^{-2}), which is estimated from the leaf area index (LAI) following *Paloscia and Pampaloni* [1988], and θ is the incident angle (55˚ for AMSR-E). Empirical coefficients (b' and x) depend on vegetation type and are also subject to update through RA in this study.

3.3.2 Data sets

1) AMSR-E brightness temperature observations

In this study, AMSR-E/Aqua Daily Global Quarter–Degree Gridded Brightness Temperatures (NISDC-0302; http://nsidc.org/data/nsidc-0302) data [*Knowles et al.*, 2006] were assimilated into model simulations. AMSR-E is a microwave radiometer flown on NASA's Earth Observing System (EOS) Aqua satellite. It observes TOA vertically (V-pol) and horizontally (H-pol) polarized microwave radiance at 6 frequencies: 6.925, 10.65, 18.7, 23.8, 36.5, and 89.0 GHz. *Durand and Margulis* [2006] reported that the 36.5 GHz channel contains the most significant information with respect to snow RA. Theoretically, it has been shown that microwave radiance at 18.7 GHz channel is sensitive to snow depth [e.g., *Tsang et al.*, 2000]. Therefore, two frequency channels (i.e., 18.7 and 36.5 GHz V-pol) were used in our RA experiments. Horizontally polarized brightness temperatures were not assimilated because they are sensitive to ice layer properties [*Mätzler*, 1987; *Durand et al.*, 2008; *Rees et al.*, 2010], which cannot be realistically represented by the five-layer snow model.

In *Durand and Margulis* [2006], the 18.7 GHz channel does not significantly contribute to correcting the SWE estimates due to competing relationships, i.e., a negative relationship between snow depth and T_B (based on sensitivity analysis) and a positive relationship between snow depth and T_B (resulting from a negative relationship between snow depth and snow grain size). This issue is also emphasized in our previous error characterization study [i.e., *Kwon et al.*, 2015]. As we hypothesized, however, the simultaneous update of states and parameters and the rule-based approach may be able to mitigate the problem. Although, the lower frequency channels (i.e., 6.925 and 10.65 GHz) provide valuable information for deep snowpack [*Durand and Margulis*, 2006], they were not exploited in this paper due to the huge computational demand of the

continental-scale RA experiments. However, the use of these additional frequencies may further improve the snow RA performance.

For computational efficiency, AMSR-E T_B observations (0.25˚ spatial resolution) were scaled up to the CLM4 grid (0.9˚ × 1.25˚). The use of the upscaled T_B reduced the computational demand to about 1/10 of the original demand. The observation error was roughly assumed to be 2 K. As recommended in *Kwon et al.* [2015], we used only nighttime T_B observations to minimize the effect of the snowpack wetness error.

2) Atmospheric ensemble forcing

We constructed 40 ensemble members of CLM4 simulations at 0.9˚ × 1.25˚ spatial resolution using the coupled DART/Community Atmospheric Model (CAM4) reanalysis [*Raeder et al.*, 2012] as atmospheric forcing. Compared to traditional approaches that perturb each atmospheric forcing field separately to produce the ensemble [e.g., *Andreadis and Lettenmaier*, 2006; *Su et al.*, 2008], the use of the DART/CAM4 reanalysis offers the advantage of physical consistency between forcing fields (such as downward short-wave radiation, air temperature, precipitation, wind speed, humidity, and atmospheric pressure).

All grid cells in CLM4 have the same UTC, whereas T_B has been observed by AMSR-E at approximately the same local time (1:30 am LST for the descending pass) for each grid cell. Therefore, based on the method suggested in *Zhao et al.* [submitted], we temporally shifted the original time series of DART/CAM4 reanalysis for each grid cell so that the CLM4 simulation time matches the AMSR-E observation time.

3) Independent snow data sources for validation

RA results were compared with two independent snow data sources, i.e., the Canadian Meteorological Centre (CMC) daily snow depth analysis data and the Moderate Resolution Imaging Spectroradiometer (MODIS) snow cover fraction (SCF) observations. The CMC product provides Northern Hemisphere daily snow depth [*Brasnett*, 1999; *Brown and Brasnett*, 2010] with approximately 24-km spatial resolution. The CMC analysis data are produced using snow depth data from surface synoptic observations and meteorological and special aviation reports acquired from the World Meteorological Organization (WMO) information system [*Brown and Brasnett*, 2010]. These daily snow depth data are considered the best available snow depth reference for model evaluations over the Northern Hemisphere [e.g., *Su et al.*, 2010; *Reichle et al.*, 2011].

The 0.05° MODIS/Terra level-3 daily global snow cover products (MOD10C1) [*Hall et al.*, 2006] are used for additional validation of the RA results. MODIS retrieves snow cover information using 36 spectral bands. A tile of daily snow cover data product at 500 m spatial resolution (MOD10A1) is produced using a snow-mapping algorithm based on a normalized difference snow index (NDSI), a normalized difference vegetation index (NDVI), and several criteria tests classifying image pixels [see *Riggs et al.*, 2006]. The MOD10C1 snow product is generated by merging MOD10A1 daily tiles and binning them to the 0.05° Climate Modeling Grid (CMG). For comparison purposes, we upscaled the original MOD10C1 data to the CLM4 grid ($0.9^{\circ} \times 1.25^{\circ}$) using the CMG confidence indices (CI) [see *Riggs et al.*, 2006 for further information on CI]. A higher CI indicates less cloud cover within a pixel and thus better quality SCF estimates. Only CMG grid cells that have the CI greater than 20% and a non-zero daily percentage of snow cover were considered during upscaling.

3.3.3 Experimental design

We hypothesized that continental-scale snow estimates in RA can be enhanced by simultaneously updating all model physical states of snow and soil and RTM parameters required for calculating T_B and through rule-based prior innovations. To demonstrate our hypothesis that the rule-based update can improve the RA performance, we conducted three classes of experiments (see Table 3.1): 1) open-loop run without assimilation, 2) default update in RA, and 3) rule-based update in RA. Ten sub-experiments were set up to demonstrate the effect of the simultaneous update of snow and soil states and RTM parameters on the RA performance (see Table 3.1). In the RA_{SWE} and $RA_{SWE\text{-}R}$ cases, only SWE related states including snow depth were updated. Additional updates of snow grain radius (RA_{SR} and $RA_{SR\text{-}R}$), snow temperature (RA_{SRT} and $RA_{SRT\text{-}R}$), soil water content and temperature (RA_{SRTS} and $RA_{SRTS\text{-}R}$), and RTM parameters (RA_{SRTSP} and $RA_{SRTSP\text{-}R}$) were considered in the other eight sub-experiments. In the RA_{SRTSP} and $RA_{SRTSP\text{-}R}$ cases, initial values of three RTM parameters were randomly generated for each grid cell and each ensemble member within the given ranges (i.e., $0.1 \leq$ snow stickiness ≤ 0.5, $-1.656 \leq x \leq -0.804$, and $0.496 \leq b' \leq 0.744$). For all other RA cases, we used constant values of 0.2 (for stickiness), –1.23 (for x), and 0.62 (for b') for all grid cells and ensemble members during the simulation period. All 11 experiments were driven by the 40 randomly chosen ensemble members of the DART/CAM4 reanalysis over North America for December 2002 to February 2003. In the RA cases, AMSR-E T_B observations at two frequency channels (i.e., 18.7-V and 36.5-V) were assimilated. Note

that the states and parameters in the current RA system are not updated when one or more of the ensemble members in a grid cell have no snow.

Table 3.1. List of experiments and updated states and parameters in each experiment.

Cases		Updated states and parameters					
		SWE	Snow depth	Snow grain radius	Snow temperature	Soil water content and soil temperature	RTM parameters
Open-loop		·	·	·	·	·	·
Default update in RA	RA_{SWE}	○	○	·	·	·	·
	RA_{SR}	○	○	○	·	·	·
	RA_{SRT}	○	○	○	○	·	·
	RA_{SRTS}	○	○	○	○	○	·
	RA_{SRTSP}	○	○	○	○	○	○
Rule-based update in RA	RA_{SWE-R}	○	○	·	·	·	·
	RA_{SR-R}	○	○	○	·	·	·
	RA_{SRT-R}	○	○	○	○	·	·
	RA_{SRTS-R}	○	○	○	○	○	·
	$RA_{SRTSP-R}$	○	○	○	○	○	○

Rodell and Houser (2004) suggested a rule-based DA method to assimilate MODIS SCF observations because of a threshold (non-continuous) relationship between SCF and SWE. In their rule-based DA, a thin snow layer (i.e., 5 mm SWE) is added to model grid cells where MODIS SCF is greater than 0.4 but the model simulated no snow. When MODIS SCF is less than 0.1, the simulated SWE is set to zero. For grid cells where the observed SCF is between 0.1 and 0.4, no change is applied to the modeled SWE. However, our rule-based approach in RA is different in that the rule is determined based on a sensitivity analysis. Only when correlations between the prior estimates (of snow/soil states and RTM parameters) and the prior T_B have the same signs as the sensitivity index, are the priors updated.

We analyzed the sensitivity of T_B to snow/soil states and RTM parameters, i.e., SWE, snow grain radius, snow temperature, soil temperature, soil water content, snow stickiness (in DMRT-ML), and two empirical parameters (x and b' in the vegetation RTM), all of which are updated in the RA scheme. The sensitivity index was calculated using an equation suggested by *Lenhart et al.* [2002]:

$$I = \frac{(y_2 - y_1)/y_0}{2\Delta x / x_0} \tag{3.2}$$

where I is the dimensionless sensitivity index, x_0 is the initial value of states and parameters being tested, Δx is the variation, and y_0, y_1 and y_2 are brightness temperatures estimated using x_0, x_1 (= $x_0 - \Delta x$), and x_2 (= $x_0 + \Delta x$), respectively. For the sensitivity analysis, a single-layer dry snowpack was assumed and ±10% perturbations were applied to default values of SWE (181.6 kg m^{-2}), snow grain radius (251 μm), soil water content (0.1), snow stickiness (0.2), x (–1.23), and b' (0.62). In reality, snow temperature (270 K) and soil temperature (270 K) were perturbed by ±3 K. As mentioned previously, we assumed that the SWE update determines the snow depth update, whereas snow density is not changed during the assimilation. In addition, SWE is not an input to DMRT-ML but snow depth is used to estimate T_B. Therefore, the sensitivity of T_B to SWE was calculated by applying the variation (= 18.16 kg m^{-2}) of SWE to the variation (= 0.08 m) of snow depth (the default was set to 0.8 m).

The use of small ensemble size for the computational efficiency of the DA system can cause a large sampling error and subsequently lead to spurious large correlations between two uncorrelated variables [*Anderson*, 2007]. DART has a localization distance parameter, which can be tuned for different observation types. The localization distance minimizes this negative effect by reducing the impact of observations on model states of neighboring grid cells [*Anderson et al.*, 2009]. For the above-mentioned experiments, we used the localization distance of 0.03 radians according to *Zhang et al.* [2014]. Here, we conducted additional RA experiments (with localization distances of 0.01, 0.05, 0.07, 0.1, 0.15, 0.2, and 0.3 radians) to find out the proper localization distance for the coupled RA system used in this study.

We also tested the effect of inflation on the snow RA performance. In ensemble DA, the ensemble spread decreases as more information from observations is assimilated into the system. This may cause filter divergence [*Anderson et al.*, 2009]. Inflation helps the DA system to maintain adequate variability by increasing the variance (uncertainty) of the ensemble estimate [*Anderson*, 2009]. The spatially and temporally varying adaptive inflation [*Anderson*, 2009] in DART was employed in this study. In the localization and inflation experiments, all model states and RTM parameters were simultaneously updated with and without the rule.

3.4 RESULTS AND DISCUSSION

In this section, we present the assimilation results using the coupled RA system. The RA results are assessed using the CMC daily snow depth analysis and MODIS SCF observations.

3.4.1 Simultaneous update of states and parameters

1) Snow depth estimation

Figure 3.2 shows the results of the open-loop case without assimilation. Compared to the CMC snow depth analysis data, CLM4 greatly overestimated snow depth for most of northern North America while the difference between the CMC and CLM4 snow depth is relatively small for the United States and southern Canada.

By updating only SWE related snow states in RA (RA_{SWE}), we were not able to improve snow depth estimates (see Figure 3.3a). In Figure 3.3, which shows the snow depth root mean square error (RMSE) differences between the RA and open-loop cases, negative (or positive) values denote the improvement (or degradation) of the RA performance. Although compared to the open-loop run, the RA_{SWE} shows a minor improvement in snow depth estimates for some areas, the snow depth error is much greater for most of the study area, especially for northeastern North America.

This degeneration of the RA performance is much ameliorated in the RA_{SR} case by additionally updating snow grain size (see Figures 3.3b and 3.3f). As emphasized in *Kwon et al.* [2015], when snow grain radius is greatly biased, the T_B error (= simulation – observation) is contributed primarily by the snow grain radius error but not by the SWE error. In this case, we cannot expect a proper update of SWE in RA, even though SWE and T_B show a high correlation. Accordingly, we might improve the RA performance by reducing the effect of the snow grain radius error on the T_B error in the RA_{SR} case.

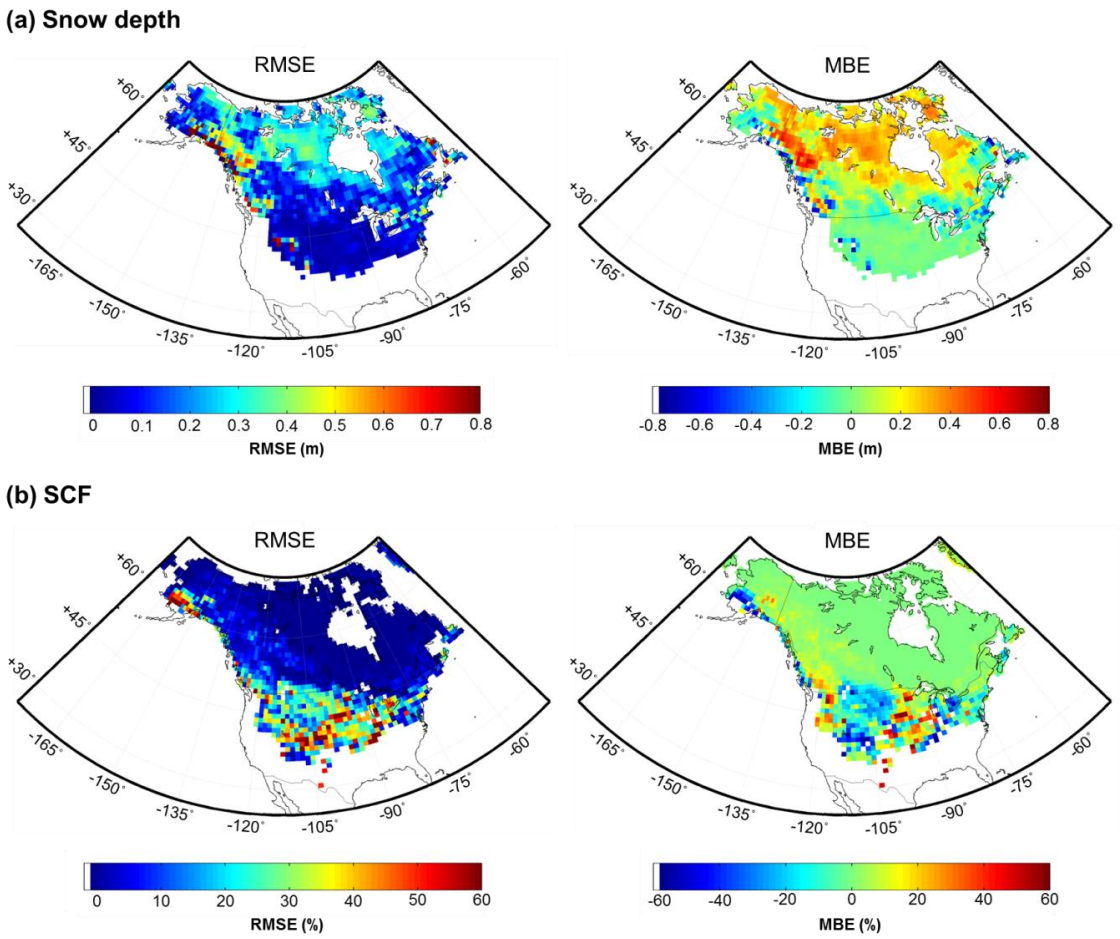

Figure 3.2. Simulation results of the open-loop case for (a) snow depth and (b) SCF. The root mean square error (RMSE) and mean bias error (MBE) were calculated by comparing the results with the CMC snow depth and MODIS SCF for December 2002 to February 2003.

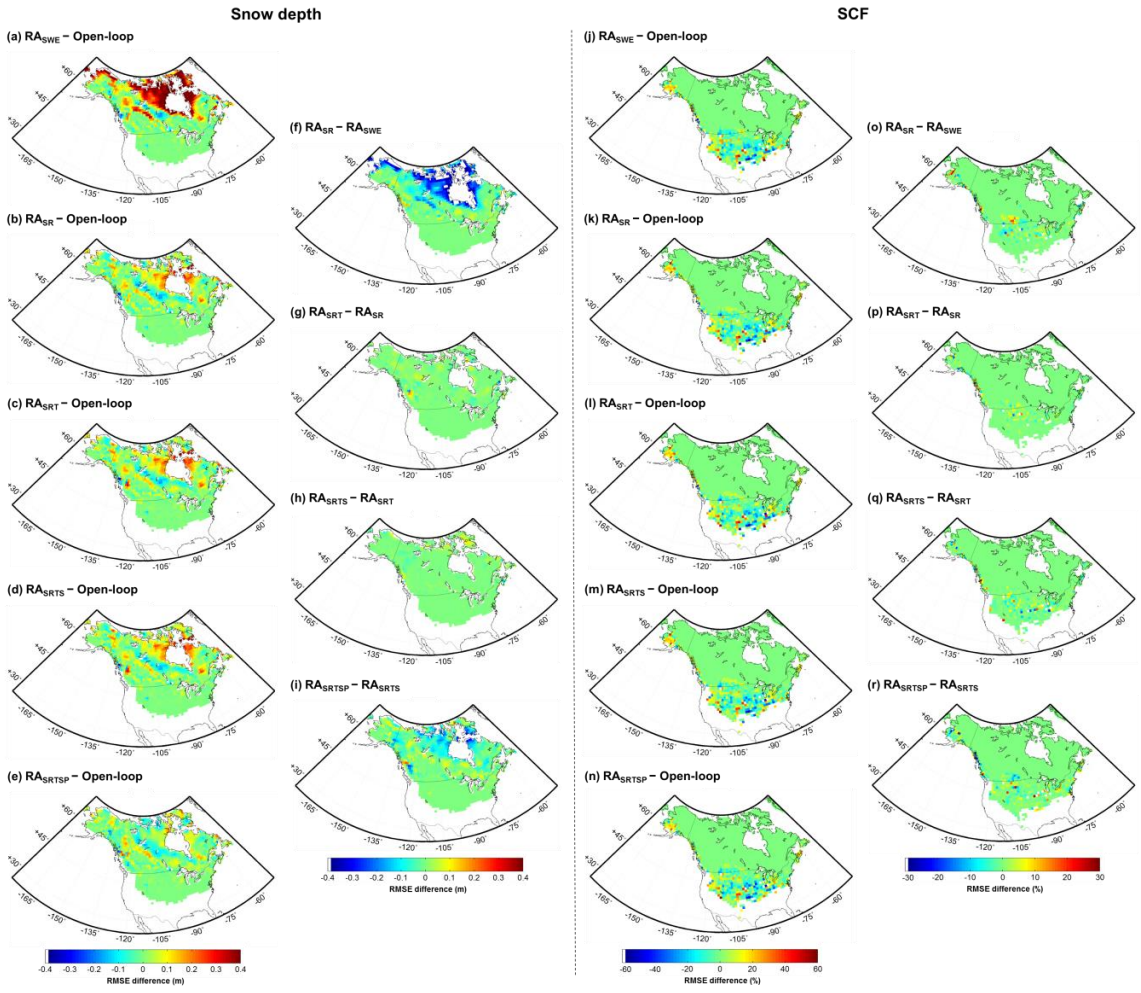

Figure 3.3. RMSE differences for (a to i) snow depth and (j to r) SCF: (a and j) RA_{SWE} − Open-loop, (b and k) RA_{SR} − Open-loop, (c and l) RA_{SRT} − Open-loop, (d and m) RA_{SRTS} − Open-loop, (e and n) RA_{SRTSP} − Open-loop, (f and o) RA_{SR} − RA_{SWE}, (g and p) RA_{SRT} − RA_{SR}, (h and q) RA_{SRTS} − RA_{SRT}, and (i and r) RA_{SRTSP} − RA_{SRTS}. In the RA cases, the default update method was used.

However, additional updates of snow temperature (RA_{SRT}) and soil temperature and water content (RA_{SRTS}) did not significantly improve the RA performance (see Figures 3.3c, 3.3d, 3.3g, and 3.3h). As shown in *Kwon et al.* [2015], CLM4 provides a

relatively accurate simulation of snow temperature. In addition, the ensemble spread of snow temperature was much smaller than that of other snow physical states, especially snow grain radius (not shown here). Therefore, the snow temperature uncertainty could not significantly contribute to the uncertainty of the simulated T_B despite T_B is highly and positively sensitive to snow temperature. As a result, the additional snow temperature update did not make a substantial difference in the RA performance between the RA_{SRT} and RA_{SR} cases. Meanwhile, the marginal improvement in the RA_{SRTS} case can be attributed to the fact that the effect of the underlying soil on microwave emission from the snowpack is insignificant over the region where snow depth is relatively deep and mostly overestimated by the model (see Figure 3.2a).

In the RA_{SRTSP} case, we achieved noticeable improvement in the snow depth estimation in particular for the northeastern and western parts of Canada (see Figures 3.3e and 3.3i). This implies that the constant values of snow stickiness (0.2), x (–1.23), and b' (0.62) adopted in this study are not applicable to all continental grid cells and that the update of parameters in the DA system is a large-scale alternative where parameter optimization is difficult. Figure 3.4 shows the spatial distributions of the parameter ensemble mean updated in the coupled RA system. The figure shows that the parameter values were not significantly changed during the simulation period after they approached certain values for each grid cell.

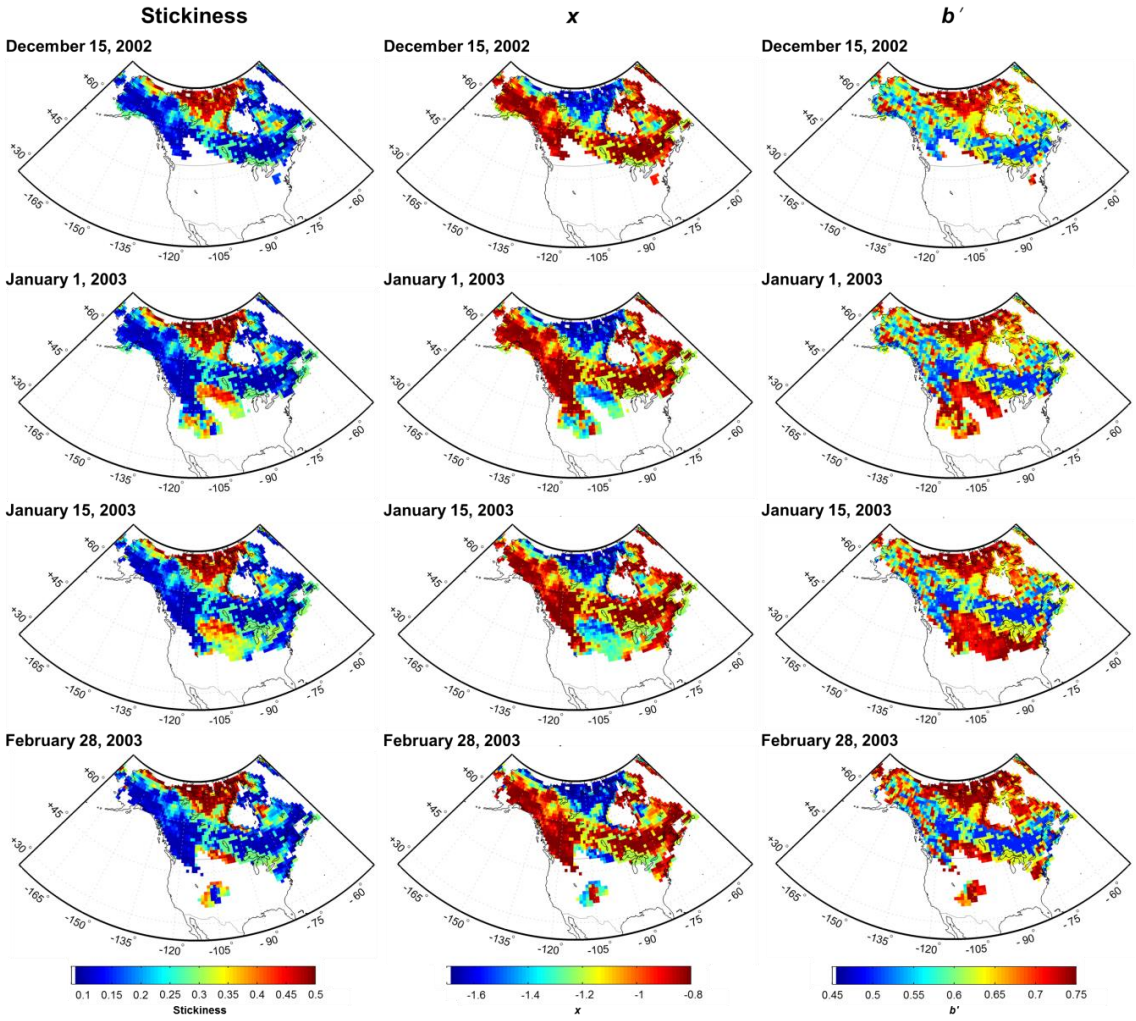

Figure 3.4. Spatial distributions of the ensemble mean of the RTM parameters (i.e., snow stickiness in DMRT-ML and x and b' in the vegetation RTM) on 15 December 2002, 1 and 15 January 2003, and 28 February 2003.

2) SCF estimation

In contrast to the snow depth estimation, the SCF bias of the open-loop run was very small for most of Canada while SCF was greatly overestimated or underestimated over the United States including Alaska (see Figure 3.2b). CLM4 estimates SCF from the

simulated snow depth and density using the snow cover parameterization developed by *Niu and Yang* [2007], which is based on monthly averaged snow depth and SCF and thus it may not be applicable to the simulation at a daily time scale [*Swenson and Lawrence*, 2012]. Therefore, the large SCF bias in the United States may result from this snow cover parameterization because the snow depth bias was marginal for the same region (see Figure 3.2a). The SCF RMSE was almost zero for deep snowpack regions in northeastern North America (see Figure 3.2b), where snow depth was greatly overestimated (see Figure 3.2a) and SCF is saturated (i.e., 100% SCF).

Overall, for many areas of the United States, the SCF estimation in RA was better than the open-loop run, although it was not as accurate for some regions including southwest Alaska (see Figures 3.3j to 3.3n). However, unlike the snow depth estimation, the improvement of the RA performance resulting from the simultaneous update was not that obvious (see Figures 3.3o to 3.3r).

The results in Figure 3.3 show that RA is effective in improving the snow depth estimation for relatively deep snowpack regions and the SCF estimation for relatively shallow snowpack regions. Because SCF in the observation and model simulation was already saturated (i.e., SCF was almost 100%) for deep snowpack regions over Canada, the improvement of snow depth in RA did not affect the SCF estimation for these regions. As reported by previous DA studies using SCF observations [e.g., *Rodell and Houser*, 2004; *Andreadis and Lettenmaier*, 2006; *Su et al.*, 2008; *Zaitchik and Rodell*, 2009; *De Lannoy et al.*, 2012; *Zhang et al.*, 2014), SCF DA does not work for areas where SCF already approaches 100% because satellite SCF data cannot detect additional snow mass or snow depth variations when the ground is fully covered with snow. The results in this paper imply that RA can complement SCF DA as it provides more information about snow for deep snowpack regions.

3.4.2 Rule-based RA

1) Snow depth estimation

In the rule-based RA, as previously mentioned, we hypothesized that only when the sign of the correlation between the forecasted states/parameters and the predicted T_B is the same as the sign of the sensitivity index, the T_B difference will provide meaningful information for each of the priors. The sensitivity analysis results are shown in Figure 3.5. T_B is negatively sensitive to SWE, snow grain radius, and soil water content while it is positively sensitive to snow and soil temperature, snow stickiness, and b' for both 18.7-V and 36.5-V channels. The sensitivity of T_B to x is positive for 18.7-V and negative for 36.5-V. In the rule-based RA, the states and parameters were updated when the signs of their correlations with the prior T_B coincided with those of the sensitivity indices.

In the rule-based RA cases, the performance of the coupled RA system was also enhanced via the simultaneous update of states and parameters (see Figures 3.6a to 3.6i). The additional update of snow grain radius ($RA_{SR\text{-}R}$) greatly reduced the snow depth error in the central to southern parts of Canada (see Figure 3.6f). However, the effects of the updates of snow temperature ($RA_{SRT\text{-}R}$) and soil temperature and water content ($RA_{SRTS\text{-}R}$) on the RA performance were insignificant (see Figures 3.6g and 3.6h). The snow depth RMSE largely diminished in the southern and western parts of Canada by additionally updating the RTM parameters ($RA_{SRTSP\text{-}R}$) (see Figure 3.6i).

Compared to the default RA cases, snow depth estimates in the rule-based RA were more accurate in many areas of North America, especially northeastern Canada (see Figures 3.7a to 3.7e). However, the rule-based RA performed worse than the default RA in mid-latitudes of Canada, particularly in the $RA_{SWE\text{-}R}$ case (see Figure 3.7a).

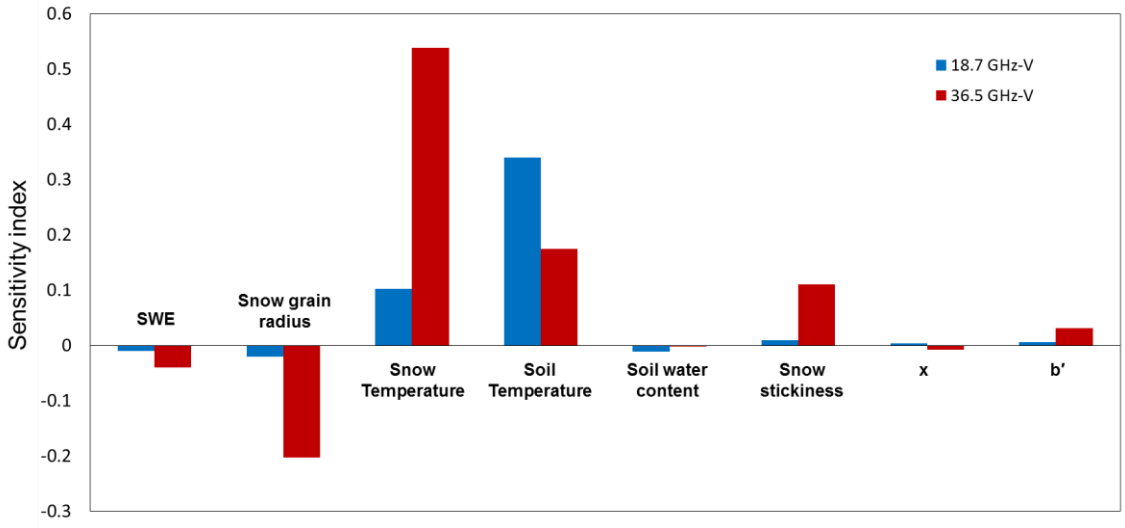

Figure 3.5. Sensitivity of brightness temperature to snow and soil physical properties (i.e., SWE, snow grain radius, snow temperature, soil temperature, and soil water content) and RTM parameters (i.e., snow stickiness in DMRT-ML and two empirical parameters (x and b') in the vegetation RTM). Dimensionless sensitivity indices were calculated based on the method suggested by *Lenhart et al.* [2002].

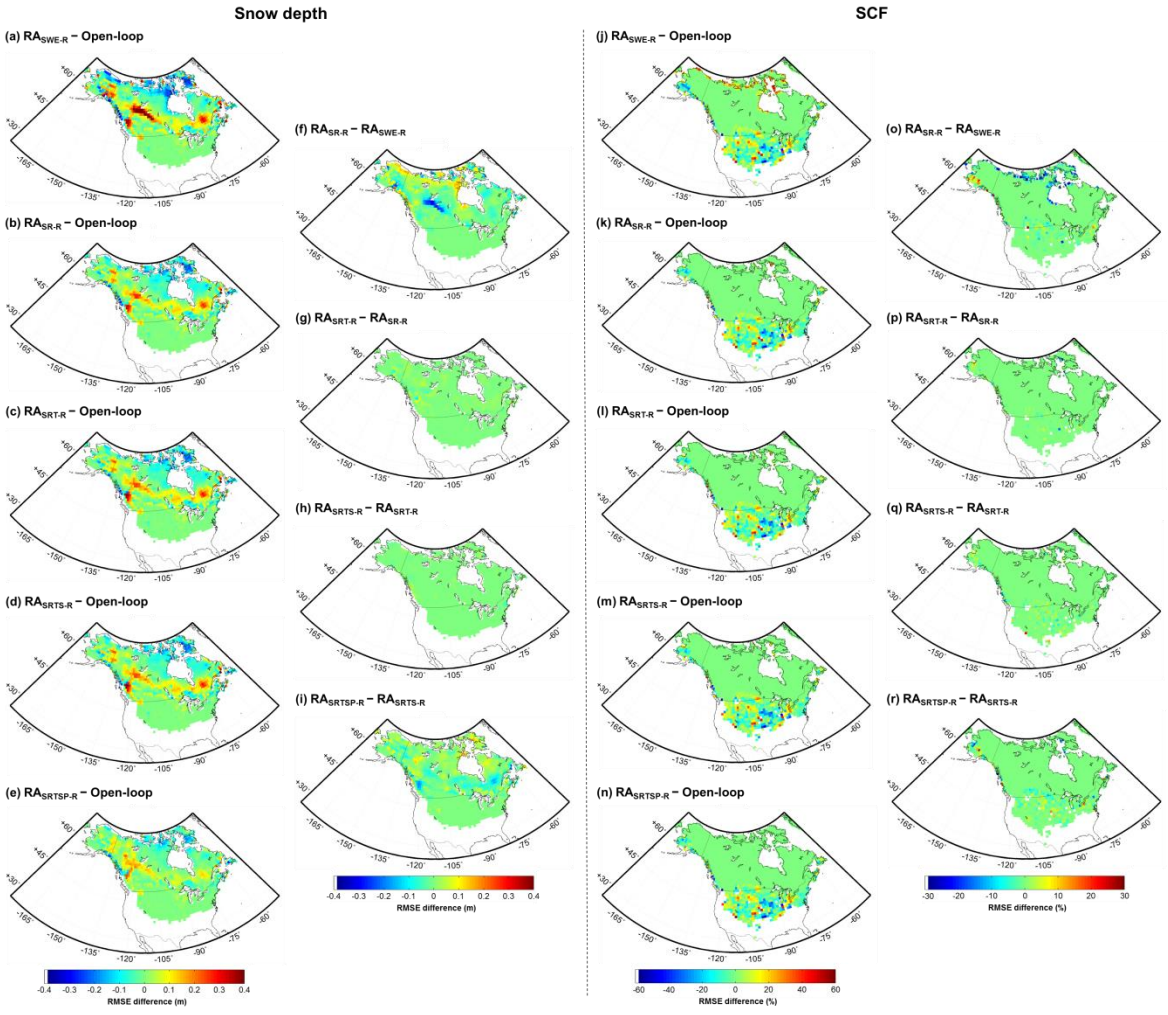

Figure 3.6. RMSE differences for (a to i) snow depth and (j to r) SCF: (a and j) RA_{SWE-R} − Open-loop, (b and k) RA_{SR-R} − Open-loop, (c and l) RA_{SRT-R} − Open-loop, (d and m) RA_{SRTS-R} − Open-loop, (e and n) $RA_{SRTSP-R}$ − Open-loop, (f and o) RA_{SR-R} − RA_{SWE-R}, (g and p) RA_{SRT-R} − RA_{SR-R}, (h and q) RA_{SRTS-R} − RA_{SRT-R}, and (i and r) $RA_{SRTSP-R}$ − RA_{SRTS-R}. In the RA cases, the rule-based update method was used.

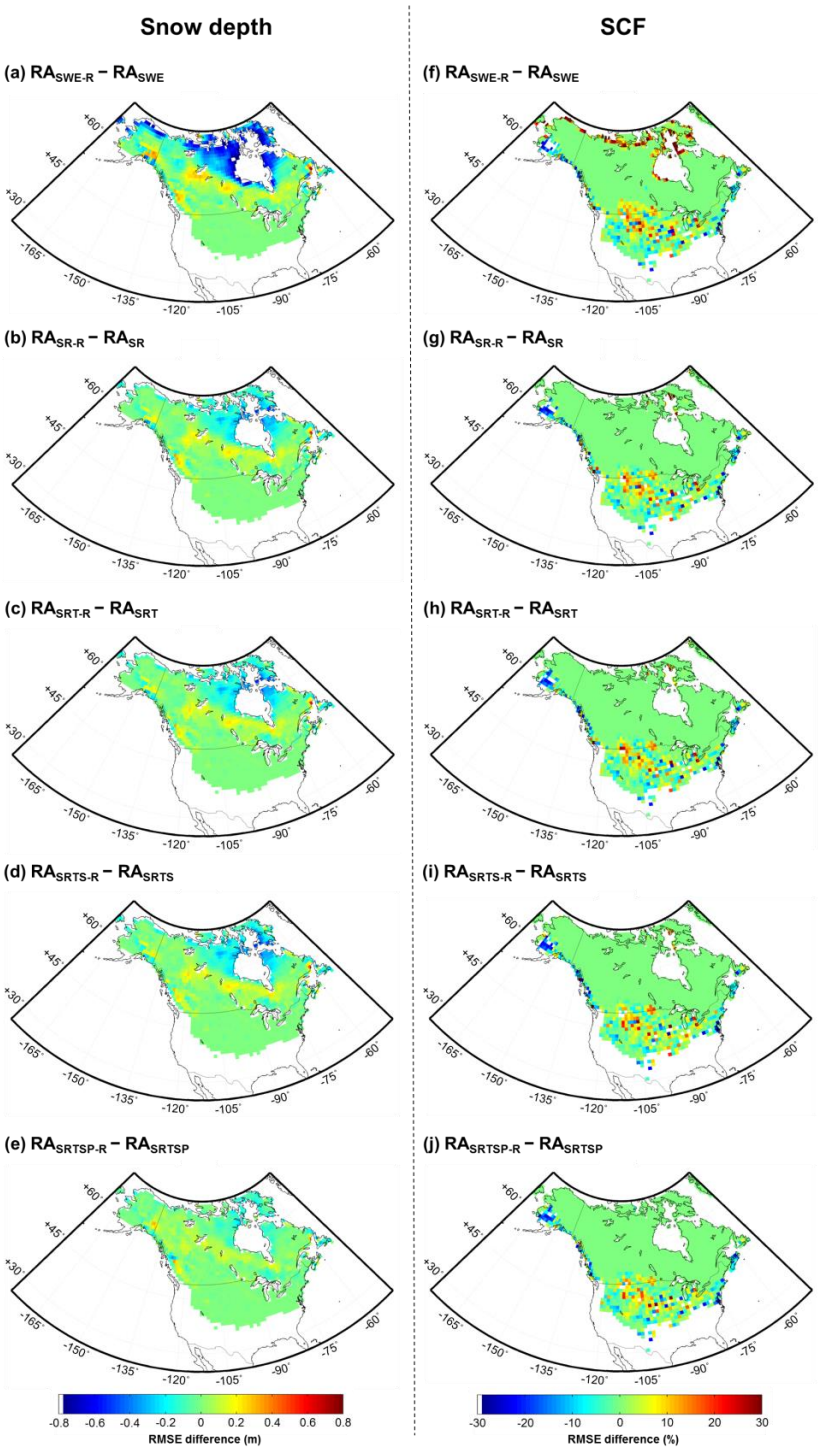

Figure 3.7. The snow depth (a to e) and SCF (f to j) RMSE differences between the RA cases with a rule-based update and with default update.

The RA performance deteriorates in two possible cases: 1) the prior SWE (or snow depth) is positively correlated with the prior T_B, and SWE (or snow depth) and T_B are overestimated and underestimated, respectively, as described in Figure 3.8a, and 2) the prior SWE and T_B show a negative correlation but both SWE (or snow depth) and T_B are overestimated due to the effects of other factors, such as a greatly underestimated snow grain radius (see Figure 3.8b). Ideally the prior SWE (or snow depth) should have a negative correlation with the prior T_B based on the sensitivity analysis results. However, a positive correlation between the prior SWE and T_B can happen when the T_B signal is dominated by snow density, when SWE (or snow depth) is negatively correlated with snow grain radius [*Kwon et al.*, 2015], or when imprecise values of the RTM parameters are used. In the first possible case of degeneration (see Figure 3.8a), the RA system tries to raise T_B and as a result SWE (or snow depth) is further overestimated as shown in Figure 3.3a because of the positive correlation between SWE and T_B. This negative effect of RA can be moderated by two approaches, i.e., the simultaneous update of states and parameters (see Figures 3.3a to 3.3e) and the rule-based update (see Figure 3.7a). As we can see from Figure 3.7e, snow depth RMSE differences between the rule-based and default RA cases are reduced when all the model physical states of snow and soil and RTM parameters are simultaneously updated.

In the second possible case of degradation (see Figure 3.8b), the RA system tries to lower T_B and as a result SWE (or snow depth) is further overestimated. This may be the principal reason for the degraded performance of the rule-based RA in mid-latitudes of Canada as shown in Figure 3.6a. This problem was partly resolved by additionally updating snow grain radius (see Figure 3.6f) and parameters (see Figure 3.6i); however, RA still degraded the snow depth estimates compared to the open-loop run for the region (see Figure 3.6e).

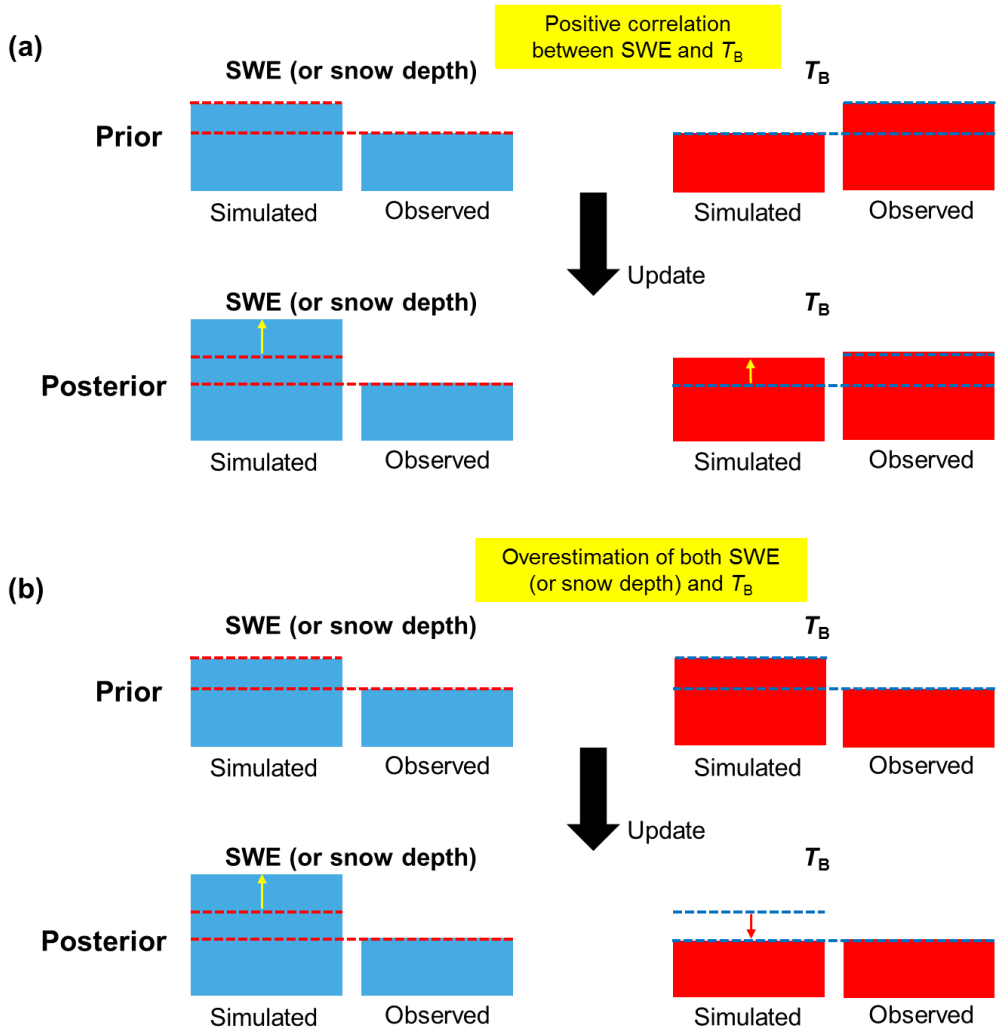

Figure 3.8. Degradation of the RA performance due to: (a) incorrect relationships between the prior SWE (or snow depth) and T_B and (b) overestimation of both SWE (or snow depth) and T_B with a negative correlation between them.

2) SCF estimation

Compared to the open-loop run, the rule-based RA improved the SCF estimates for many areas in the United States including Alaska (see Figure 3.6). Although the SCF estimation error of the $RA_{SWE\text{-}R}$ case was larger than that of the open-loop run in the

coastal areas of northern Canada (see Figure 3.6j), the RA performance for those areas was reinforced by additionally updating snow grain size (see Figures 3.6k and 3.6o). However, like the default RA cases, the improvement of the SCF estimates by simultaneously updating states and parameters was not significant (see Figures 3.6o to 3.6r). The rule-based RA outperformed the default RA over Alaska and western and eastern coastal areas of North America (see Figures 3.7f to 3.7j) but overall both the default and rule-based RA showed comparable performance in estimating SCF over the United States (see Figure 3.7j).

3.4.3 Localization and adaptive inflation

The results of the localization and inflation experiments are shown in Figure 3.9. The T_B RMSE was calculated by comparing the results with AMSR-E T_B observations. As shown in Figure 3.9, the rule-based RA was superior to the default RA with respect to T_B estimations and the localization distance of 0.01 radians provided the smallest T_B RMSE for both the default and rule-based RA. The localization distance (0.01 radians) obtained here is smaller than that from *Zhang et al.* [2014] (0.03 or 0.05 radians) using MODIS SCF observations. This can likely be explained by high spatial heterogeneity of various factors (i.e., snow depth, snow temperature, snow density, snow grain size, snow wetness, soil temperature, soil water content, and vegetation) influencing T_B over snow-covered regions.

In the inflation experiments, the localization distance of 0.01 radians was used. Adaptive inflation further improved T_B estimations for the default RA (see the solid red triangle in Figure 3.9) while the T_B RMSE of the rule-based RA with inflation was almost the same as that without applying inflation (see the hollow red triangle in Figure 3.9).

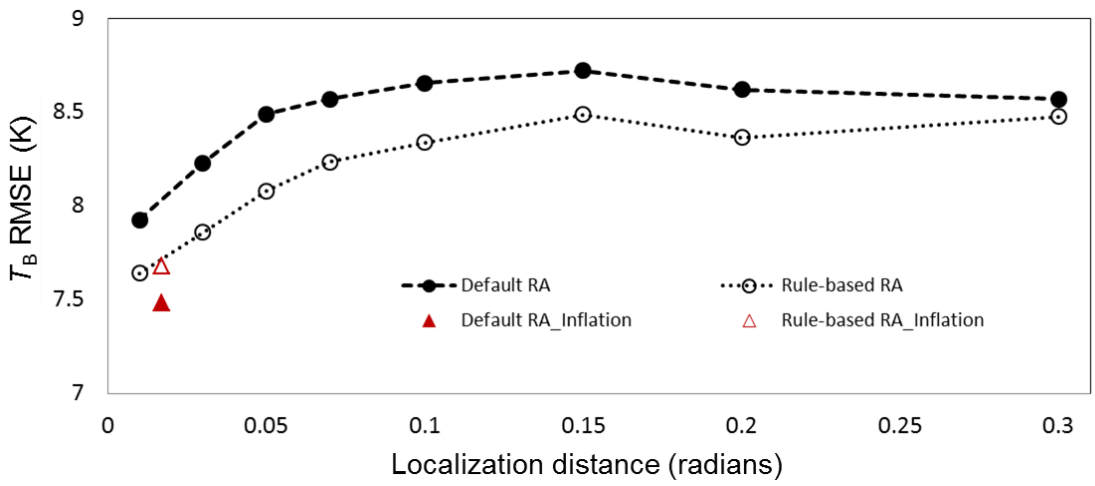

Figure 3.9. The prior T_B RMSE of the RA cases with localization distances of 0.01, 0.03, 0.05, 0.07, 0.1, 0.15, 0.2, and 0.3 radians. The RMSE values were averaged over North America. The solid and hollow symbols represent the default and rule-based RA cases, respectively. The red triangle symbols denote the results of RA using the adaptive inflation and the localization distance of 0.01 radians, which are plotted slightly displaced laterally from their original position for clearness.

The RA performance in estimating snow depth was analyzed for snow classes and land covers (Tables 3.2 and 3.3). For all RA cases in Tables 3.2 and 3.3, the localization distance of 0.01 radians was used. In the $RA_{SRTSP/INF}$ and $RA_{SRTSP\text{-}R/INF}$ cases, adaptive inflation was additionally applied. Snow cover was classified into six classes (i.e., tundra, taiga, alpine, maritime, prairie, and ephemeral) as defined in *Sturm et al.* [1995] (see Figure 3.10a) and land cover was classified into five groups (i.e., bare soil, forest, shrub, grass, and crop) using CLM4 plant functional types (PFTs) (see Figure 3.10b). Tables 3.2 and 3.3 exhibit that the rule-based RA outperforms the default RA in estimating snow depth and the rule-based RA without inflation ($RA_{SRTSP\text{-}R}$) provides the most improved snow depth estimates. Compared to the open-loop run, the default RA (RA_{SRTSP})

degraded snow depth estimates for most snow classes and land covers, except for maritime snow class and crop land cover.

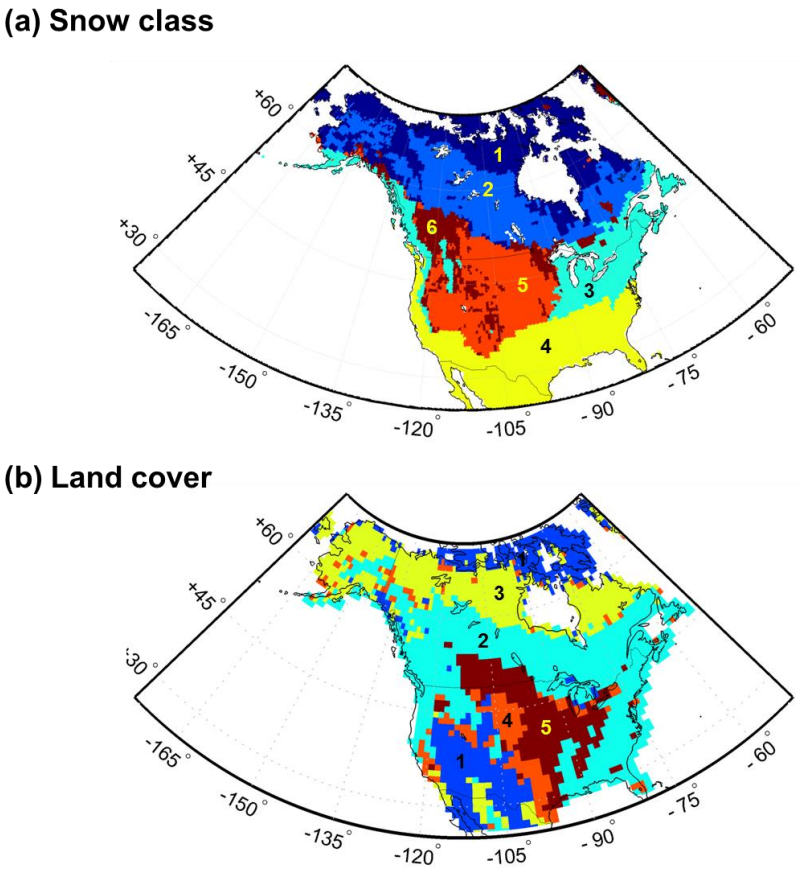

Figure 3.10. Maps of (a) snow classes and (b) land cover types over North America. Snow cover was classified into six classes (1: tundra, 2: taiga, 3: maritime, 4: ephemeral, 5: prairie, and 6: alpine) according to *Sturm et al.* [1995]. Land cover was classified into five groups (1: bare soil, 2: forest, 3: shrub, 4: grass, and 5: crop) using CLM4 plant functional types (PFTs).

Although the T_B estimation in the default RA was enhanced by using adaptive inflation (see Figure 3.9), it did not ensure improved snow depth estimates (see the results of the $RA_{SRTSP/INF}$ case in Tables 3.2 and 3.3). The use of inflation also degraded the

snow depth estimates in the rule-based RA (see the results of the $RA_{SRTSP-R/INF}$ case in Tables 3.2 and 3.3). One possible reason is that the current inflation scheme in DART would not be able to consider the physical relationships between snow/soil states updated simultaneously in the RA system. As a result, inflation would result in the abnormal update of model states in this RA study. However, because adaptive inflation is a helpful method to improve the data assimilation performance, future RA studies need to address this issue for the proper use of the method.

The rule-based RA without inflation ($RA_{SRTSP-R}$) was effective only for tundra and maritime but it degraded the snow depth estimates for other snow classes, in particular for taiga (see Table 3.2). The use of only one snowpack RTM may be one of possible reasons for the results because the existing snowpack RTMs show limited performance in estimating T_B for different snow conditions [*Tedesco and Kim*, 2006]. Using multiple RTMs for snowpack T_B, as suggested in *Kwon et al.* [2015], the coupled RA system would enhance the snow estimates for various snow types. The other plausible reason is the poor performance of our coupled RA system for forested areas (see Table 3.3). Table 3.3 shows that compared to the open-loop run, the $RA_{SRTSP-R}$ case enhanced the snow depth estimates for all land cover types, except for forest. As shown in Figure 3.10, most areas of the snow classes, where the RA system exhibited worse performance, overlap with forest areas. Significant improvement of the snow depth estimates in the rule-based RA ($RA_{SRTSP-R}$) was observed for bare soil (see Table 3.3 and Figure 3.11). Although the $RA_{SRTSP-R}$ improved the snow depth estimates for shrub, grass, and crop land cover types, it was marginal as shown in Figure 3.11. We used a simple empirical equation to estimate the vegetation effect on T_B at the TOA (see equation (1)). Although the empirical coefficients in the equation were updated in the RA system, it may not be enough to accurately represent the vegetation effect. The use of more sophisticated vegetation

RTMs, applicable to large scale, would further improve the RA performance for vegetated areas.

Table 3.2. The snow depth RMSE of each case for snow classes as defined in *Sturm et al.* [1995]. The localization distance of 0.01 radians was used for all RA cases. Adaptive inflation was applied in the RASRTSP/INF and RASRTSP-R/INF cases. The percentage values in parentheses represent the relative improvement (negative values) or degradation (positive values) in the performance of the RA cases compared to the open-loop run.

	RMSE (m) for snow classes						
Cases	Tundra	Taiga	Maritime	Ephemeral	Prairie	Alpine	Total
Open-loop	0.2383	0.1758	0.1521	0.0270	0.0448	0.1251	0.1708
RA_{SRTSP}	0.2478 (3.99%)	0.1839 (4.61%)	0.1497 (**–1.58%**)	0.0402 (48.89%)	0.0466 (4.02%)	0.1288 (2.96%)	0.1769 (3.57%)
$RA_{SRTSP\text{-}R}$	0.2108 (**–11.54%**)	0.1883 (7.11%)	0.1493 (**–1.84%**)	0.0396 (46.67%)	0.0463 (3.35%)	0.1312 (4.88%)	01680 (**–1.64%**)
$RA_{SRTSP/INF}$	0.6372 (167.39%)	0.3635 (106.77%)	0.1719 (13.02%)	0.0403 (49.26%)	0.0538 (20.09%)	0.1730 (38.29%)	0.3795 (122.19%)
$RA_{SRTSP\text{-}R/INF}$	0.5499 (130.76%)	0.3861 (119.62%)	0.1669 (9.73%)	0.0394 (45.93%)	0.0518 (15.63%)	0.1918 (53.32%)	0.3651 (113.76%)

Table 3.3. Same as Table 3.2 but for land covers.

	RMSE (m) for land covers					
Cases	Bare soil	Forest	Shrub	Grass	Crop	Total
Open-loop	0.2100	0.1614	0.2211	0.1068	0.0474	0.1708
RA_{SRTSP}	0.2142 (2.00%)	0.1692 (4.83%)	0.2294 (3.75%)	0.1092 (2.25%)	0.0470 (**–0.84%**)	0.1769 (3.57%)
$RA_{SRTSP\text{-}R}$	0.1817 (**–13.48%**)	0.1731 (7.25%)	0.2095 (**–5.25%**)	0.1050 (**–1.69%**)	0.0471 (**–0.63%**)	0.1680 (**–1.64%**)
$RA_{SRTSP/INF}$	0.5093 (142.52%)	0.3074 (90.46%)	0.5418 (145.05%)	0.2769 (159.27%)	0.0604 (27.43%)	0.3795 (122.19%)
$RA_{SRTSP\text{-}R/INF}$	0.4165 (98.33%)	0.3402 (110.78%)	0.4969 (124.74%)	0.2604 (143.82%)	0.0551 (16.24%)	0.3651 (113.76%)

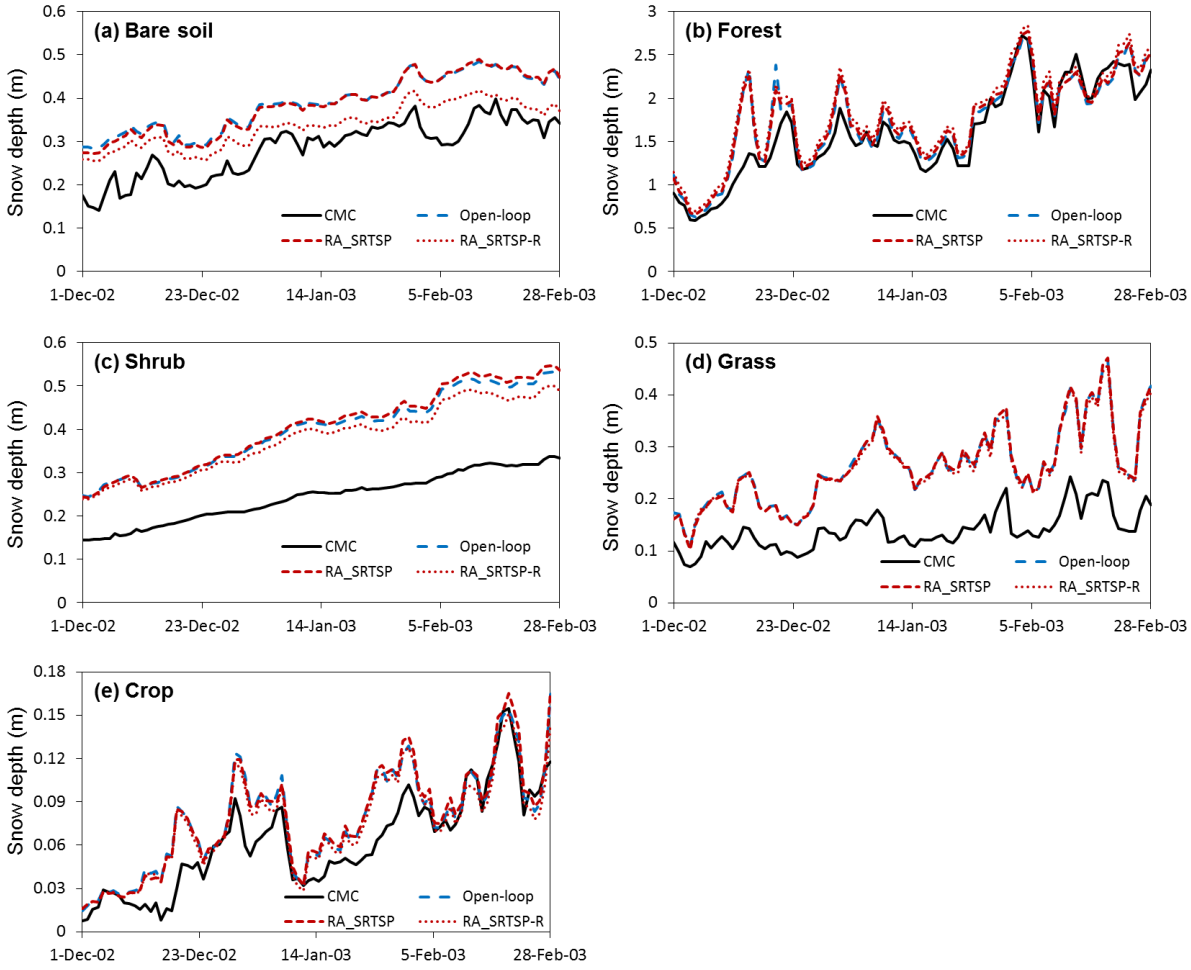

Figure 3.11. Time series of snow depth (in meters) for land covers: (a) bare soil, (b) forest, (c) shrub, (d) grass, and (e) crop. The localization distance of 0.01 radians was used for the radiance assimilation (RA) cases.

3.5 CONCLUSIONS

In this study, we aimed to demonstrate the feasibility of the coupled RA system (i.e., coupled CLM4/DART/RTMs) to enhance snow estimation at the continental scale. To this end, two hypotheses were established: 1) the simultaneous update of model states and parameters can improve snow estimation by minimizing the effects of their errors on

the T_B error; and 2) updating states and parameters based on a rule, the degradation of RA performance, which is attributed to incorrect relationships between the prior SWE (or snow depth) and T_B, can be managed. AMSR-E T_B at 18.7-V and 36.5-V were assimilated into the coupled RA system and the results were assessed using the CMC daily snow depth and MODIS SCF observations. In total, 11 experiments were conducted over North America for December 2002 to February 2003 and their performances were compared to each other.

The results in this paper show that RA performance is improved by both the simultaneous update and rule-based update. The additional updates of snow grain radius and RTM parameters greatly improved the snow depth estimates over North America while the improvement by updating snow temperature, soil temperature, and soil water content was not significant. For both the default and rule-based RA cases, the additional updates of states and parameters could not obviously improve the SCF estimates.

The rule-based RA was more effective in estimating snow depth than the default RA when only SWE related snow states were updated. Simultaneously updating all states and parameters, the degradation of the performance of both the default and rule-based RA was mitigated and eventually the default RA showed comparable performance to the rule-based RA. This indicates that the updates of all states and parameters can reduce the T_B errors related to them and consequently lead to considerable improvement of the relationship between SWE (or snow depth) and T_B. The results also demonstrate that the parameter update in the DA system can be an alternative way of optimizing parameter values on a large scale.

RA was effective in improving snow depth simulations for relatively deep snowpack regions, especially over northeastern Canada, where SCF observations could not provide additional information about snow mass or snow depth variations. This

implies that RA can complement SCF DA and thus a multi-sensor snow DA using T_B and SCF could provide improved snow estimates at the continental (or larger) scale. This idea will be addressed in our future studies.

The effects of the localization and inflation on the RA performance were additionally tested. The smallest T_B RMSE was achieved using the localization distance of 0.01 radians for both the default and rule-based RA and the T_B estimation of the default RA was further enhanced by applying adaptive inflation. The results show that the rule-based RA is superior to the default RA in estimating snow depth and the most improved performance is achieved by the rule-based RA without adaptive inflation. However, even in the best performance RA case, snow estimates were degenerated for some snow classes and land covers, particularly for taiga and forest, respectively. Our future studies will focus on addressing these issues by 1) using multiple RTMs for snowpack T_B and 2) employing more refined vegetation RTMs.

3.6 ACKNOWLEDGEMENT

This work is funded in part by the National Aeronautics and Space Administration under Grant NNX11AJ43G and in part by the National Natural Science Foundation of China under Grant 91337217. The authors would like to thank Michael Durand and Ghislain Picard for providing their computer codes and for discussions on the use of them. The authors also wish to thank Patricia A. Bobeck for language assistance. Computational resources were provided by the UT Texas Advanced Computing Center. (TACC).

CHAPTER 4: Improving the radiance assimilation performance in estimating snow water storage across snow and land cover types in North America[3]

4.1 ABSTRACT

Continental-scale snow radiance assimilation (RA) experiments are conducted in order to improve snow estimates across snow and land cover types in North America. In the experiments, the ensemble adjustment Kalman filter is applied and the Advanced Microwave Scanning Radiometer–Earth Observing System (AMSR-E) brightness temperature (T_B) observations are assimilated into an RA system comprised of the Community Land Model version 4 (CLM4), radiative transfer models (RTMs), and the Data Assimilation Research Testbed (DART). The performance of two snowpack RTMs, the Dense Media Radiative Transfer–Multi Layers model (DMRT-ML) and the Microwave Emission Model for Layered Snowpacks (MEMLS), in improving snow depth estimates through RA is compared. The experimental results show that the 23.8 and 18.7 GHz channels are the best and next-best performing frequency channels in the RA system. Continental-scale snow estimates are enhanced through RA by using these better-performing frequency channels and by considering the vegetation single scattering albedo (ω). The contribution of T_B of the vegetation canopy to T_B at the top of the atmosphere is better represented by considering ω in the RA system, and improvements in the resulting snow depth are evident for the forest land cover type and the taiga and alpine snow classes, especially in MEMLS case. Compared to the open-loop run, the total snow water volume and snow cover area in North America are reduced in the RA cases.

[3] This chapter was previously submitted to *Journal of Hydrometeorology*.

4.2 INTRODUCTION

At the continental (or larger) scale, the physical properties of snow vary widely with local climate conditions (e.g., air temperature, precipitation, and wind speed). According to *Sturm et al.* [1995], seasonal snow cover can be classified into six classes (i.e., tundra, taiga, alpine, maritime, prairie, and ephemeral). While existing radiative transfer models (RTMs) do show different sensitivities to snowpack properties (such as snow depth, density, grain size, temperature, and wetness) and simulate significantly different T_B, no single RTM has been shown to be able to accurately reproduce the observed T_B for such a wide range of snow classes [*Tedesco and Kim*, 2006]. In an RA scheme, an RTM is an observational operator predicting T_B; therefore, the quality of the assimilation results may strongly depend upon the RTM used [*Tedesco and Kim*, 2006; *Durand et al.*, 2008] as well as the LSM. Through synthetic experiments, *Kwon et al.* [2015] showed that two snowpack RTMs, i.e., the Dense Media Radiative Transfer–Multi Layers model (DMRT-ML) [*Picard et al.* 2013] and the Microwave Emission Model for Layered Snowpacks (MEMLS) [*Wiesmann and Mätzler*, 1999] coupled with the Community Land Model version 4 (CLM4) [*Oleson et al.*, 2010; *Lawrence et al.*, 2011], have substantially different RA performance.

Meanwhile, vegetation canopy masks the microwave emission from the underlying surface and adds its own emission [*Foster et al.*, 1991; *Chang et al.*, 1996; *Pampaloni*, 2004]. In this regard, snow estimates for vegetated areas using microwave radiance observations by both retrieval algorithms [e.g., *Hall et al.*, 1982; *Chang et al.*, 1996] and radiance assimilation methods [e.g., *Kwon et al.*, submitted] involve considerable uncertainties. In particular, the microwave T_B exhibits a significantly lower sensitivity to snow in dense forest [*Hallikainen and Jolma*, 1992; *Roy et al.*, 2012]. Therefore, precise estimates of the impact of the vegetation (i.e., vegetation emission and

transmission) on T_B at the top of the atmosphere (TOA) are essential for applications of the RA method in vegetated areas. Without such estimates, the vegetation canopy could result in an inaccurate modeling of the relationship between T_B and snow (i.e., snow water equivalent (SWE) or snow depth) and, in turn, snow estimates via RA would be degraded as presented in *Kwon et al.* [submitted].

Our objective in this study is to improve the performance of the snow RA system in estimating continental-scale snow water storage across snow and land cover types. To this end, we attempt to address the following research questions: (1) Which microwave frequency channels are most useful in improving snow estimates through RA? (2) Which of the two snowpack RTMs (i.e., DMRT-ML and MEMLS) performs better for different snow cover types at the continental scale? (3) Is vegetation single scattering albedo an important parameter for estimating the effect of vegetation on T_B at the TOA and improving the RA performance in estimating snow?

Section 4.3 describes the coupled radiance assimilation system used in this study. The design of the radiance assimilation experiments is explained in section 4.4. The results are presented and discussed in section 4.5 and conclusions are drawn in section 4.6.

4.3 COUPLED RADIANCE ASSIMILATION SYSTEM

In the coupled RA system employed in this study, we use CLM4 as a land surface model (LSM) and RTMs as observational operators. DA is implemented by the Data Assimilation Research Testbed (DART) [*Anderson et al.*, 2009], which is a community data assimilation system developed by the National Center for Atmospheric Research (NCAR) for ensemble-based DA. We employ this particular coupled RA system to

maintain continuity with our previous RA papers [i.e., *Kwon et al.*, 2015; *Kwon et al.*, submitted].

CLM4 [*Oleson et al.*, 2010; *Lawrence et al.*, 2011] simulates snow dynamics for up to five snow layers, depending on the total snow depth. CLM4 can simulate snow melt-refreeze cycles for each snow layer. It is also able to simulate snow densification by considering destructive and melting metamorphism and compaction by snow load. These make CLM4 suitable for this RA study. CLM4 estimates soil temperature for 15 soil layers, and it simulates hydrological processes over the top 10.

Two snowpack RTMs, i.e., DMRT-ML and MEMLS are used in this study while *Kwon et al.* [submitted] used only DMRT-ML to calculate T_B from the snowpack. DMRT-ML and MEMLS estimate T_B of a layered snowpack based on different theories; DMRT-ML is based on the Dense Media Radiative Transfer (DMRT) theory [*Tsang and Kong*, 2001] while MEMLS is based on the six-flux model (see *Wiesmann and Mätzler* [1999] for more details). DMRT-ML involves a stickiness parameter which is related to the size of the scatterers and which must be optimized. However, continental-scale optimization of stickiness parameter is difficult and thus it is updated during assimilation as suggested by *Kwon et al.* [submitted]. The extinction coefficient in MEMLS is calculated based on the improved Born approximation [*Mätzler*, 1998]. Unlike DMRT-ML and CLM4 which both use an effective grain radius for the grain size representation, MEMLS employs an exponential correlation length. Therefore, for MEMLS, simulated CLM4 snow grain radius is converted to the exponential correlation length using the conversion equation suggested in *Kwon et al.* [2015] and based on the work by *Mätzler* [2002] and *Debye et al.* [1957]:

$$p_{ex} = r_e\left(1-\frac{\rho}{\rho_{ice}}\right) \tag{4.1}$$

where p_{ex} is the exponential correlation length (m), r_e is the effective grain radius (m), ρ is the snow density (kg m^{-3}), and ρ_{ice} is the ice density (=917 kg m^{-3}). To calculate T_B from the snowpack, both RTMs require snow inputs such as snow layer thickness, density, temperature, wetness, and grain radius, all of which are provided by CLM4 in the coupled RA system. The reflectivity of the underlying soil is calculated by the rough bare soil reflectivity model [*Wegmüller and Mätzler*, 1999] using the estimated soil temperature and soil water content from CLM4.

T_B at the TOA is calculated as implemented in *Durand and Margulis* [2007]. The effect of the atmosphere is estimated following *Ulaby et al.* [1981]. The vegetation optical depth (τ) and transmissivity (t_c) are estimated using equation (4.2) [*Jackson and Schmugge*, 1991] and equation (4.3) [*Schmugge and Jackson*, 1992], respectively.

$$\tau = b'\lambda^x w_c / \cos\theta \tag{4.2}$$

$$t_c = \exp(-\tau) \tag{4.3}$$

where λ is the wavelength (cm); b' and x are the empirical parameters, which depend upon the vegetation canopy type and are updated in the RA system; w_c is the vegetation water content (kg m^{-2}), calculated based on *Paloscia and Pampaloni* [1988] using the leaf area index (LAI); and θ is the incident angle.

Among a variety of ensemble-based assimilation algorithms available in DART, we use the ensemble adjustment Kalman filter (EAKF) (see *Anderson* [2001] for more

detailed explanations of the EAKF), which is a deterministic ensemble square root filter [*Tippett et al.*, 2003] and does not need randomly perturbed observations. *Anderson* [2001] reports that in the cases compared in the paper, the performance of the EAKF was much better than that of the traditional ensemble Kalman filter [EnKF; *Evensen*, 1994; *Burgers et al.*, 1998], especially for a small ensemble size.

4.4 EXPERIMENTAL DESIGN

The experiments are designed to address our three research questions related to the microwave frequency channels, snowpack RTMs, and vegetation single scattering albedo. In all experimental cases (Table 4.1) including the open-loop run (without assimilation), CLM4 was run at 0.9˚ × 1.25˚ spatial resolution forced by the 40 randomly chosen ensemble members of the coupled DART/Community Atmospheric Model (CAM4) reanalysis [*Raeder et al.*, 2012], which includes air temperature, atmospheric pressure, precipitation, humidity, wind speed, and downward short-wave radiation. The experiments were conducted for North America during December 2002 to February 2003. In all RA cases, the Advanced Microwave Scanning Radiometer–Earth Observing System (AMSR-E) T_B observations were assimilated.

The physical states and parameters updated during the assimilation include SWE, snow grain radius, snow temperature, soil temperature, soil water content, snow stickiness (in DMRT-ML), and two empirical parameters (x and b' in equation (4.2)) of the vegetation RTM. The single scattering albedo was also updated in some experimental cases. As suggested in *Zhang et al.* [2014] and *Kwon et al.* [submitted], among the snow-mass-related states in CLM4 (i.e., the mass of snow liquid water and ice (kg m^{-2}), SWE (kg m^{-2}), snow density (kg m^{-3}), and snow depth (m)), only SWE was updated during the assimilation procedure to avoid excessive snow mass updating. Snow depth and the mass

of snow liquid water and ice were adjusted according to their physical relationships with SWE. Snow density was not updated in the RA system because it is simply calculated from SWE and snow depth in CLM4.

Table 4.1. Radiance assimilation (RA) experimental cases with respect to snowpack RTMs, frequency channels, and single scattering albedo.

Experimental cases	Snowpack RTM	Frequency (GHz)	Single scattering albedo (ω)
D10	DMRT-ML	10.65	·
D18	DMRT-ML	18.7	·
D23	DMRT-ML	23.8	·
D36	DMRT-ML	36.5	·
D89	DMRT-ML	89.0	·
M10	MEMLS	10.65	·
M18	MEMLS	18.7	·
M23	MEMLS	23.8	·
M36	MEMLS	36.5	·
M89	MEMLS	89.0	·
D1823	DMRT-ML	18.7 and 23.8	·
D1836	DMRT-ML	18.7 and 36.5	·
M1823	MEMLS	18.7 and 23.8	·
M1836	MEMLS	18.7 and 36.5	·
D1823(ω)	DMRT-ML	18.7 and 23.8	0.064
D1836(ω)	DMRT-ML	18.7 and 36.5	0.064
M1823(ω)	MEMLS	18.7 and 23.8	0.064
M1836(ω)	MEMLS	18.7 and 36.5	0.064
D1823(ω_up)	DMRT-ML	18.7 and 23.8	Updated
D1836(ω_up)	DMRT-ML	18.7 and 36.5	Updated
M1823(ω_up)	MEMLS	18.7 and 23.8	Updated
M1836(ω_up)	MEMLS	18.7 and 36.5	Updated

Kwon et al. [submitted] demonstrated two approaches which are effective in improving the continental-scale snow estimates: (1) simultaneous updates of all model physical states and parameters involved in predicting T_B; and (2) a rule-based approach in which the states and parameters are updated only when the signs of their correlations with

the prior T_B coincide with those of the sensitivity indices. These approaches were simultaneously applied in the RA cases. It should be noted that the assimilation was not performed if any ensemble members within a grid cell predicted no snow.

A localization distance parameter in DART restricts the effect of assimilated observations on model states of nearby grid cells [*Anderson et al.*, 2009]. This mitigates the degradation of assimilation performance resulting from correlations between two uncorrelated variables due to sampling error [*Anderson*, 2007]. According to *Kwon et al.* [submitted], the localization distance of 0.01 radians was used in all RA experimental cases.

The assimilation results were evaluated for each snow class and land cover type using the Canadian Meteorological Centre (CMC) daily snow depth data [*Brasnett*, 1999; *Brown and Brasnett*, 2010]. Based on *Sturm et al.* [1995], six snow classes (tundra, taiga, alpine, maritime, prairie, and ephemeral) were used (Figure 3.10a). Dominant land cover types (bare soil, forest, shrub, grass, and crop) in grid cells were determined using CLM4 plant functional types (Figure 3.10b).

4.4.1 Microwave frequency channels

In this study, we assimilated the AMSR-E/Aqua Daily Global Quarter–Degree Gridded Brightness Temperatures data (NISDC-0302; http://nsidc.org/data/nsidc-0302) [*Knowles et al.*, 2006] into the coupled RA system. Vertically (V) and horizontally (H) polarized TOA microwave radiances at 6 frequencies (i.e., 6.925, 10.65, 18.7, 23.8, 36.5, and 89.0 GHz) are observed by AMSR-E. In all RA cases, only vertically polarized T_B observations were assimilated because horizontally polarized T_B is significantly influenced by ice layers within the snowpack [*Mätzler*, 1987; *Durand et al.*, 2008; *Rees et al.*, 2010], which are not accurately represented in the five-layer snow model.

Previous snow RA studies mostly used passive microwave observations at 18.7 and/or 36.5 GHz [e.g., *Durand et al.*, 2009; *Dechant and Moradkhani*, 2011; *Toure et al.*, 2011; *Bateni et al.*, 2015; *Kwon et al.*, submitted]. However, through a synthetic test, *Durand and Margulis* [2006] suggested that all frequency channels provide valuable information for snowpack. In this paper, we compared the RA performance of the experimental cases (Table 4.1) using different AMSR-E frequency channels. Only nighttime observations were used, thereby avoiding error due to snow wetness. The 6.925 GHz T_B was excluded from the experiments due to the high potential for radio frequency interference over the United States [*Njoku et al.*, 2005].

It has been reported that the total bias error of the AMSR-E sensor ranges from 0.66 K at 100 K to 0.68 K at 250 K [*Lobl*, 2001]. However, the constructed AMSR-E T_B data used in this study may have more error resulting from two sources (see http://nsidc.org/data/docs/daac/ae_l2a_tbs.gd.html#errorsource): (1) a mismatch between the construction and the ideal antenna pattern, and (2) random measurement error. In addition, the original AMSR-E T_B data, which have 0.25˚ spatial resolution, were scaled up to the CLM4 grid (0.9˚ × 1.25˚) for computational efficiency; this may introduce additional error into the T_B observations. Therefore, to consider these additional error sources, the observation error was set to 2 K, as assumed by *Durand and Margulis* [2007]. However, quantification of the AMSR-E T_B observational error needs to be further investigated.

4.4.2 Snowpack radiative transfer models

We employed two snowpack RTMs (DMRT-ML and MEMLS) to estimate the snowpack T_B. Due to the different T_B sensitivities of DMRT-ML and MEMLS to the physical properties of snow and underlying soil, the correlations between the SWE error

(simulation minus observation) and T_B error produced by coupled CLM4/DMRT-ML and CLM4/MEMLS also exhibit considerable differences [*Kwon et al.*, 2015] as shown in Figure 4.1. More grid cells with higher positive correlations are observed in the CLM4/DMRT-ML results (Figure 4.1a) while those with higher negative correlations are found in the CLM4/MEMLS results (Figure 4.1b). This is consistent with the synthetic experimental results of *Kwon et al.* [2015], in which CLM4/DMRT-ML and CLM4/MEMLS were apt to yield more positive and negative correlations, respectively, for both shallow and deep snowpack conditions. Furthermore, the two coupled models estimate correlations of the opposite sign for some locations (Figures 4.1c and 4.1d).

RA using ensemble Kalman-based data assimilation methods assumes that the SWE error is correlated with the T_B error [*Kwon et al.*, 2015]. Therefore, two coupled models (CLM4/DMRT-ML and CLM4/MEMLS) may show varying RA performance for different snow cover types. *Kwon et al.* [submitted] showed that the RA system using DMRT-ML significantly improves the snow depth estimates for the tundra and maritime snow classes. Here, we added MEMLS to the RA system and compared the RA performance using DMRT-ML and MEMLS for various snow and land cover types (see Table 4.1 for the experimental cases).

4.4.3 Vegetation single scattering albedo

The most commonly used vegetation RTM is the τ–ω model [*Mo et al.*, 1982], which is a simplified approach to model the vegetation effect on T_B. Two parameters, namely the vegetation optical depth (τ) and the single scattering albedo (ω), are involved in the model. The single scattering albedo parameterizes all processes within the vegetation canopy layer such as the absorption and scattering effects [*Kurum et al.*, 2012]. In many cases, ω is neglected [e.g., *Kruopis et al.*, 1999; *Langlois et al.*, 2011]

because previous studies have reported that it is generally less than 0.1 [*Pampaloni and Paloscia*, 1986; *Grant et al.*, 2008; *Roy et al.*, 2012].

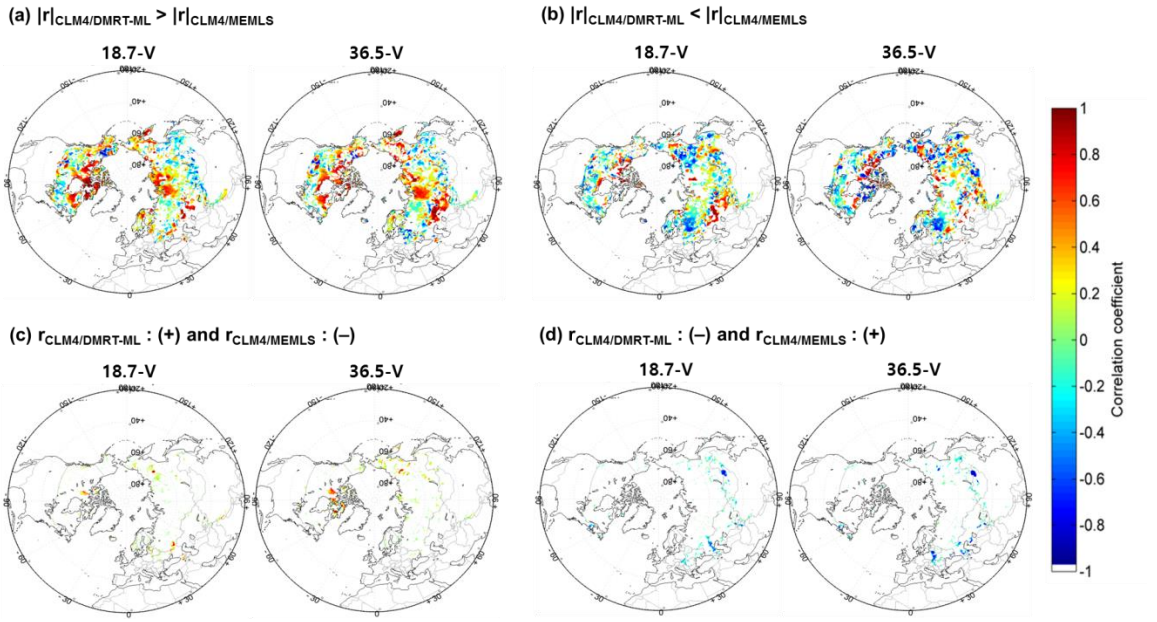

Figure 4.1. Spatial distribution of the correlations between the SWE error and T_B error in February 2003 (where error = simulation – observation). The SWE error is calculated using the SWE estimates obtained by *Reichle et al.* [2011] from the CMC snow depth and climatological snow densities suggested by *Sturm et al.* [2010]. The T_B error is estimated using the AMSR-E T_B observations at 18.7 and 36.5 GHz vertical (V) and horizontal (H) polarization channels.

Our coupled RA system, which uses the approach of *Durand and Margulis* [2007], initially neglects ω in its estimate of T_B at the TOA. However, this assumption of ω = 0 results in an overestimation of the microwave emission of the vegetation canopy [*Ferrazzoli et al.*, 2002]. Therefore, the contribution of ω was additionally considered in representing T_B as follows:

$$T_{B,TOA} = \left[\{1+(t_c-1)V_c\}T_{B,sn} + V_c(1-\omega)(1-t_c)T_c\right]t_a + T_{B,a} \quad (4.4)$$

$$T_{B,BC} = \{1+(t_c-1)V_c\}(T_{B,sp}t_a + T_{B,a}) + V_c(1-\omega)(1-t_c)T_c \quad (4.5)$$

where $T_{B,TOA}$ is the brightness temperature at the TOA (K); t_c and t_a are the vegetation and atmospheric transmissivity, respectively; V_c is the vegetation fraction within a grid cell; $T_{B,sn}$ is the brightness temperature from the snowpack (K), which is estimated by DMRT-ML or MEMLS and includes the effect of the underlying soil; T_c is the vegetation physical temperature (K); $T_{B,a}$ is the atmospheric brightness temperature (K); $T_{B,BC}$ is the boundary condition T_B for snowpack RTMs to model $T_{B,sn}$; and $T_{B,sp}$ is the space brightness temperature (=2.7 K).

Firstly, the improvement of the RA performance by considering ω was tested using a constant value of ω=0.064 as suggested in *Roy et al.* [2012] (see the D1823(ω), D1836(ω), M1823(ω), and M1836(ω) cases in Table 4.1). However, ω value depends on vegetation type, frequency, and polarization [*Langlois et al.*, 2011]. Although *Roy et al.*, [2012] suggested that ω is mostly frequency- and polarization-independent for coarse-scale observations, it is still influenced by vegetation properties. Yet, no measurements of ω are available at the continental scale and thus an optimization procedure for ω is required. Several studies [e.g., *Paloscia*, 1995; *Njoku and Li*, 1999; *Pellarin et al.*, 2006; *Grant et al.*, 2008; *Roy et al.*, 2012] have been published on the optimization of ω values for different vegetation types, but they are not in agreement. This is attributed to the fact that surface parameterizations (e.g., snow and/or soil), data sets, and assumptions can influence the optimization results [*Roy et al.*, 2012; *Pellarin et al.*, 2006]. Fortunately, however, most of the ω values suggested by these studies are within the range of 0.05 to 0.1. Therefore, in the D1823(ω_up), D1836(ω_up), M1823(ω_up), and M1836(ω_up) cases (Table 4.1), ω was updated in the RA system using the range of 0.05 to 0.1. Based on the sensitivity analysis (not shown here), T_B at the TOA is negatively sensitive to ω;

that is, an increase in ω leads to a decrease in T_B at the TOA. Using the rule-based approach suggested by *Kwon et al.* [submitted], the update of ω was performed only if the correlation between the prior T_B and ω was negative.

4.5 RESULTS AND DISCUSSION

4.5.1 Performance of the RA system using AMSR-E frequencies and snowpack RTMs

The T_B observation at each AMSR-E frequency channel (10.65, 18.7, 23.8, 36.5, and 89.0 GHz vertical polarization) was separately assimilated into the RA system and the resulting snow depth root mean square error (RMSE) of the RA experimental cases using DMRT-ML and MEMLS for North America are shown in Figure 4.2. Among the five frequency channels assimilated, only the 18.7 and 23.8 GHz channels led to an overall improvement in snow depth estimates in both DMRT-ML and MEMLS cases. The DMRT-ML cases (D18 and D23) slightly outperformed the MEMLS cases (M18 and M23). Compared to the open-loop run without assimilation (the horizontal dotted line in Figure 4.2), the performance of the RA system was marginally improved in the D36 case, whereas it was degraded in the M36 case. This is at least partly due to the different saturation depth of the 36.5 GHz signal in DMRT-ML and MEMLS. Figure 4.3 shows that the sensitivity of the 36.5 GHz T_B to snow depth variation is higher in MEMLS than in DMRT-ML and, as a result, the 36.5 GHz signal is saturated for a shallower snowpack in MEMLS. It should also be noted in Figure 4.3 that for both DMRT-ML and MEMLS, the 10.65 GHz T_B is largely insensitive to snow depth while the 89.0 GHz T_B is saturated for a very shallow snow. This might explain the poor performance of the RA cases using the 10.65 or 89.0 GHz channels (Figure 4.2).

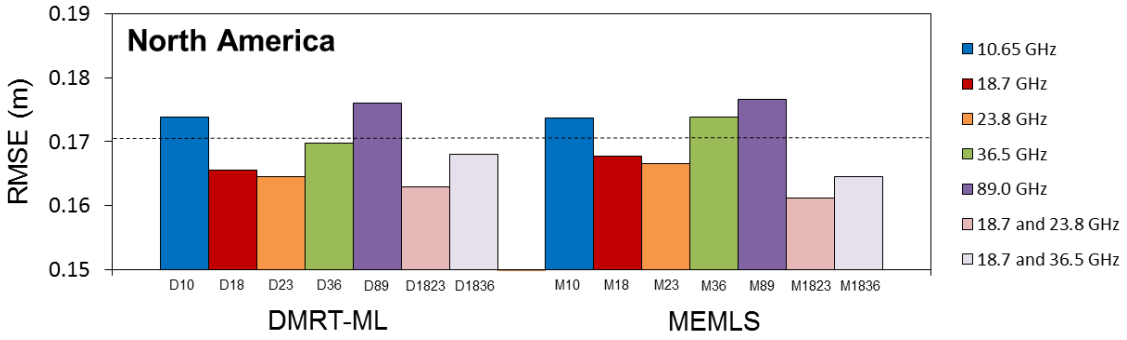

Figure 4.2. The snow depth RMSE (m) in the radiance assimilation (RA) experimental cases, using different snowpack RTMs (DMRT-ML and MEMLS) and assimilating different AMSR-E frequency channels, for North America. The horizontal dotted line represents the RMSE of the open-loop run (without assimilation).

Meanwhile, the results obtained here contradict the synthetic experiment results of *Durand and Margulis* [2006] in which the 10.65 and 36.5 GHz channels contributed more than the 18.7 and 23.8 GHz channels in improving the snow estimates in their RA system. There are three potential reasons for our different results. First, RA methods applied in the real world might produce different results than when used in synthetic experiments. Second, different results could be due to differences among RA schemes in terms of LSM, RTM, updated states/parameters during the assimilation, or assimilation methods employed (e.g., EnKF and KAKF). Finally, a rule-based approach was applied in our RA experiments but was not used by *Durand and Margulis* [2006]. The use of rule-based approach can avoid improper updates of states and parameters resulting from their false correlations with the prior T_B [*Kwon et al.*, submitted]. This approach probably influenced the relative contribution of different frequency channels to the RA performance.

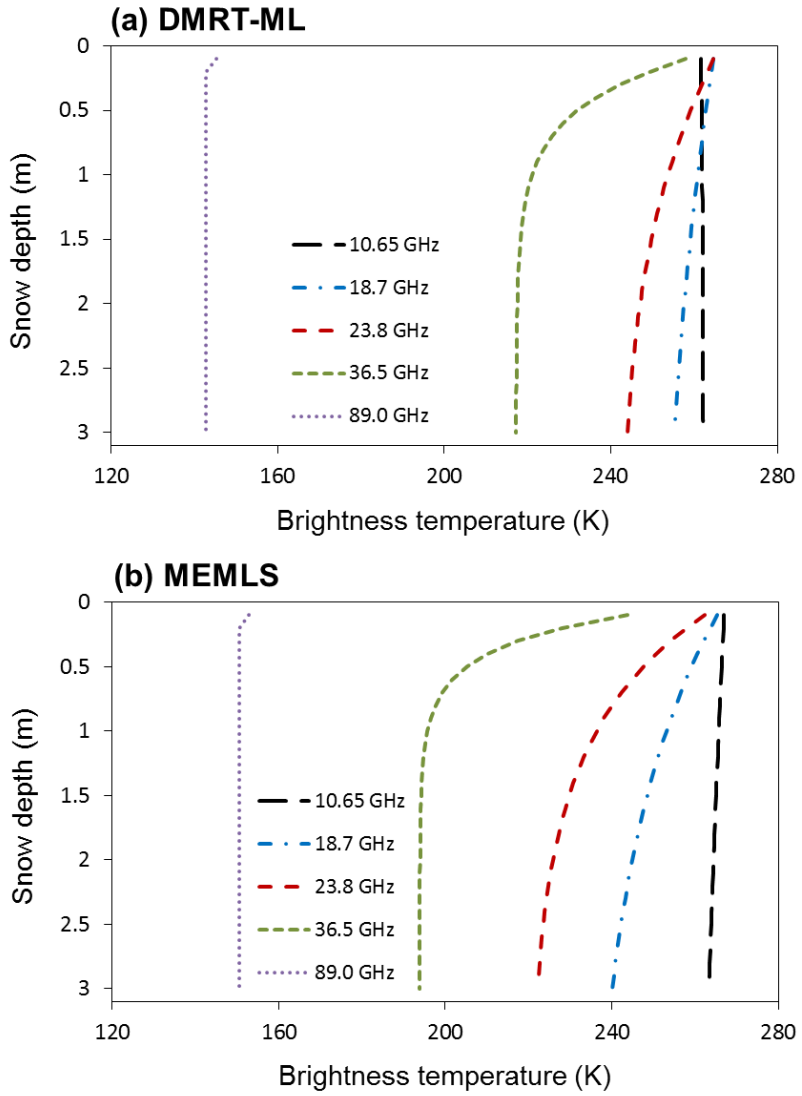

Figure 4.3. Brightness temperature (T_B) at 10.65, 18.7, 23.8, 36.5, and 89 GHz vertical polarization channels estimated by (a) DMRT-ML and (b) MEMLS with varying snow depth (0.1 to 3 m). Other snow and soil physical properties were set as follows: snow grain radius=350 μm, snow temperature=270 K, snow density=300 kg m^{-3}, snow wetness=0 m^3 m^{-3}, soil temperature=270 K, and soil water content=0.1 m^3 m^{-3}. The snow stickiness in DMRT-ML was set to 0.2 and the exponential correlation length (p_{ex}) for MEMLS was calculated using equation (1).

We additionally analyzed the effect of assimilating two frequency channels simultaneously on the RA performance in estimating snow depth (Figure 4.2). Because

the 23.8 and 18.7 GHz channels were the best and next-best performing frequency channels, respectively, these two were assimilated in the D1823 and M1823 cases. For comparison purposes, T_B observations at 18.7 and 36.5 GHz channels were also simultaneously assimilated in the D1836 and M1836 cases because these two channels have been frequently used in snow RA systems as well as in snow retrieval algorithms.

As shown in Figure 4.2, except for the D1836 case, the assimilation of two frequency channels improved the overall performance of the RA system as compared to the separate use of each frequency channel. The D1836 case performed better than D36 but worse than D18. It should be noted that compared to the D1836 and M1836 cases, greatly improved estimates of snow depth were obtained by assimilating the two best performing frequency channels, i.e., 18.7 and 23.8 GHz. The improvement of the snow estimates by the RA system using multiple frequency channels was more obvious in MEMLS cases. When two frequency channels were simultaneously assimilated, the performance of MEMLS cases (M1823 and M1836) was superior to that of DMRT-ML cases (D1823 ad D1836) even though MEMLS cases showed worse performance than DMRT-ML cases for a single frequency channel (Figure 4.2).

In general, without considering the vegetation single scattering albedo (ω), DMRT-ML cases produced better estimates of snow than MEMLS cases for the taiga and alpine snow classes while MEMLS cases were more effective for tundra (Figure 4.4). For the maritime, ephemeral, and prairie snow classes, DMRT-ML and MEMLS cases showed comparable performance. Compared to the open-loop run, however, DMRT-ML and MEMLS cases only improved snow depth estimates for the tundra and maritime snow classes. While the snow depth RMSE of the open-loop run for the ephemeral and prairie snow classes was already very small and RA marginally increased the RMSE, the degradation of the snow depth estimates by RA was considerable for the taiga and alpine

snow classes. The poor performance of the RA system for the taiga and alpine snow classes could be due to the effect of vegetation (especially forest) on T_B estimations. The difficulty of characterizing snowpack under the vegetation canopy using microwave radiance observations has been reported by many previous studies [e.g., *Hallikainen and Jolma*, 1992; *Chang et al.*, 1996; *Foster et al.*, 2005]. Figure 4.5 shows that regardless of the snowpack RTMs and microwave frequency channels, the RA system could not improve the snow depth estimates for forest land cover, the dominant land cover type for the taiga and alpine snow classes (Figure 3.10). This implies that the effect of the vegetation canopy on T_B at the TOA was not accurately represented in our current RA system. Further improvement of the performance of the RA system for vegetated areas by introducing ω is discussed in the next section.

4.5.2 The impact of the vegetation single scattering albedo (ω) on the RA performance

To analyze the effect of ω on the estimation of T_B emitted by vegetation and on the performance of the RA system, two approaches were compared: (1) the use of the constant ω value (=0.064) obtained in *Roy et al.* [2012] and (2) the use of an ω updated during the assimilation. The experimental results are presented in Figures 4.6, 4.7 and 4.8.

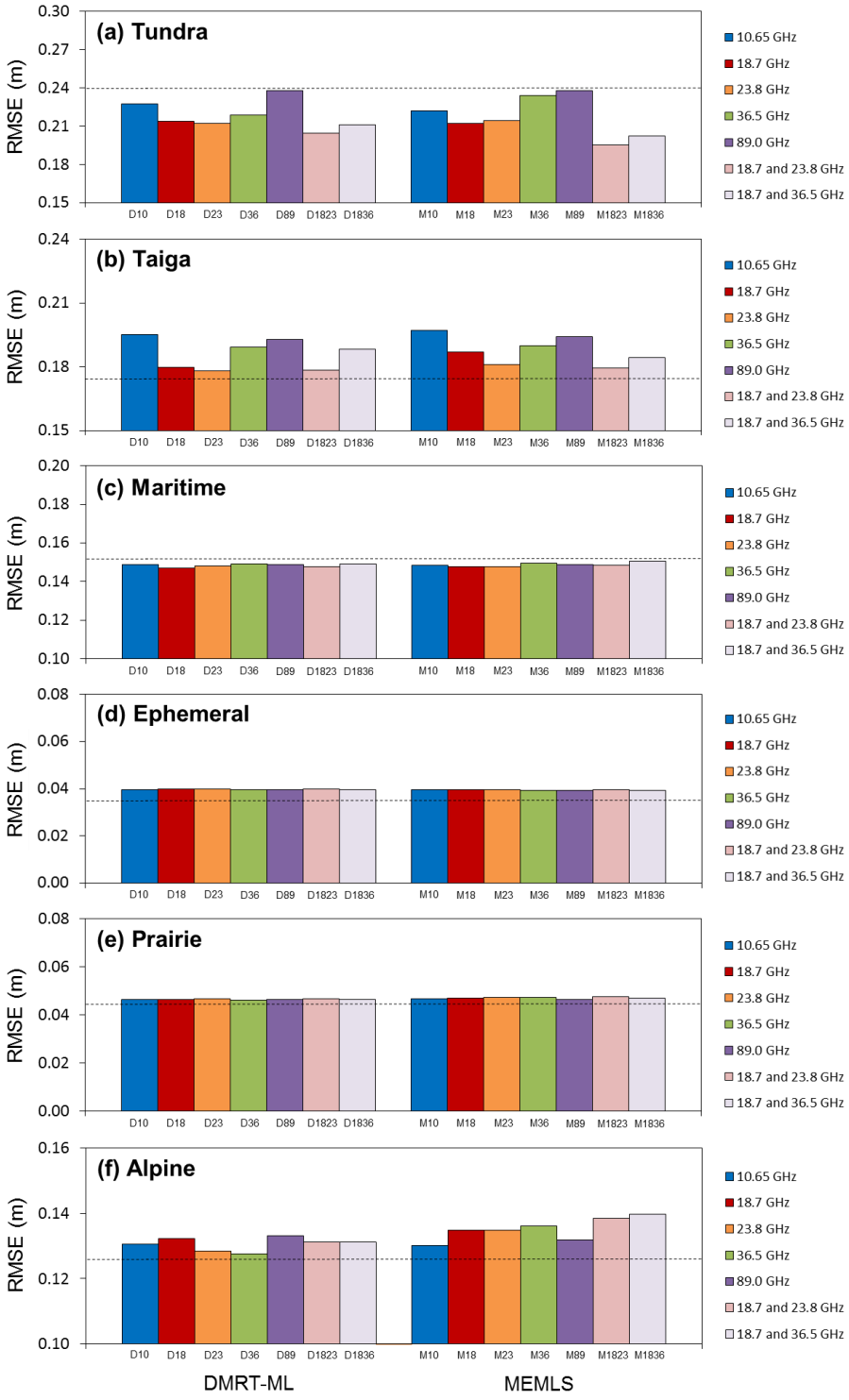

Figure 4.4. Same as Figure 4.2 but for snow classes as defined in Sturm et al. (1995): (a) tundra, (b) taiga, (c) maritime, (d) ephemeral, (e) prairie, and (f) alpine.

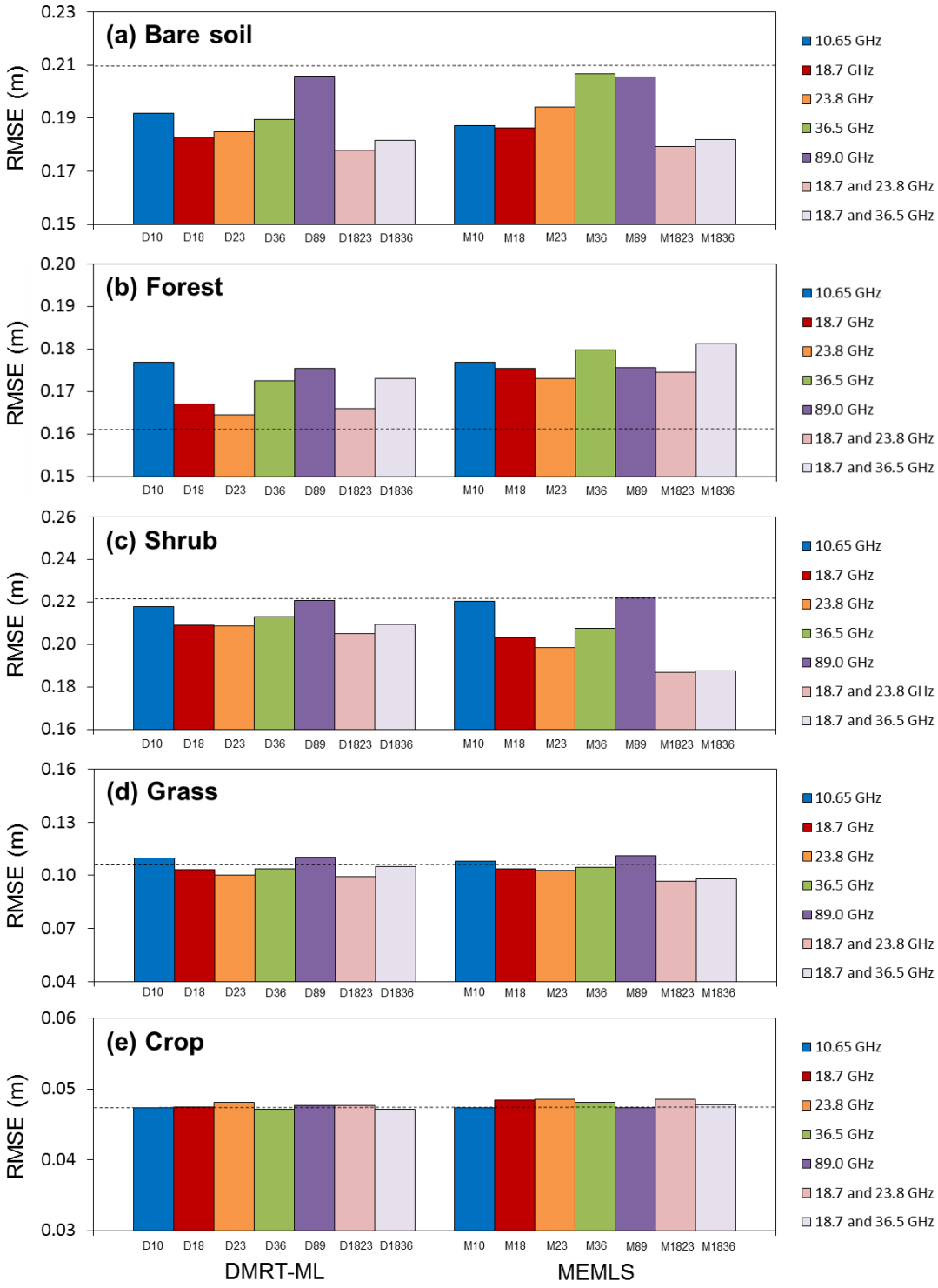

Figure 4.5. Same as Figure 4.2 but for land cover types: (a) bare soil, (b) forest, (c) shrub, (d) grass, and (e) crop.

By considering the constant ω, the overall snow depth RMSE for North America was reduced (Figure 4.6) and improved snow depth estimates were observed for all vegetated areas except crop land cover (Figure 4.8). The most considerable improvement was achieved for forest land cover (Figure 4.8) and accordingly the snow estimates for the taiga and alpine snow classes were also enhanced compared to the RA cases neglecting ω (Figure 4.7). Improvements in performance resulting from the use of ω were more noticeable in MEMLS cases (M1823(ω) and M1836(ω)) than in DMRT-ML cases (D1823(ω) and D1836(ω)), especially for the forest land cover type and the taiga snow class (Figures 4.7 and 4.8). The overall performance of the DMRT-ML case (D1823(ω)) was worse than the MEMLS case (M1823(ω)) (Figure 4.6). However, the D1823(ω) case yielded better snow depth estimates than the open-loop run for all land cover types, whereas the M1823(ω) case degraded the estimates for crop land cover (Figure 4.8). The performance of the cases assimilating the 18.7 and 36.5 GHz channels was slightly better than that of the cases assimilating the 18.7 and 23.8 GHz channels for crop land cover (Figure 4.8e). This is due to the fact that the 36.5 GHz channel exhibited better performance in estimating snow depth than the 23.8 GHz channel for this land cover type (Figure 4.5e). Our RA experimental results show that substantial improvements to snow estimates made through RA are achieved by taking ω into account even when the ω value is less than 0.1. This suggests that ω should be considered in representing the effect of vegetation on T_B at the TOA from the RA perspective.

Figure 4.9 shows that the vegetation transmissivity estimated in the RA experimental cases which neglect ω (D1823 and M1823) ranges from 0.4 to 0.6 for forested areas. The saturation levels of the vegetation transmissivity obtained by *Langlois et al.* [2011] for the Canadian boreal forest are 0.51 and 0.55 for the 19 GHz-V and 19 GHz-H channels, respectively, and 0.53 for both the 37 GHz-V and 37 GHz-H channels.

Roy et al. [2012] suggested that the vegetation transmissivities for dense boreal forests are 0.69, 0.62, 0.497, and 0.423 for 6.9, 10.7, 18.7, and 36.5 GHz channels, respectively. Based on the values suggested in previous studies, the range of vegetation transmissivity we obtained for forest land cover is reasonable.

However, in the D1823 and M1823 cases, more than 70% of T_B at the TOA ($T_{B,TOA}$) was contributed by T_B emission from the vegetation canopy ($T_{B,v}$) in areas dominated by forest land cover (Figures 4.10a and 4.10b). Compared to the results by *Roy et al.* [2012] in which $T_{B,v}$ constituted about 46% and 50% of $T_{B,TOA}$ at 18.7 and 36.5 GHz-V, respectively, the contribution of $T_{B,v}$ was overestimated in our experiments by neglecting ω. By considering ω in the D1823(ω) and M1823(ω) cases, more reasonable estimates of the vegetation contribution were obtained (Figures 4.10c and 4.10d). A better estimate of the $T_{B,v}$ contribution was observed in the MEMLS case than in the DMRT-ML case (Figure 4.10). This could explain why the reduction in the snow depth RMSE associated with ω was greater in MEMLS cases than in DMRT-ML cases for forest land cover (Figure 4.8b).

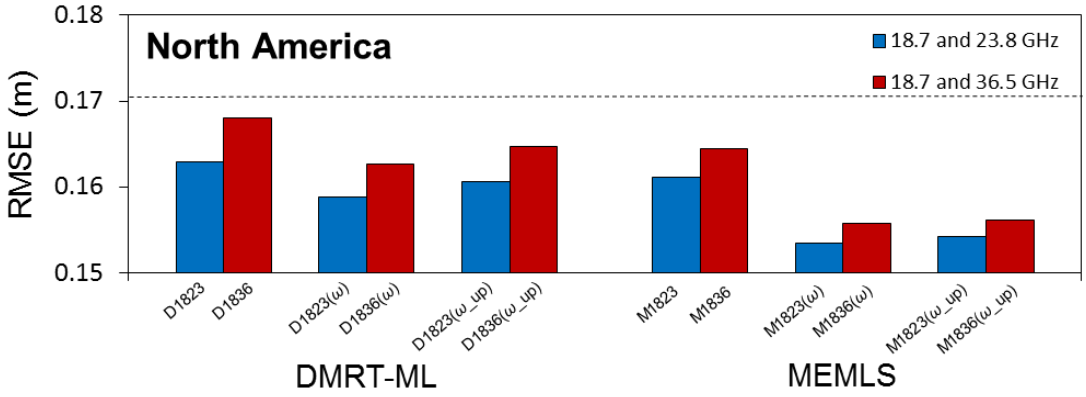

Figure 4.6. The snow depth RMSE (m) in the radiance assimilation (RA) experimental cases using different snowpack RTMs (DMRT-ML and MEMLS) and assimilating two frequency channels simultaneously (i.e., 18.7 and 23.8 GHz or 18.7 and 36.5 GHz) for North America. The vegetation single scattering albedo (ω) was neglected (in the D1823, D1836, M1823 and M1836 cases), was set to 0.064 (in the D1823(ω), D1836(ω), M1823(ω), and M1836(ω) cases), or was updated during the assimilation (in the D1823(ω_up), D1836(ω_up), M1823(ω_up), and M1836(ω_up) cases). The horizontal dotted line represents the RMSE of the open-loop run (without assimilation).

Updating ω during the assimilation in the RA system did not improve the RA performance beyond what was already achieved using a constant ω (Figures 4.6, 4.7 and 4.8). Rather, the snow depth RMSE slightly increased in the D1823(ω_up) and M1823(ω_up) cases. Nonetheless, the performance of the RA cases using an updated ω was still superior to that of the cases neglecting ω.

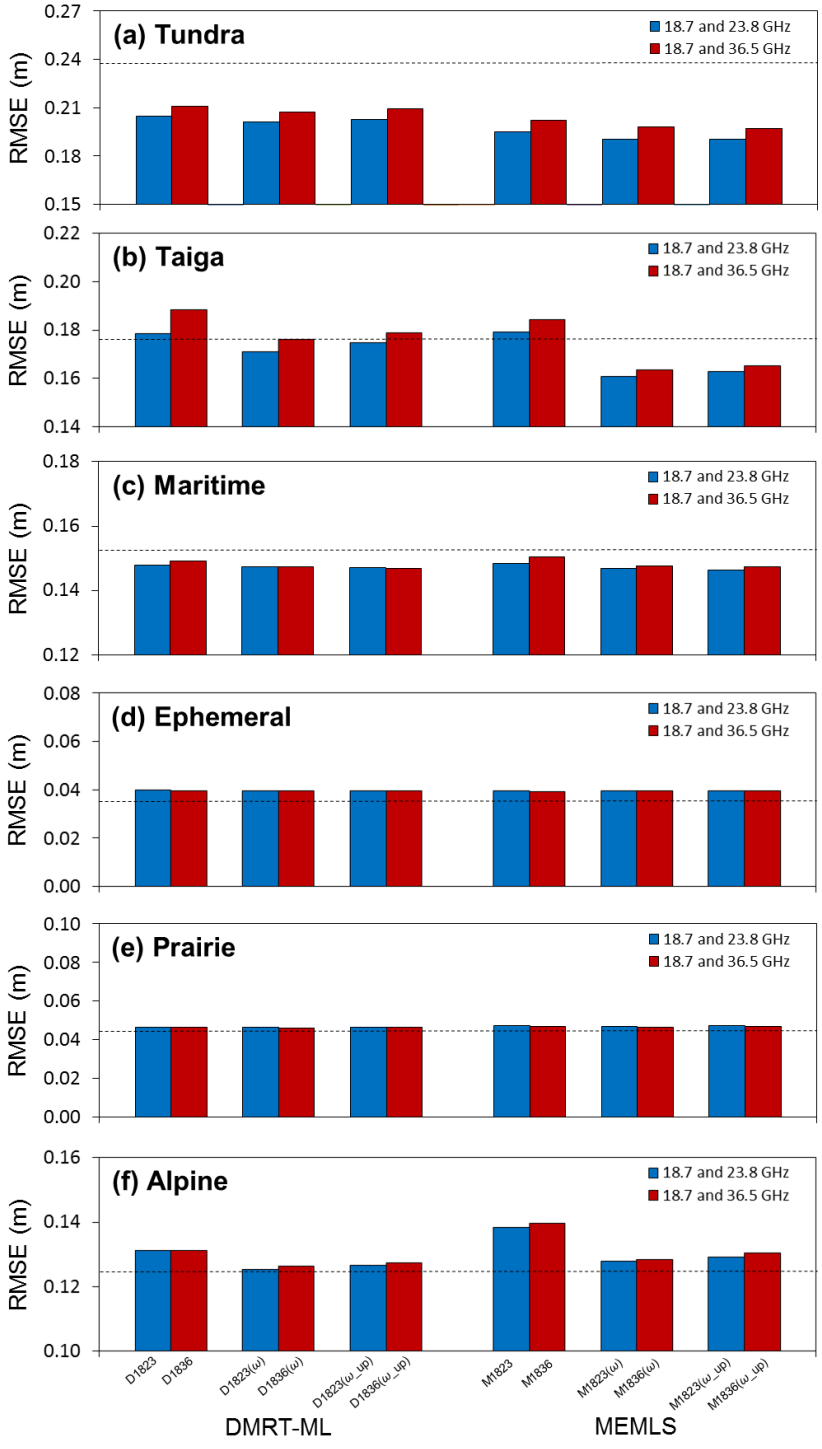

Figure 4.7. Same as Figure 4.6 but for snow classes as defined in Sturm et al. (1995): (a) tundra, (b) taiga, (c) maritime, (d) ephemeral, (e) prairie, and (f) alpine.

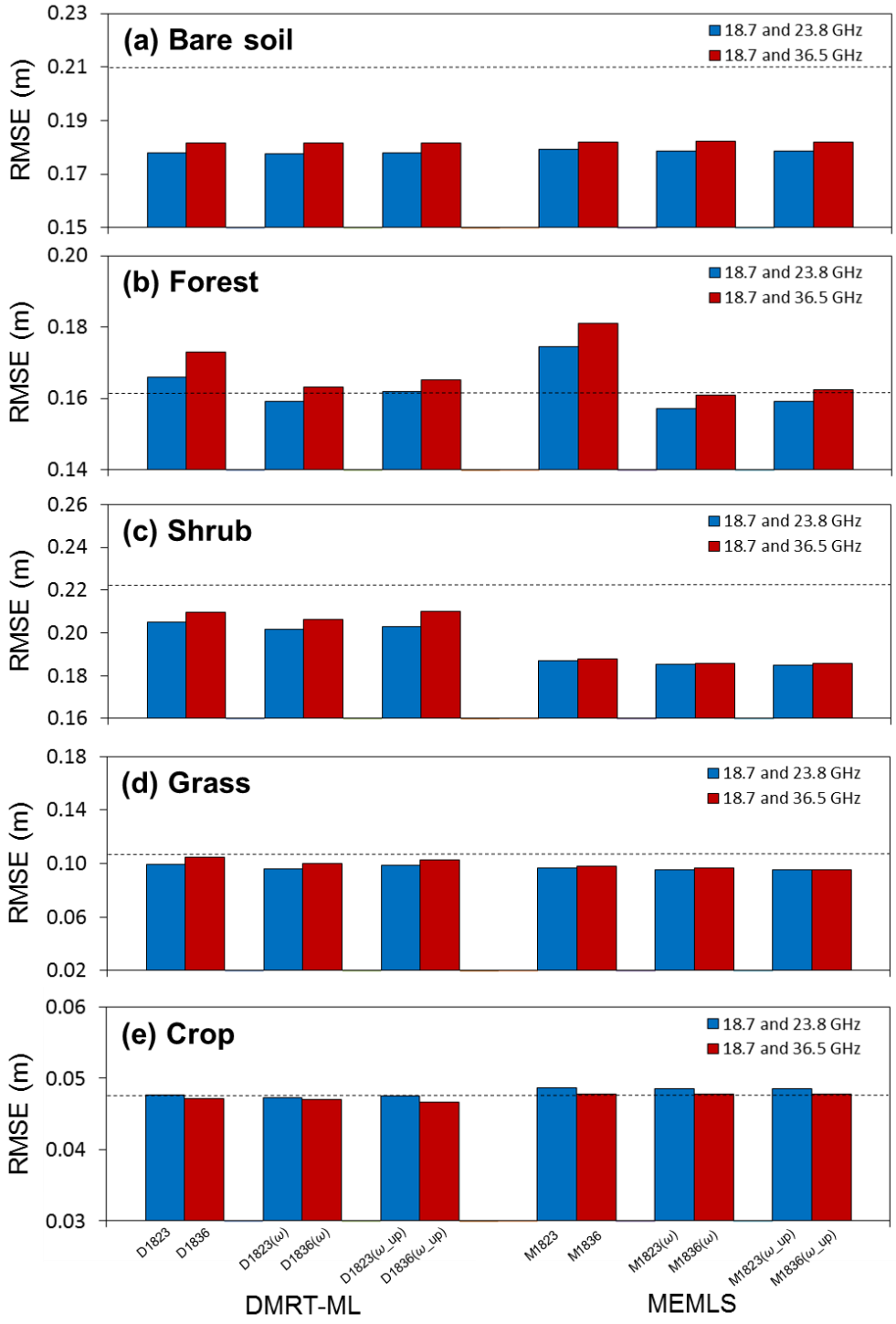

Figure 4.8. Same as Figure 4.6 but for land cover types: (a) bare soil, (b) forest, (c) shrub, (d) grass, and (e) crop.

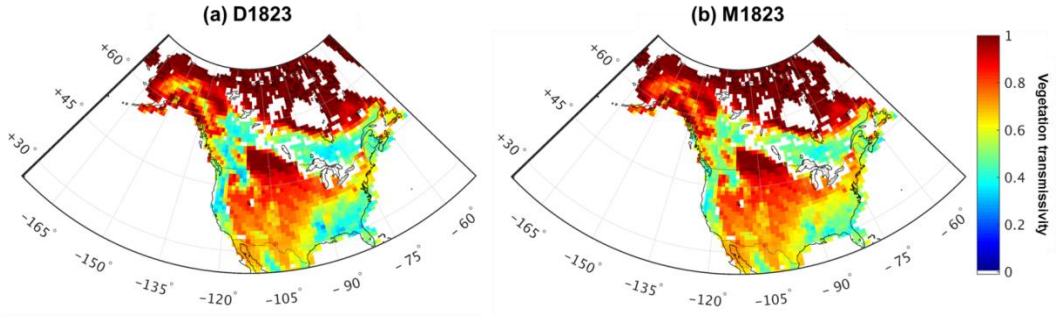

Figure 4.9. The estimated (ensemble mean) vegetation transmissivity in the (a) D1823 and (b) M1823 cases. The values were averaged over two frequency channels (18.7 and 23.8 GHz vertical polarizations) during the assimilation period.

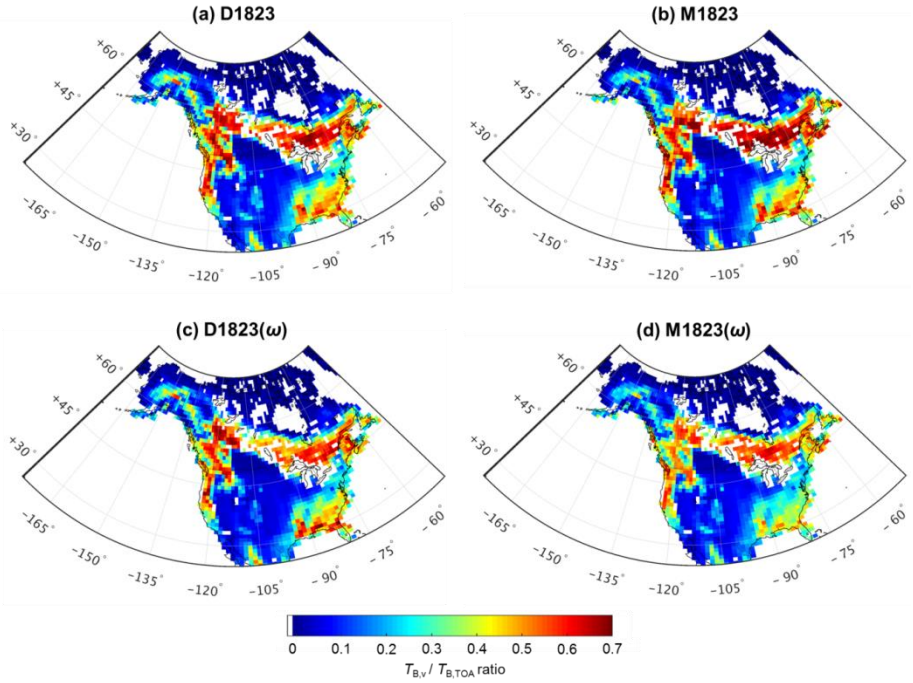

Figure 4.10. The ratio of the estimated (ensemble mean) $T_{B,v}$ (T_B emitted by the vegetation canopy) to the estimated (ensemble mean) $T_{B,TOA}$ (T_B at the top of the atmosphere) in the cases neglecting ω ((a) D1823 and (b) M1823) and in the cases considering ω ((c) D1823(ω) and (d) M1823(ω)). The values were averaged over two frequency channels (18.7 and 23.8 GHz vertical polarizations) during the assimilation period.

4.5.3 Snow water volume and snow cover area in North America

Snow water volume was calculated by multiplying the estimated (ensemble mean) SWE by grid area and summing the result over North America (Figure 4.11a). Compared to the open-loop run, the snow water volume was reduced in the RA cases throughout the assimilation period (i.e., the snow accumulation season). The difference in the snow water volume between the RA cases and open-loop run increased with time and approached 110 and 132 km^3 for the D1823(ω) and M1823(ω) cases, respectively, by the end of the assimilation period. This represented 7.8 and 9.5% of the snow water volume from the open-loop run, respectively.

In CLM4, snow cover fraction (SCF) is a diagnostic variable and is estimated from snow density and depth using the snow cover parameterization suggested by *Niu and Yang* [2007]. The ensemble mean snow cover area in North America was calculated from SCF estimated by CLM4 (Figure 4.11b). Compared to the open-loop run, the snow cover area also decreased in the RA cases but the magnitude of the decrease was very small. The maximum difference in the snow cover area between the RA cases and open-loop run was 68,969 km^2 for the D1823(ω) case and 122,998 km^2 for the M1823(ω) case, corresponding to 0.5 and 0.8% of the snow cover area from the open-loop run, respectively. The insignificant changes in the snow cover area through RA may be attributed to the fact that RA was primarily effective in improving snow depth (and SWE) estimates for relatively deep snowpack regions where SCF was already saturated (i.e., 100% SCF).

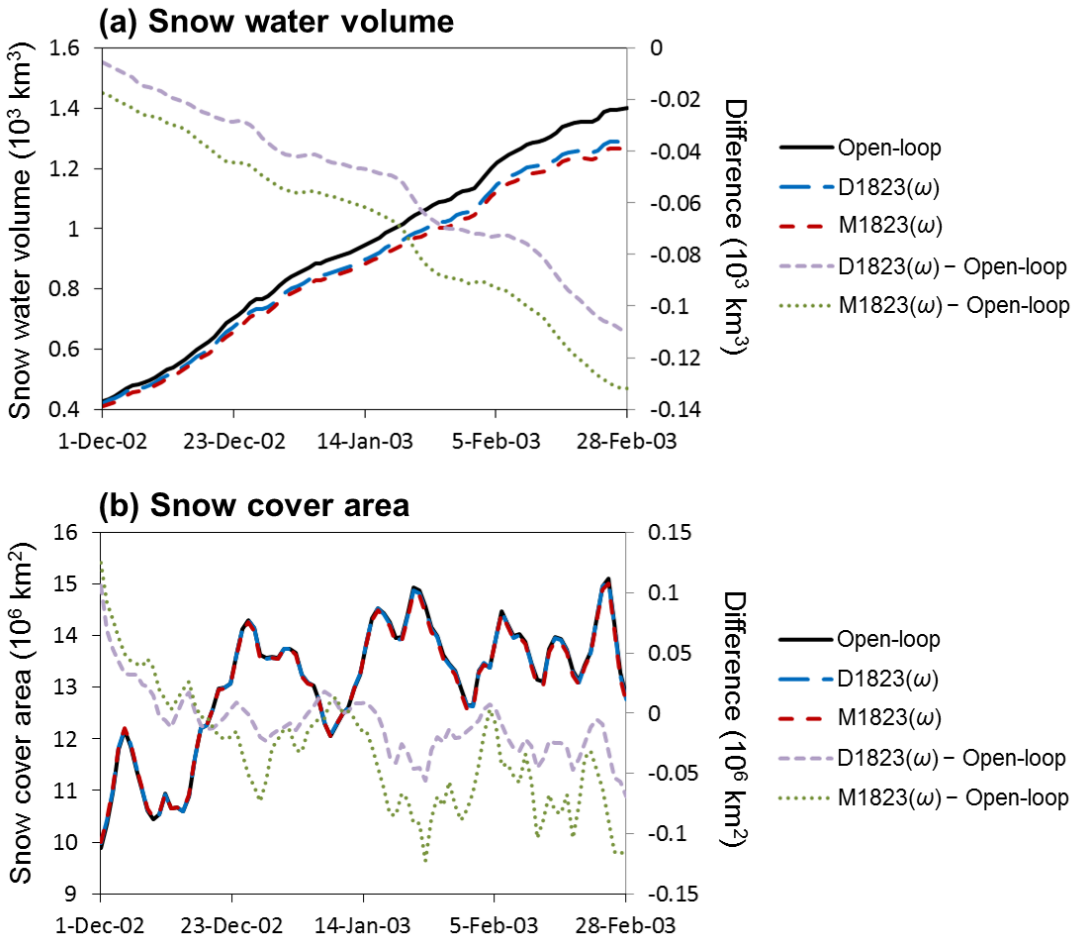

Figure 4.11. The estimated (ensemble mean) (a) snow water volume (10^3 km^3) and (b) snow cover area (10^6 km^2) in North America.

4.6 CONCLUSIONS

In this study, three research questions related to microwave frequency channels, snowpack RTMs, and vegetation single scattering albedo (ω) were addressed for the purpose of improving the snow RA performance across snow classes and land cover types in North America. Our coupled RA system employed CLM4 (for snow modeling), RTMs (for T_B estimates), and DART (for ensemble-based data assimilation). Two

different snowpack RTMs (DMRT-ML and MEMLS) were compared in terms of their relative performance in improving snow depth estimates through RA. RA experiments were conducted during the snow accumulation season (December 2002 to February 2003) by assimilating AMSR-E T_B observations using the EAKF. The experimental results were assessed for six snow classes (tundra, taiga, alpine, maritime, prairie, and ephemeral) and five land cover types (bare soil, forest, shrub, grass, and crop) using the CMC snow depth data.

The results showed that the 23.8 and 18.7 GHz channels are the best and next-best performing frequency channels, respectively, in our RA system. Due to microwave signal saturation for relatively shallow snow depth, higher frequency channels (i.e., 36.5 and 89.0 GHz) performed worse than the 18.7 and 23.8 GHz channels. The poor performance of the 10.65 GHz channel was attributed to its low sensitivity to snow depth in the snowpack RTMs used in this study. We obtained a significant improvement in snow depth estimates, especially in MEMLS cases, by assimilating the two best performing frequency channels (18.7 and 23.8 GHz).

By introducing ω, the contribution of vegetation T_B emission ($T_{B,v}$) to T_B at the TOA ($T_{B,TOA}$) was more reasonably represented in the RA system. Consequently, substantial improvements in the RA performance were achieved for vegetated areas, in particular for the forest land cover type and the taiga and alpine snow classes. Although we could not further improve the RA performance by updating ω during the assimilation, the results suggested that from the RA perspective, ω is an essential factor in the RA system for characterizing snow under the vegetation canopy. By establishing the ω values for various land cover types (or vegetation types), the performance of snow RA will be further enhanced.

When ω was neglected, the DMRT-ML cases were superior to the MEMLS cases for the taiga and alpine snow classes while the MEMLS cases produced better snow estimates for the tundra snow class. When ω was considered, however, improvement of the RA performance was more noticeable in the MEMLS cases than in the DMRT-ML cases, and the MEMLS cases outperformed the DMRT-ML cases for the taiga snow class as well as for the tundra snow class.

RA tended to decrease the total snow water volume and snow cover area in North America compared to the open-loop run. These changes in snow estimates will alter modeled energy fluxes and hydrological cycles through feedback mechanisms such as the snow albedo-temperature feedback and soil moisture-precipitation feedback, further affecting seasonal hydroclimatic predictions [e.g., *Lin et al.*, 2015].

This study demonstrated that continental-scale snow estimates can be improved through RA by using the better-performing frequency channels (i.e., 18.7 and 23.8 GHz) and by considering ω. However, we focused on limited spatial (North America) and temporal scales (single snow accumulation season). Our RA system needs to be further evaluated at the global scale over multi-year snow seasons. This will be our aim in future studies.

4.7 ACKNOWLEDGEMENT

This work is supported in part by the National Aeronautics and Space Administration under Grant NNX11AJ43G and in part by the National Natural Science Foundation of China under Grant 91337217. The authors would like to thank Michael Durand, Ghislain Picard, and Christian Mätzler for providing their computer codes and for discussions on the use of them. The Data Assimilation Research Testbed (DART)/Community Atmospheric Model (CAM4) atmospheric ensemble reanalysis data

are prepared by Kevin Raeder (raeder@ucar.edu). The authors would also like to thank Adam S. Papendieck for language assistance and Long Zhao for processing the time-shifted atmospheric forcing. Computational resources were provided by the UT Texas Advanced Computing Center. (TACC).

CHAPTER 5: Conclusions and future perspective

This dissertation aimed to develop an advanced RA system to improve snow water storage estimates at the continental scale. The developed RA system employs CLM4 as a land surface model, DMRT-ML and MEMLS as snowpack radiative transfer models (RTMs), and DART for ensemble-based data assimilation. Four research questions have been addressed in this dissertation.

Is the RA method applicable to continental-scale snow water storage estimations? In order to answer this first question, the following three chapters were organized to address the other three questions. Chapter 2 tried to answer the second research question, i.e., Which error characteristics of estimated snow physical properties and T_B impede continental-scale applications of the RA method? The errors of two coupled land surface–radiative transfer models, i.e., CLM4/DMRT-ML and CLM4/MEMLS, were characterized by evaluating the CLM4 snowpack state simulations, by assessing the RTMs performance in simulating T_B, and by analyzing the correlations between SWE error and T_B error from the RA perspective. The error characterizations were carried out at point scale and mesoscale using *in situ* measurements and synthetic experiments were additionally conducted for shallow and deep snowpack conditions. The results showed that the magnitude of the snow grain radius error and its relationship to the SWE error significantly affect the correlations between the SWE error and the T_B error. The results also exhibited that errors of all physical properties of soil and snow required to estimate T_B have substantial impacts on the correlations between the SWE error and the T_B error and subsequent RA performance. Chapter 2 suggests that (a) in addition to SWE (snow depth and density), all other related physical properties should be properly updated in the RA system to minimize errors related to them; and (b) a rule-based approach is required

to avoid the degradation of the RA performance due to incorrect relationships between the prior SWE (or snow depth) and T_B.

Based on the results and discussions in Chapter 2, Chapter 3 addressed the third research question "Can the effect of these error sources be mitigated in the RA system?" It was hypothesized that the continental-scale RA performance in estimating snow water storage can be improved by simultaneously updating all model physical states and parameters determining T_B using a rule-based approach, in which prior estimates were updated depending on their correlations with a prior T_B. This hypothesis has been tested through analysis of results from a series of RA experiments, which assimilated AMSR-E T_B observations at 18.7 and 36.5 GHz vertical polarizations using the ensemble adjustment Kalman filter. The experimental results showed that the continental-scale snow estimates are improved by applying the hypothesis. However, the results also suggested that the RA system needs to be further refined to improve snow estimates for vegetated areas.

By overcoming the limitations of the RA system discussed in Chapter 3, Chapter 4 answered the fourth research question (i.e., How to improve the performance of the RA system in characterizing snow under the vegetation canopy?). The results showed that the 23.8 and 18.7 GHz channels are the best and next-best performing frequency channels and a significant improvement in snow depth estimates was obtained by assimilating these two frequency channels into the RA system. The contribution of the vegetation canopy to T_B at the TOA was better represented by considering the vegetation single scattering albedo (ω) and consequently the performance of the RA system was considerably improved for the forest land cover types and the taiga and alpine snow classes.

After having answered the second through fourth questions, the answer to the first research question becomes an obvious "yes". Indeed, this dissertation demonstrated that the performance of the RA system in estimating snow depth over North America is enhanced by simultaneously updating model states and parameters involved in simulating T_B based on the rule, by using the best-performing frequency channels (18.7 and 23.8 GHz), and by considering ω (Figure 5.1a). Especially, the RA system performed much better than the open-loop run for areas without vegetation cover (Figure 5.1b). The snow depth estimates by RA were also enhanced for forested areas (Figure 5.1c) by better representing the vegetation contribution to T_B at the TOA.

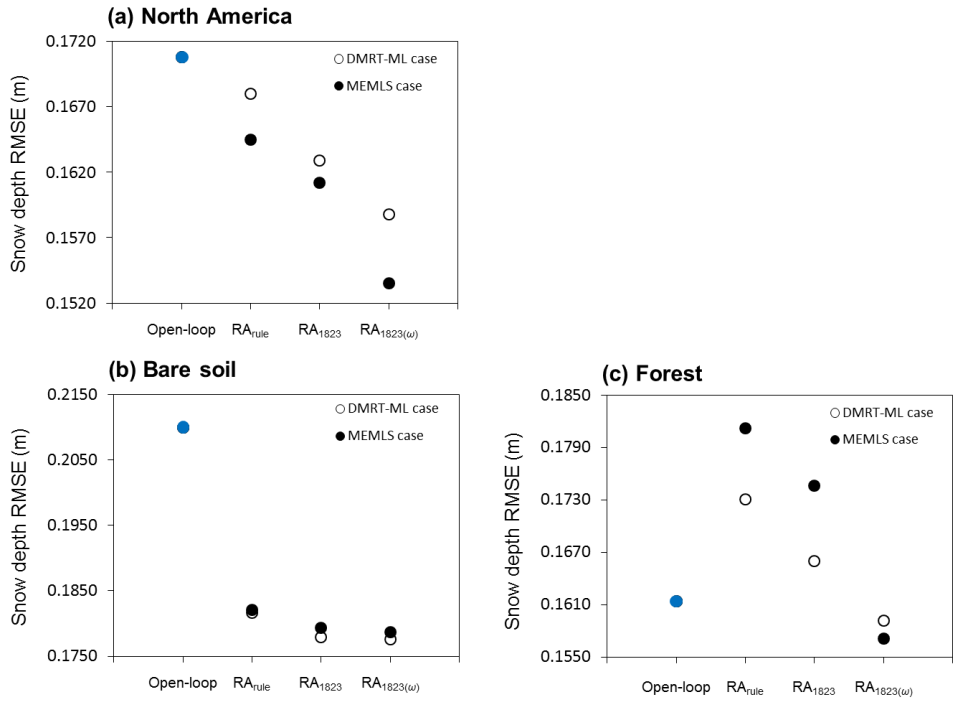

Figure 5.1. The improvement of the RA performance in estimating snow depth for (a) North America, (b) bare soil land cover, and (c) forest land cover by simultaneously updating all model physical states and parameters determining T_B based on a rule (RA_{rule}), by assimilating the best-performing frequency channels, i.e., 18.7 and 23.8 GHz (RA_{1823}), and by considering the vegetation single scattering albedo ($RA_{1823(\omega)}$).

Throughout the dissertation, we have learned that the improvement of snow estimates is not guaranteed by just assimilating microwave radiance data into the RA system. As shown in Chapters 2, 3, and 4, we should identify limitations of the RA method and attempt to resolve them for continental-scale and/or global-scale snow estimates. Although this dissertation made significant progress in using microwave radiance data to characterize the continental-scale snow water storage, several remaining issues still need to be resolved.

First, RTM parameters should be established for snow classes and vegetation types found in the continental domain. Although this dissertation demonstrated that the update of parameters in the RA system can be an alternative for continental-scale optimizations of parameters, this approach is suboptimal. If we can have established parameter values for each snow class and vegetation type, further improvement of the RA performance will be achieved. However, this work requires extensive data sets including *in situ* snowpit, T_B, and vegetation measurements.

Second, the CLM4 snow layering scheme may be an additional uncertainty source for degrading the performance of the current RA system. The importance of snowpack stratigraphy in T_B predictions has been emphasized in many studies [e.g., *Boyarskii and Tikhonov*, 2000; *Rosenfeld and Grody*, 2000; *Andreadis et al.*, 2008; *Durand et al.*, 2008, 2011; *Andreadis and Lettenmaier*, 2012]. Microwave emissions are strongly modulated by snow layer properties, especially when the snowpack has significantly different dielectric properties between neighboring layers [*Colbeck*, 1991; *Rees et al.*, 2010]. Permittivity of a dielectric medium determines how much electric charge can be transmitted by the medium; therefore, the dielectric permittivity of snow is a main parameter affecting microwave radiation scattering and absorption by snowpack [*Mätzler*, 1996]. Permittivity differences between adjacent snow and ice layers increase

the reflectivity of the interface [*Wiesmann and Mätzler*, 1999]; thus, the presence of ice layers within a snowpack has a significant effect on T_B [*Durand et al.*, 2008]. In particular, as shown in Figure 5.2, horizontally polarized brightness temperatures are more sensitive to ice layer properties than vertical channels [*Mätzler*, 1987; *Durand et al.*, 2008; *Rees et al.*, 2010] and the uncertainty of ice-layer density is the most critical error source in T_B predictions at horizontal polarization [*Durand et al.*, 2008]. It has been demonstrated that at the point-scale, assimilating both vertical and horizontal channels provides significant improvement in estimating snowpack characteristics as compared to the use of only vertical channels [*Toure et al.*, 2011]. Therefore, representing ice layers in LSM may improve large-scale RA as well.

In CLM4 snow physics, ice layers are not explicitly created; however, the model implicitly represents ice layers by the refrozen liquid water content of each snow layer. In addition, because the snow layering scheme in the current CLM4 combines or subdivides snow layers according to the prescribed minimum and maximum layer thickness, the lower snow layers are always thicker than the upper layers. Furthermore, since the maximum number of snow layers is limited to five, the model cannot create thin ice layers within the snowpack. The effect of thin ice layers with higher density on microwave propagation within the snowpack may be different from that of thick layers with lower density resulting from layer-averaging. The improvement of the CLM4 snow layering scheme for ice layer representation will further improve the RA performance.

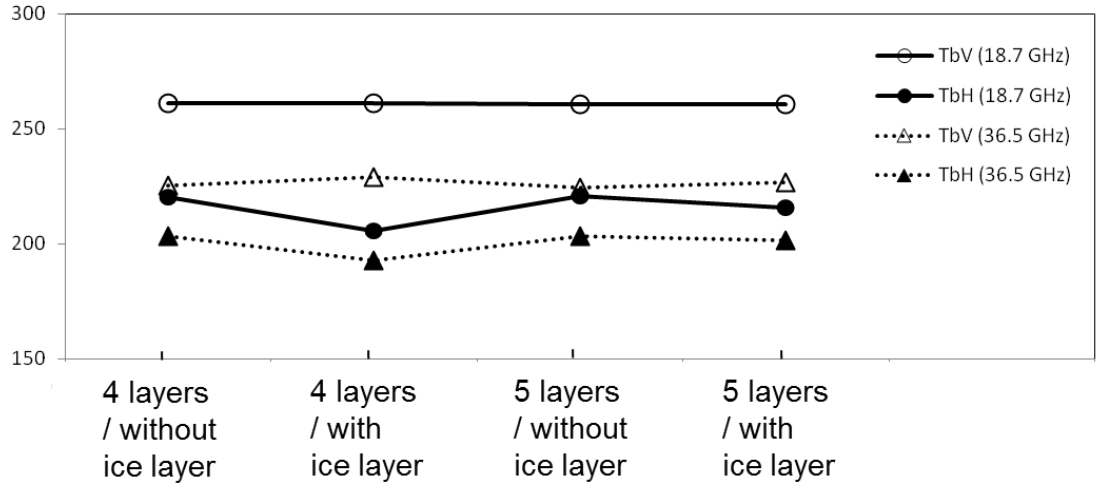

Figure 5.2. T_B estimated by DMRT-ML for four- and five-layered snowpack with and without ice layer.

Third, snow intercepted by the vegetation canopy may be an additional uncertainty source of the current RA system. Boreal forests, which cover approximately 15% of the terrestrial land area [*Pomeroy and Dion*, 1996], are the largest terrestrial biome in North America [*Girard et al.*, 2008]. These forests are primarily composed of evergreen coniferous tree species that intercept and retain snowfall during winter [*Pomeroy and Dion*, 1996; *Lundberg et al.*, 2004]. *Bunnell et al.* [1985] reported that intercepted snow by the coniferous canopy approaches 30 mm SWE. According to *Lundberg and Halldin* [2001], snow accumulation in forests is reduced by up to 40% compared with open areas due to interception and sublimation, which are considerable parts of the winter water budget. Based on a three-year field experiment on mountain maritime climates, *Storck et al.* [2002] reported that approximately 60% (up to about 40 mm SWE) of snowfall is intercepted by the coniferous canopy.

Intercepted snow can be retained in the forest canopy by snow strength and cohesion. Snow crystals adhere to needles and branches by cohesion of snow resulting

from the rapid formation of micro-scale ice bonds [*Hedstrom and Pomeroy*, 1998]. Snow strength is determined by bonding between snow crystals [*Hedstrom and Pomeroy*, 1998], which strengthens at cold temperature and weakens near the melting point [*Langham*, 1981]. Therefore, in cold boreal forests, canopy-intercepted snow may persist for several days to a month [*Pomeroy and Schmidt*, 1993; *Zierl and Bugmann*, 2005], while it quickly sublimates in temperate forests [*Hedstrom and Pomeroy*, 1998].

Canopy-intercepted snow is involved in scattering and absorption of microwave emission from the underlying snowpack [*Derksen and MacKay*, 2006; *Clifford*, 2010] and also emits its own microwave energy [*Chang et al.*, 1996; *Hall et al.*, 2002; *Dong et al.*, 2005]. Melt-refreeze cycles result in the formation of liquid water or ice crystals within the intercepted snow; this condition may also contribute to the microwave signal. As a result, microwave emission from intercepted snow is a significant source of T_B observed at the TOA; therefore, it may influence the quality of RA results for these forested areas. However, CLM4 does not separate liquid and solid phases of canopy water; therefore, the effect of canopy-intercepted snow on T_B at the TOA was neglected in the current study. Further improvement of the RA performance could be achieved by considering it.

Fourth, as mentioned in Chapter 4, this dissertation mainly focused on North America during a single snow accumulation season. To provide better understanding of snow and to improve hydroclimatic predictions, global-scale applications of the RA system over multi-year snow seasons should be explored. Regarding a longer-term RA study, the use of T_B observations from the Advance Microwave Scanning Radiometer-2 (AMSR2) can be considered. In this dissertation, AMSR-E T_B observations were assimilated into the RA system. AMSR-E had observed global T_B since 2002 but unfortunately it halted its scientific observation in October 2011 due to its antenna

rotation problems [*Imaoka et al.*, 2010]. AMSR2 was launched in May 2012 and has been providing T_B observations since January 2013. Basic performance of AMSR2 is almost identical to that of AMSR-E, except for several important improvements [*Imaoka et al.*, 2010]: 1) additional channels (7.3 GHz) in C-band receiver to mitigate radio frequency interference (RFI) issue, 2) larger main reflector (2.0 m diameter) to improve the spatial resolution, and 3) improved calibration system. Therefore, it is expected that assimilation of AMSR2 T_B observations will provide better estimates of snow water storage.

Finally, although the assimilation of microwave T_B observations improved overall snow estimates, it still degraded the estimates for some regions including the ephemeral and alpine snow classes. In addition, microwave radiance data will add more uncertainties to snow estimates for snowmelt seasons due to the effect of liquid water within the snowpack. A multi-sensor snow data assimilation is required to overcome the limitations of microwave radiance data. Previous studies [*Rodell and Houser*, 2004; *Andreadis and Lettenmaier*, 2006; *Clark et al.*, 2006; *Su et al.*, 2010; *De Lannoy et al.*, 2012; *Zhang et al.*, 2014] showed that the assimilation of MODIS SCF is effective for ephemeral snowpack during snowmelt periods. Previous members of our group *Su et al.*, [2010] and *Zhang* [2015] demonstrated that when the Gravity Recovery and Climate Experiment (GRACE) terrestrial water storage (TWS) data are additionally assimilated, much improved snow estimates can be obtained. We can also consider the use of a recently emerging approach, i.e., lidar, when measuring snow depth. However, MODIS SCF, GRACE TWS, and lidar also have their own limitations. MODIS provides high resolution data, but it cannot distinguish between snow cover and cloud, and it cannot detect snow mass variations when the ground is full covered with snow. Although GRACE observes mass variations in terrestrial water storage, its spatial and temporal

resolutions are coarse. Lidar is not influenced by the snow wetness, which is one of significant factors degrading T_B observations, and can provide accurate snow depth observations at about 1 m horizontal spatial resolutions; however, it cannot pass through clouds. The assimilation of these multi-sensor data (i.e., AMSR-E T_B, MODIS SCF, GRACE TWS, and lidar snow depth) will complement each other's limitations and provide much improved large-scale snow water storage estimates.

These potential future researches can benefit from the SnowEX campaign (http://neptune.gsfc.nasa.gov/hsb/index.php?section=322), now being planned by NASA. SnowEX is a multi-year snow campaign to collect airborne observations using various remote-sensing instruments such as radar, lidar, multispectral imagers, passive microwave detector, and passive visible light/infrared detector. In addition, it will also collect ground truth data. The campaign sites will be in the forested areas ranging from no trees to dense forests. The data collection will start in February 2017 and continue to 2019–2021.

To make more efficient use of the collected data, the following aspects need to be considered during the SnowEX campaign. First, as the CLPX data sets, the SnowEX *in situ* snowpit measurements should include snow layer thickness, density, temperature, wetness, and snow grain size. Especially, the information about the presence of ice lens, and its thickness and location within the snowpack are required. Second, the snowpit and airborne observations must be available for the same dates (and time, if possible). We experienced from the use of CLPX data sets that many data sets could not be used because they were not available at the same dates. Third, microwave frequency channels provided by the airborne sensor need to match those by satellite. Fourth, vegetation data such as vegetation types, density, and LAI should be provided. Fifth, snow intercepted by

the vegetation canopy should also be measured. Finally, the campaign should cover the full snow season so that we can have measurements for dry and wet snow conditions.

REFERENCES

Anderson, J. L. (2001), An ensemble adjustment Kalman filter for data assimilation, *Mon. Wea. Rev.*, 129, 2884–2903.

Anderson, J. L. (2007), Exploring the need for localization in ensemble data assimilation using a hierarchical ensemble filter, *Physica D*, 230, 99–111.

Anderson, J. L. (2009), Spatially and temporally varying adaptive covariance inflation for ensemble filters, *Tellus*, 61A, 72–83.

Anderson, J. L., T. Hoar, K. Raeder, H. Liu, N. Collins, R. Torn, and A. Arellano (2009), The data assimilation research testbed: A community facility, *Bull. Am. Meteorol. Soc.*, 90, 1283–1296.

Andreadis, K. M., and D. P. Lettenmaier (2006), Assimilating remotely sensed snow observations into a macroscale hydrology model, *Adv. Water Resour.*, 29, 872–886.

Andreadis, K. M., and D. P. Lettenmaier (2012), Implications of representing snowpack stratigraphy for the assimilation of passive microwave satellite observations, *J. Hydrometeor.*, 13, 1493–1506, doi: http://dx.doi.org/10.1175/JHM-D-11-056.1.

Andreadis, K. M., D. Liang, L. Tsang, D. P. Lettenmaier, and E. G. Josberger (2008), Characterization of Errors in a Coupled Snow Hydrology–Microwave Emission Model, *J. Hydrometeorol.*, 9, 149–164.

Bateni, S. M., S. A. Margulis, E. Podest, and K. C. McDonald (2015), Characterizing snowpack and the freeze–thaw state of underlying soil via assimilation of multifrequency passive/active microwave data: a case study (NASA CLPX 2003), *IEEE Trans. Geosci. Remote Sens.*, 53, 173–189, doi:10.1109/TGRS.2014.2320264.

Brasnett, B. A. (1999), Global analysis of snow depth for numerical weather prediction, *J. Appl. Meteorol.*, 38, 726–740.

Brodzik, M. (2004), *CLPX-Satellite: AMSR-E Brightness Temperature Grids*. Boulder, CO: Nat. Snow Ice Data Center. Digital Media.

Brown, R. D., and B. Brasnett (2010), Canadian Meteorological Centre (CMC) Daily Snow Depth Analysis Data. Environment Canada, National Snow and Ice Data Center, Boulder, CO, digital media, updated annually. [Available online at https://nsidc.org/data/docs/daac/nsidc0447_CMC_snow_depth/.]

Brucker, L., A. Royer, G. Picard, A. Langlois, and M. Fily (2011), Hourly simulations of the microwave brightness temperature of seasonal snow in Quebec, Canada, using a coupled snow evolution-emission model, *Remote Sens. Environ.*, 115, 1966–1977.

Brun, E. (1989), Investigation of wet-snow metamorphism in respect of liquid water content, *Ann. Glaciol.*, 13, 22-26.

Brun, E., P. David, M. Sudul, and G. Brunot (1992), A numerical model to simulate snow-cover stratigraphy, *J. Glaciol.*, 38, 13–22.

Bunnell, F. L., R. S. McNay, and C. C. Shank (1985), *Trees and snow: the deposition of snow on the ground - a review and quantitative synthesis*, IWIFR-17, Res. Branch, Minist. of Environ. and For., Victoria, British Columbia, Canada.

Burgers, G., P. J. van Leeuwen, and G. Evensen (1998), Analysis scheme in the ensemble Kalman filter, *Mon. Wea. Rev.*, 126, 1719–1724.

Chang, A. T. C., J. L. Foster, and D. K. Hall (1987), Nimbus-7 SMMR derived global snow cover parameters, *Ann. Glaciol.*, 9, 39–44.

Chang, A. T. C., J. L. Foster, and D. K. Hall (1996), Effects of forest on the snow parameters derived from microwave measurements during the BOREAS winter field experiment, *Hydrol. Process.*, 10, 1565–1574.

Chapin, F. S., M. Sturm, M. C. Serreze, J. P. McFadden, J. R. Key, A. H. Lloyd, A. D. McGuire, T. S. Rupp, A. H. Lynch, J. P. Schimel, J. Beringer, W. L. Chapman, H. E. Epstein, E. S. Euskirchen, L. D. Hinzman, G. Jia, C. –L. Ping, K. D. Tape, C. D. C. Thompson, D. A. Walker, and J. M. Welker (2005), Role of land-surface changes in Arctic summer warming, *Science*, 310, 657–660, doi: 10.1126/science.1117368.

Clark, M. P., A. G. Slater, A. P. Barrett, L. E. Hay, G. J. McCabe, B. Rajagopalan, and G. H. Leavesley (2006), Assimilation of snow covered area information into hydrologic and land-surface models, *Adv. Water Resour.*, 29, 1209–1221.

Clifford, D. (2010), Global estimates of snow water equivalent from passive microwave instruments: history, challenges and future developments, *Int. J. Remote Sens.*, 31, 3707–3726.

Cline, D., R. Armstrong, R. Davis, K. Elder, and G. Liston (2002), CLPX-Ground: ISA Snow Pit Measurements, Version 2.0, M. Parsons and M. J. Brodzik, Eds. Boulder, CO: Nat. Snow Ice Data Center, updated July 2004, http://dx.doi.org/10.5060/D4H41PBP.

Cline, D., R. Armstrong, R. Davis, K. Elder, and G. Liston (2003), CLPX LSOS snow pit measurements," in CLPX-Ground: Snow Measurements at the Local Scale Observation Site (LSOS), M. Parsons and M. J. Brodzik, Eds. Boulder, CO: Nat. Snow Ice Data Center. Digital Media, 2002. J. Hardy, J. Pomeroy, T. Link, D. Marks, D. Cline, K. Elder, R. Davis, updated July 2004.

Cohen, J., and D. Entekhabi (1999), Eurasian snow cover variability and Northern Hemisphere climate predictability, *Geophys. Res. Let.*, 26, 345–348.

Debye, P., H. R. Anderson, and H. Brumberger (1957), Scattering by an inhomogeneous solid. II. The Correlation function and its application, *J. Appl. Phys.*, 28, 679–683.

Dechant, C., and M. Moradkhani (2011), Radiance data assimilation for operational snow and streamflow forecasting, *Adv. Water Resour.*, 34, 351–364.

De Lannoy, G. J. M., R. H. Reichle, K. R. Arsenault, P. R. Houser, S. Kumar, N. E. C. Verhoest, and V. R. N. Pauwels (2012), Multiscale assimilation of Advanced Microwave Scanning Radiometer–EOS snow water equivalent and Moderate Resolution Imaging Spectroradiometer snow cover fraction observations in northern Colorado, *Water Resour. Res.*, 48, W01522, doi:10.1029/2011WR010588.

Derksen, C., and M. MacKay (2006), The Canadian boreal snow water equivalent band, *Atmosphere-Ocean*, 44, 305–320.

Ding, K. H., L. Tsang, and S. E. Shih (2001), Monte Carlo simulations of particle positions for densely packed multispecies sticky particles, *Microw. Opt. Technol. Lett.*, 30, 187–192.

Dobson, M. C., F. T. Ulaby, M. T. Hallikainen, and M. A. El-Rayes (1985), Microwave dielectric behavior of wet soil-Part II: Dielectric mixing models, *IEEE Trans. Geosci. Remote Sens.*, GE-23, 35–46, doi:10.1109/TGRS.1985.289498.

Dong, J., J. P. Walker, and P. R. Houser (2005), Factors affecting remotely sensed snow water equivalent uncertainty, *Remote Sens. Environ.*, 97, 68–82.

Dong, J., J. P. Walker, P. R. Houser, and C. Sun (2007), Scanning multichannel microwave radiometer snow water equivalent assimilation, *J. Geophys. Res.*, 112, D07108, doi:10.1029/2006JD007209.

Durand, M., and S. A. Margulis (2006), Feasibility Test of Multifrequency Radiometric Data Assimilation to Estimate Snow Water Equivalent, *J. Hydrometeor.*, 7, 443–457.

Durand, M., and S. A. Margulis (2007), Correcting first-order errors in snow water equivalent estimates using a multifrequency, multiscale radiometric data assimilation scheme, *J. Geophys. Res.*, 112, D13121, doi:10.1029/2006JD008067.

Durand, M., E. J. Kim, and S. A. Margulis (2008), Quantifying uncertainty in modeling snow microwave radiance for a mountain snowpack at the point-scale, including stratigraphic effects, *IEEE Trans. Geosci. Remote Sens.*, 46, 1753–1767.

Durand, M., E. J. Kim, and S. A. Margulis (2009), Radiance assimilation shows promise for snowpack characterization, *Geophys. Res. Lett.*, 36, L02503, doi:10.1029/2008GL035214.

Elder, K. and A. Goodbody (2004), *CLPX-Ground: ISA Main Meteorological Data*. Boulder, CO: Nat. Snow Ice Data Center. Digital Media.

Evensen, G. (1994), Sequential data assimilation with a nonlinear quasi-geostrophic model using Monte Carlo methods to forecast error statistics, *J. Geophys. Res.*, 99, 10143–10162.

Ferrazzoli, P., L. Guerriero, and J.-P. Wigneron (2002), Simulating L-band emission of forests in view of future satellite applications, *IEEE Trans. Geosci. Remote Sens.*, 40, 2700–2708.

Flanner, M. G. and C. S. Zender (2006), Linking snowpack microphysics and albedo evolution, *J. Geophys. Res.*, 111, D12208, doi:10.1029/2005JD006834.

Foster, J. L., A. T. C. Chang, D. K. Hall, and A. Rango (1991), Derivation of snow water equivalent in boreal forests using microwave radiometry, *Arctic*, 44, 147–152.

Foster, J. L., C. Sun, J. P. Walker, R. Kelly, A. Chang, J. Dong, and H. Powell (2005), Quantifying the uncertainty in passive microwave snow water equivalent observations, *Remote Sens. Environ.*, 94, 187–203.

Gent, P. R., and Coauthors (2011), The community climate system model version 4, *J. Clim.*, 24, 4973–4991, doi: 10.1175/2011JCLI4083.1.

Girard, F., S. Payette, and R. Gagnon (2008), Rapid expansion of lichen woodlands within the closed-crown boreal forest zone over the last 50 years caused by stand disturbances in eastern Canada, *J. Biogeogr.*, 35, 529–537.

Gong, G., D. Entekhabi, and J. Cohen (2003), Modeled Northern Hemisphere winter climate response to realistic Siberian snow anomalies, *J. Climate*, 16, 3917–3931.
Graf, T., T. Koike, H. Fujii, M. Brodzik, and R. Armstrong (2003), *CLPX-Ground: Ground Based Passive Microwave Radiometer (GBMR-7) Data*. Boulder, CO: Nat. Snow Ice Data Center. Digital Media.
Grant, J. P., K. Saleh, J.-P. Wigneron, M. Guglielmetti, Y. H. Kerr, M. Schwank, N. Skou, and A. Van de Griend (2008), Calibration of the L-MEB model over a coniferous and a deciduous forest, *IEEE Trans. Geosci. Remote Sens.*, 46, 808–818.
Hall, D. K., J. L. Foster, and A. T. C. Chang (1982), Measurement and modeling of microwave emission from forested snowfields in Michigan, *Nordic Hydrology*, 13, 129–138.
Hall, D. K., V. V. Salomonson, and G. A. Riggs (2006), MODIS/Terra Snow Cover Daily L3 Global 0.05deg CMG. Version 5. National Snow and Ice Data Center, Boulder, CO, digital media. [Available online at http://nsidc.org/data/docs/daac/modis_v5/mod10c1_modis_terra_snow_daily_global_0.05deg_cmg.gd.html.]
Hall, D. K., R. E. J. Kelly, G. A. Riggs, A. T. C. Chang, and J. L. Foster (2002), Assessment of the relative accuracy of hemispheric-scale snowcover maps, *Ann. Glaciol.*, 34, 24–30.
Hallikainen, M. T., and P. A. Jolma (1992), Comparison of algorithms for retrieval of snow water equivalent from Nimbus-7 SMMR data in Finland, *IEEE Trans. Geosci. Remote Sens.*, 30, 124–131.
Hedstrom, N. R., and J. W. Pomeroy (1998), Measurements and modeling of snow interception in the boreal forest, *Hydrol. Process.*, 12, 1611–1625.
Imaoka, K., M. Kachi, M. Kasahara, N. Ito, K. Nakagawa, and T. Oki (2010), Instrument performance and calibration of AMSR-E and AMSR2. *International Archives of the Photogrammetry, Remote Sensing and Spatial Information Sciences*, XXXVIII, 13–16.
Jackson, T. J., and T. J. Schmugge (1991), Vegetation effects on the microwave emission of soils, *Remote Sens. Environ.*, 36, 203–212.
Jin, Y. Q. (1994), *Electromagnetic scattering modelling for quantitative remote sensing*. World Scientific, 348pp.
Knowles, K. W., M. H. Savoie, R. L. Armstrong, and M. J. Brodzik (2006), AMSR-E/Aqua Daily EASE-Grid Brightness Temperatures. National Snow and Ice Data Center, Boulder, CO, digital media, updated current year. [Available online at https://nsidc.org/data/docs/daac/nsidc0301_amsre_gridded_tb.gd.html.]
Kruopis, N., J. Praks, A. N. Arslan, H. M. Alasalmi, J. T. Koskinen, and M. T. Hallikainen (1999), Passive microwave measurements of snow-covered forest area in EMAC'95, *IEEE Trans. Geosci. Remote Sens.*, 37, 2699–2705.
Kurum, M., P. E. O'Neill, R. H. Lang, A. T. Joseph, M. H. Cosh, and T. J. Jackson (2012), Effective tree scattering and opacity at L-band, *Remote Sens. Environ.*, 118, 1–9.

Kwon, Y., A. M. Toure, Z.-L. Yang, M. Rodell, and G. Picard (2015), Error characterization of coupled land surface–radiative transfer models for snow microwave radiance assimilation, *IEEE Trans. Geosci. Remote Sens.*, 53, 5247–5268, doi: 10.1109/TGRS.2015.2419977.

Kwon, Y., Z.-L. Yang, L. Zhao, T. J. Hoar, A. M. Toure, M. Rodell, Estimating snow water storage in North America using CLM4, DART, and snow radiance data assimilation, submitted to *Journal of Hydrometeorology*.

Langham, E. J. (1981), Physics and properties of snowcover, in: *Handbook of Snow: principles, processes, management and use*. Gray, D. M., and D. H. Male (eds), Pergamon Press, Toronto, pp. 275-337.

Langlois, A., A. Royer, F. Dupont, A. Roy, K. Goïta, and G. Picard (2011), Improved corrections of forests effects on passive microwave satellite remote sensing of snow over boreal and subarctic regions, *IEEE Trans. Geosci. Remote Sens.*, 49, 3824–3837.

Lawrence, D., et al. (2011), Parameterization improvements and functional and structural advances in version 4 of the community land model, *J. Adv. Model. Earth Syst.*, 3, M03001, doi:10.1029/2011MS000045.

Lemke, P., J. Ren, R. B. Alley, I. Allison, J. Carrasco, G. Flato, Y. Fujii, G. Kaser, P. Mote, R.H. Thomas, and T. Zhang (2007), Observations: Changes in snow, ice and frozen ground, *Climate Change 2007: The Physical Science Basis*, S. Solomon et al., Eds. Cambridge Univ. Press, 337–383.

Lenhart, T., K. Eckhardt, N. Fohrer, and H.-G. Frede (2002), Comparison of two different approaches of sensitivity analysis, *Phys. Chem. Earth*, 27, 645–654.

Liang, X., D. P. Lettenmaier, E. F. Wood, and S. J. Burges (1994), A simple hydrologically based model of land-surface water and energy fluxes for general-circulation models, *J. Geophys. Res.*, 99, 14415–14428.

Lin, P., J. Wei, Y.-F. Zhang, and Z.-L. Yang (2015), The impact of land initialization on seasonal forecasts of surface air temperature: role of Northern Hemisphere snow data assimilation. *Proc. AGU Fall Meeting*, San Francisco, CA, USA, Amer. Geophys, Union.

Lobl, E. (2001), Joint Advanced Microwave Scanning Radiometer (AMSR) Science Team meeting, *Earth Observer*, 13, 3–9.

Lundberg, A., and S. Halldin (2001), Snow interception evaporation. Review of measurement techniques, processes, and models, *Theor. Appl. Climatol.*, 70, 117–133.

Lundberg, A., Y. Nakai, H. Thunehed, and S. Halldin (2004), Snow accumulation in forests from ground and remote-sensing data, *Hydrol. Process.*, 18, 1941–1955.

Mätzler, C. (1987), Applications of the interaction of microwaves with the natural snow cover, *Remote Sens. Rev.*, 2, 259–387.

Mätzler, C. (1996), Microwave permittivity of dry snow, *IEEE Trans. Geosci. Remote Sens.*, 34, 573–581.

Mätzler, C. (1998), Improved Born approximation for scattering of radiation in a granular medium, *J. Appl. Phys.*, 83, 6111–6117.

Mätzler, C. (2002), Relation between grain-size and correlation length of snow, *J. Glaciol.*, 48, 461–466.
Mätzler, C. and A. Wiesmann (1999), Extension of the Microwave Emission Model of Layered Snowpacks to Coarse-Grained Snow, *Remote Sens. Environ.*, 70, 317–325.
Mo, T., B. J. Choudhury, T. J. Schmugge, J. R. Wang, and T. J. Jackson (1982), A model for microwave emission from vegetation-covered fields, *J. Geophys. Res.*, 87, 11229–11237.
Namias, J. (1985), Some empirical evidence for the influence of snow cover on temperature and precipitation, *Mon. Wea. Rev.*, 113, 1542–1553.
Nghiem, S. V., I. G. Rigor, D. K. Perovich, P. Clemente-Colón, J. W. Weatherly, and G. Neumann (2007), Rapid reduction of Arctic perennial sea ice, *Geophys. Res. Lett.*, 34, L19504, doi:10.1029/2007GL031138.
Niu, G.-Y., and Z.-L. Yang (2006), Effects of frozen soil on snowmelt runoff and soil water storage at a continental scale, *J. Hydrometeor*., 7, 937–952.
Niu, G.-Y., and Z.-L. Yang (2007), An observation-based formulation of snow cover fraction and its evaluation over large North American river basins, *J. Geophys. Res.*, 112, D21101, doi:10.1029/2007JD008674.
Njoku, E. G., and L. Li (1999), Retrieval of land surface parameters using passive microwave measurements at 6–18 GHz, *IEEE Trans. Geosci. Remote Sens.*, 37, 79–93.
Njoku, E. G., P. Ashcroft, T. K. Chan, and L. Li (2005), Global survey and statistics of radio-frequency interference in AMSR-E land observations, *IEEE Trans. Geosci. Remote Sens.*, 43, 938–947.
Oleson, K. W., et al. (2010), Technical description of version 4.0 of the Community Land Model (CLM). NCAR Tech. Note NCAR/TN-478+STR, 257pp.
Paloscia, S. (1995), Microwave emission from vegetation, *Passive microwave remote sensing of land-atmosphere interactions*, B. J. Choudhury, Y. H. Kerr, E. G. Njoku, and P. Pampaloni, Eds., VSP Press, 357–374.
Paloscia, S., and P. Pampaloni (1988), Microwave polarization index for monitoring vegetation growth, *IEEE Trans. Geosci. Remote Sens.*, 26, 617–621.
Pampaloni, P. (2004), Microwave radiometry of forests, *Waves Random Media*, 14, S275–S298, doi:10.1088/0959-7174/14/2/009.
Pampaloni, P., and S. Paloscia (1986), Microwave emission and plant water content: A comparison between field measurements and theory, *IEEE Trans. Geosci. Remote Sens.*, 24, 900–905.
Pellarin, T., Y. H. Kerr, and J.-P. Wigneron (2006), Global simulations of brightness temperature at 6.6 and 10.7 GHz over land based on SMMR data set analysis, *IEEE Trans. Geosci. Remote Sens.*, 44, 2492–2505.
Picard, G., L. Brucker, A. Roy, F. Dupont, M. Fily, and A. Royer (2013), Simulation of the microwave emission of multi-layered snowpacks using the dense media radiative transfer theory: the DMRT-ML model, *Geosci. Model Dev.*, 6, 1061–1078. doi:10.5194/gmd-6-1061-2013.

Pomeroy, J. W., and K. Dion (1996), Winter radiation extinction and reflection in a boreal pine canopy: measurements and modeling, *Hydrol. Processes*, 10, 1591–1609.

Pomeroy, J. W., and R. A. Schmidt (1993), The use of fractal geometry in modelling intercepted snow accumulation and sublimation, *Proc. Eastern Snow Conference*, 50, 1–10.

Raeder, K., J. L. Anderson, N. Collins, T. J. Hoar, J. E. Kay, P. H. Lauritzen, and R. Pincus (2012), DART/CAM: An ensemble data assimilation system for CESM atmospheric models, *J. Clim.*, 25, 6304–6317.

Rees, A., J. Lemmetyinen, C. Derksen, J. Pulliainen, and M. English (2010), Observed and modelled effects of ice lens formation on passive microwave brightness temperatures over snow covered tundra, *Remote Sens. Environ.*, 114, 116–126.

Reichle, R. H., R. D. Koster, G. J. M. De Lannoy, B. A. Forman, Q. Liu, S. P. P. Mahanama, and A. Toure (2011), Assessment and enhancement of MERRA land surface hydrology estimates, *J. Climate*, 24, 6322–6338.

Riggs, G. A., D. K. Hall, V. V. Salomonson (2006), MODIS snow products user guide to collection 5. [Available online at https://nsidc.org/data/docs/daac/modis_v5/dorothy_snow_doc.pdf.]

Rodell, M., and P. R. Houser (2004), Updating a land surface model with MODIS derived snow cover, *J. Hydrometeor.*, 5, 1064–1075.

Roy, A., A. Royer, J.-P. Wigneron, A. Langlois, J. Bergeron, and P. Cliché (2012), A simple parameterization for a boreal forest radiative transfer model at microwave frequencies, *Remote Sens. Environ.*, 124, 371–383.

Roy, A., G. Picard, A. Royer, B. Montpetit, F. Dupont, A. Langlois, C. Derksen, and N. Champollion (2013), Brightness temperature simulations of the Canadian seasonal snowpack driven by measurements of the snow specific surface area, *IEEE Trans. Geosci. Remote Sens.*, 51, 4692–4704.

Schmugge, T. J., and T. J. Jackson (1992), A dielectric model of the vegetation effects on the microwave emission from soils, *IEEE Trans. Geosci. Remote Sens.*, 30, 757–760.

Stankov, B. and A. Gasiewski (2004), *CLPX-Airborne: Multiband Polarimetric Scanning Radiometer (PSR) Imagery*. Boulder, CO: Nat. Snow Ice Data Center. Digital Media.

Stewart, I. T., D. R. Cayan, and M. D. Dettinger (2004), Changes in snowmelt runoff timing in western North America under a 'business as usual' climate change scenario, *Clim. Change*, 62, 217–232.

Storck, P., D. P. Lettenmaier, and S. M. Bolton (2002), Measurement of snow interception and canopy effects on snow accumulation and melt in a mountainous maritime climate, Oregon, United States, *Water Resour. Res.*, 38, 1223, doi:10.1029/2002WR001281.

Stroeve, J. M. M. Holland, W. Meier, T. Scambos, and M. Serreze (2007), Arctic sea ice decline: Faster than forecast, *Geophys. Res. Lett.*, 34, L09501, doi:10.1029/2007GL029703.

Sturm, M., J. Holmgren, and G. E. Liston (1995), A seasonal snow cover classification system for local to regional applications, *J. Climate*, 8, 1261–1283.
Sturm, M., B. Taras, G. E. Liston, C. Derksen, T. Jonas, and J. Lea (2010), Estimating snow water equivalent using snow depth data and climate classes, *J. Hydrometeor.*, 11, 1380–1394.
Su, H., Z.-L. Yang, G.-Y. Niu, and R. E. Dickinson (2008), Enhancing the estimation of continental-scale snow water equivalent by assimilating MODIS snow cover with the ensemble Kalman filter, *J. Geophys. Res.*, 113, D08120, doi:10.1029/2007JD009232.
Su, H., Z.–L. Yang, G.–Y. Niu, and C. R. Wilson (2011), Parameter estimation in ensemble based snow data assimilation: A synthetic study, *Adv. Water Resour.*, 34, 407–416.
Su, H., Z.-L. Yang, R. E. Dickinson, C. R. Wilson, and G.-Y. Niu (2010), Multisensor snow data assimilation at the continental scale: The value of Gravity Recovery and Climate Experiment terrestrial water storage information, *J. Geophys. Res.*, 115, D10104, doi:10.1029/2009JD013035.
Sun, C., J. P. Walker, and P. R. Houser (2004), A methodology for snow data assimilation in a land surface model, *J. Geophys. Res.*, 109, D08108, doi:10.1029/2003JD003765.
Swenson, S. C., and D. M. Lawrence (2012), A new fractional snow-covered area parameterization for the Community Land Model and its effect on the surface energy balance, *J. Geophys. Res.*, 117, D21107, doi:10.1029/2012JD018178.
Tedesco, M. and E. J. Kim (2006), Intercomparison of electromagnetic models for passive microwave remote sensing of snow, *IEEE Trans. Geosci. Remote Sens.*, 44, 2654–2666.
Tippett, M. K., J. L. Anderson, C. H. Bishop, T. M. Hamill, and J. S. Whitaker (2003), Ensemble square root filters, *Mon. Wea. Rev.*, 131, 1485–1490.
Toure, A. M., K. Goïta, A. Royer, E. J. Kim, M. Durand, S. A. Margulis, and H. Lu (2011), A case study of using a multilayered thermodynamical snow model for radiance assimilation, *IEEE Trans. Geosci. Remote Sens.*, 49, 2828–2837.
Tsang, L., and J. A. Kong (2001), *Scattering of electromagnetic waves: Advanced Topics*. Vol. 3. Wiley-Interscience, 413pp.
Tsang, L., P. Xu, and K. S. Chen (2008), Third and fourth stokes parameters in polarimetric passive microwave remote sensing of rough surfaces over layered media, *Microw. Opt. Techn. Lett.*, 50, 3063–3069.
Tsang, L., C. Chen, A. Chang, J. Guo, and K. Ding (2000), Dense media radiative transfer theory based on quasicrystalline approximation with applications to passive microwave remote sensing of snow, *Radio Sci.*, 35, 731–749.
Ulaby, F. T., R. K. Moore, and A. K. Fung (1981), *Microwave remote sensing: active and passive*. Vol. 1. Addison-Wesley, Reading, 456 pp.
Vernekar, A. D., J. Zhou, and J. Shukla (1995), The effect of Eurasian snow cover on the Indian monsoon, *J. Climate*, 8, 248–266.
Wegmüller, U., and C. Mätzler (1999), Rough bare soil reflectivity model, *IEEE Trans. Geosci. Remote Sens.*, 37, 1391–1395.

Wiesmann, A., and C. Mätzler (1999), Microwave emission model of layered snowpacks, *Remote Sens. Environ.*, 70, 307–316.

Yang, K., T. Koike, I. Kaihotsu, and J. Qin (2009), Validation of a dual-pass microwave land data assimilation system for estimating surface soil moisture in semiarid regions, *J. Hydrometeor.*, 10, 780–793.

Zaitchik, B. F., and M. Rodell (2009), Forward-looking assimilation of MODIS-derived snow covered area into a land surface model, *J. Hydrometeor.*, 10, 130–148.

Zhang, Y.-F. (2015), Multivariate Land Snow Data Assimilation in the Northern Hemisphere: Development, Evaluation and Uncertainty Quantification of the Extensible Data Assimilation System, Ph.D. dissertation, Dept. of Geological Sciences, The University of Texas at Austin, 116 pp.

Zhang, Y.-F., T. J. Hoar, Z.-L. Yang, J. L. Anderson, A. M. Toure, and M. Rodell (2014), Assimilation of MODIS snow cover through the Data Assimilation Research Testbed and the Community Land Model version 4, *J. Geophys. Res. Atmos.*, 119, 7091–7103, doi:10.1002/2013JD021329.

Zhao, L., Z.-L. Yang, and T. J. Hoar, Global Soil Moisture Estimation by Assimilating AMSR-E Brightness Temperatures in a Coupled CLM4-RTM-DART System, submitted to *Journal of Hydrometeorology*.

Zierl, B., and H. Bugmann (2005), Global change impacts on hydrological processes in Alpine catchments, *Water Resour. Res.*, 41, W02028, doi:10.1029/2004WR003447.

Vita

Yonghwan Kwon was born in Masan, South Korea, in March, 1981. After finishing his high school study in Masan Changshin High School in 2000, he enrolled Seoul National University and majored in environmental education. He developed enthusiasm and interests for environmental sciences and decided to continue his study in the Graduate School of Environmental Studies, Seoul National University, South Korea. He earned his master's degree in Environmental Management in 2009. With encouragement and support from his family, Yonghwan continued his study in climate and hydrological sciences at the Jackson School of Geosciences, The University of Texas at Austin. He studied land surface modeling, radiative transfer modeling, and snow microwave radiance data assimilation for his PhD research at The University of Texas at Austin between September 2011 and May 2016.

Email: yhkwon@utexas.edu

This dissertation was typed by the author.